Compliant Mechanisms in Aseptic Pharmaceutical Manufacturing:

Feasibility Study on Flexure-Based Design for Particle Elimination in Sterile Environments

ME51035: ME-BMD MSc Thesis

M.C. van Ingen

Delft University of Technology

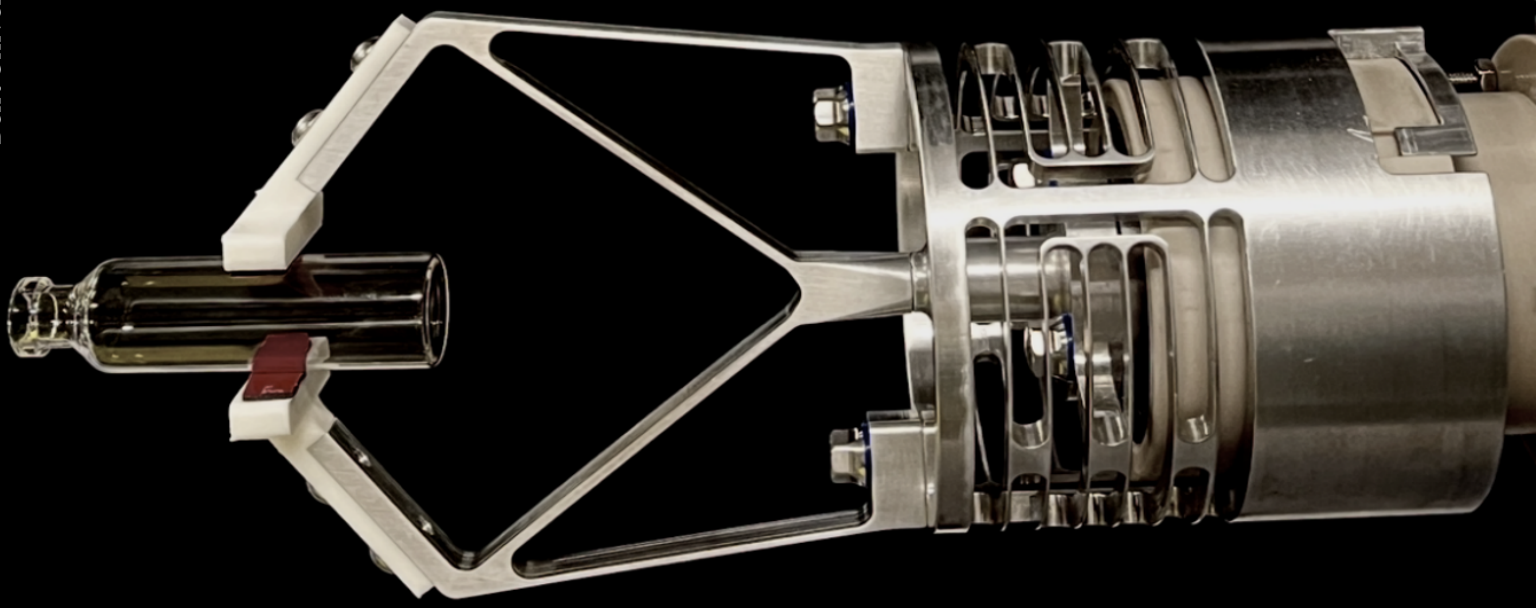

TU Delft

novo nordisk®

Compliant Mechanisms in Aseptic Pharmaceutical Manufacturing:

Feasibility Study on Flexure-Based Design for Particle Elimination in Sterile Environments

by

M.C. van Ingen

to obtain the degree of Master of Science
at the Delft University of Technology,
to be defended publicly on Monday December 15, 2025 at 2:00 PM.
Research conducted in collaboration with Novo Nordisk.

Student number:	4816978	
Project duration:	February 17, 2025 – December 15, 2025	
Thesis committee:	F.G.J. (Freek) Broeren PhD MSc,	TU Delft, supervisor
	Stienen, dr.ir. A.H.A. (Arno),	TU Delft
	Ir. N. Vacchi (Nicolo'),	Novo Nordisk

Style: TU Delft Report Style, with modifications by M.C. van Ingen

An electronic version of this thesis is available at http://repository.tudelft.nl/.

TU Delft

Preface

This rapport covers my Master of Science thesis at the Delft University of Technology, a journey that has shaped my understanding of precision engineering within the most demanding industrial contexts. Undertaking this research on compliant mechanisms in aseptic pharmaceutical manufacturing has been both a significant challenge and an incredibly rewarding experience, bridging the gap between theoretical mechanical design and real world industrial application. My deepest gratitude goes to my primary supervisor, Dr. F.G.J. Broeren, whose extensive knowledge, insightful guidance, and unwavering support were instrumental in navigating the complexities of this interdisciplinary field. His enthusiasm for compliant mechanisms and his approach to problem solving continually inspired me to push the boundaries of my research. I am also thankful to Dr.ir. A.H.A. Stienen from TU Delft, for taking up the role as chair in my graduation committee. A special acknowledgement is due to Ir. N. Vacchi from Novo Nordisk, my external daily supervisor. His practical insights into the stringent requirements of aseptic pharmaceutical manufacturing, coupled with his willingness to share his expertise, were crucial in grounding this design study in real-world applicability. The collaboration with Novo Nordisk provided an great opportunity to address a genuinely pressing industry need. The journey was not without its moments of steep learning curves and intricate design challenges, particularly at the intersection of mechanical engineering and cleanroom compatibility. I extend my sincere appreciation to my friends and family, whose encouragement, understanding, and occasional distractions provided much needed balance. It is my sincere hope that this work contributes meaningfully to the advancement of automation solutions in aseptic pharmaceutical manufacturing, demonstrating the potential of compliant mechanisms to enhance sterility assurance and operational efficiency. The experience gained during this thesis, from conceptualization to detailed analysis and preliminary validation, has been valuable, and I am grateful for the opportunity to contribute to such an impactful field

M.C. van Ingen
Delft, December 2025

Abstract

Aseptic pharmaceutical manufacturing demands ultra-clean automation to safeguard product integrity and patient safety, yet traditional rigid body mechanisms generate particles, require lubricants, and are difficult to sterilize. Compliant mechanisms (CMs), achieving motion through elastic deformation of monolithic structures, offer a compelling alternative by inherently eliminating these contamination sources. However, their feasibility within the strict constraints of Grade A aseptic environments remains underexplored.

This Master's thesis investigates the design, analysis, and preliminary validation of a flexure-based compliant gripping mechanism for sterile handling of pharmaceutical components, developed in collaboration with Novo Nordisk. The research employed a systematic approach, integrating analytical stiffness modeling (including refined corner-filleted arc leaf flexures), Pseudo-Rigid Body Models (PRBMs) for gripper kinematics, and Finite Element Analysis (FEA) for stress and kinematic performance. A cleanroom-compatible voice coil actuator (VCA) drove the system, which included a compliant linear guide mechanism (LGM) and a two-fingered gripping mechanism (GM), complemented by an aseptic bayonet locking system. Preliminary validation involved prototyping (in Al7075) and cleanability assessment via riboflavin testing.

Results demonstrated strong agreement between analytical (13.00 N/mm) and FEA (13.45 N/mm) predictions for LGM stiffness, validating the accuracy of the refined flexure models. Modal analysis confirmed robust dynamic stability, with the first axial mode (84.196 Hz) well separated from parasitic modes. The GM achieved a 7.5 mm gripping motion from a 4 mm VCA input, with optimized tapered flexures reducing peak von Mises stresses by approximately 35%. The monolithic design inherently eliminated particle-generating elements, and riboflavin tests showed high cleanability, identifying minor geometric refinements for optimal aseptic compliance. The design was subsequently re-optimized for pharmaceutical compatible material Super Duplex, preserving validated performance.

This study successfully demonstrates the viability of compliant mechanisms as a critical enabling technology for next generation automation in aseptic pharmaceutical manufacturing. By inherently minimizing particle generation, simplifying sterilization, and ensuring cleanroom compatibility, these mechanisms promise enhanced sterility assurance and improved efficiency, paving the way for advanced pharmaceutical production.

Contents

Nomenclature

Abbreviations

Abbreviation	Definition
AM	Additive Manufacturing
ASME	American Society of Mechanical Engineers
BI	Biological Indicators
BPE	Bioprocessing Equipment (ASME BPE standard)
CAD	Computer Aided Design
CFD	Computational Fluid Dynamics
CFU	Colony Forming Unit
CFLFs	Corner-Filleted Arc Leaf Flexures
CI	Chemical Indicators
CIP	Clean In Place
CM	Compliant Mechanism
CNC	Computer Numerical Control
COP	Clean Out of Place
DMLS	Direct Metal Laser Sintering
EAP	Electroactive Polymer
EC	Eligibility Criteria
EMA	European Medicines Agency
EMI	Electromagnetic Interference
EO	Ethylene Oxide
EPDM	Ethylene Propylene Diene Monomer
EU GMP	European Union Good Manufacturing Practice
FDM	Fused Deposition Modeling
FDA	Food and Drug Administration
FEA	Finite Element Analysis
FPM	Flexure Parallelogram Mechanism
GA	Geometric Advantage
GM	Gripping Mechanism
HEPA	High-Efficiency Particulate Air filter
ISO	International Organization for Standardization
LGM	Linear Guide Mechanism
MEMS	Micro-Electro-Mechanical Systems
MIR	Minimum Invasive Robotics
PA	Polyamide
PAO	Polyalphaolefin (used in particle testing)
PC	Polycarbonate
PEEK	Polyether Ether Ketone
PEG	Polyethylene Glycol (used in smoke studies)
PETP	Polyethylene Terephthalate
POM	Polyoxymethylene
PP	Polypropylene
PRBM	Pseudo-Rigid Body Model
PRISMA	Preferred Reporting Items for Systematic Reviews and Meta-Analyses
PSL	Polystyrene Latex
PSM	Point-Spring Model
PTFE	Polytetrafluoroethylene
PU	Polyurethane
RA	Roughness Average

Abbreviation	Definition
RBR	Rigid-Body Replacement
RTP	Rapid Transfer Ports
SD	Super Duplex
SDOF	Single-Degree-of-Freedom
SIP	Sterilize In Place
SLA	Stereolithography
SLM	Selective Laser Melting
SLS	Selective Laser Sintering
SMA	Shape Memory Alloys
SMP	Shape-Memory Polymers
SOP	Standard Operating Procedures
SS	Stainless Steel
TPE	Thermoplastic Elastomer
TPU	Thermoplastic Polyurethane
UDAF	Unidirectional Airflow
USP	United States Pharmacopeia
UV	Ultraviolet
VCA	Voice Coil Actuator
VHP	Vaporized Hydrogen Peroxide
VOC	Volatile Organic Compounds
W&S	Wash and Sterilization
WIP	Wash In Place

Symbols

Symbol	Definition	Unit
Latin Symbols		
a	Normalized fillet parameter (r/w_{avg})	[-]
A	Cross-sectional Area	[m^2]
b	Normalized fillet parameter (L/w_{avg})	[-]
C	Compliance Matrix	[m/N, rad/Nm]
C_{ij}	Entry in Compliance Matrix	[varies]
E	Young's Modulus	[Pa]
F	Force	[N]
F_{in}	Input Force	[N]
f_n	Natural Frequency	[Hz]
$f_{x,P}, f_{y,P}, f_{z,P}$	Local Internal Force Components	[N]
G	Shear Modulus	[Pa]
I_p	Polar Moment of Inertia (Torsional Constant)	[m^4]
I_y	Area Moment of Inertia about y-axis	[m^4]
I_z	Area Moment of Inertia about z-axis	[m^4]
J_{kin}	Jacobian Matrix	[-]
k	Stiffness	[N/m]
K_A, K_B	Torsional Stiffnesses	[Nm/rad]
k_{FPM}	Effective Stiffness of FPM System	[N/m]
$K_{mech}(x_s)$	Mechanism Stiffness at Slider Position x_s	[N/m]
k_{series}	Combined Stiffness for Series Flexures	[N/m]
k_{total}	Stiffness of Overall Linear Guide	[N/m]
k_z	Axial Stiffness	[N/m]
L	Length (Arc Length)	[m]
l_p	Number of Parallel Flexures	[-]
m	Mass	[kg]
$m_{x,P}, m_{y,P}, m_{z,P}$	Local Internal Moment Components	[Nm]
n	Number of FPM Stacks	[-]
P	Power	[W]

Symbol	Definition	Unit
r	Fillet Radius	[m]
R	Median Radius (of Arc Beam)	[m]
t	Thickness	[m]
t_b	Twist at Free End B (Displacement and Rotation Vector)	[m, rad]
U_{total}	Total Strain Energy	[J]
V	Velocity	[m/s]
V_e	Total Elastic Strain Energy	[J]
w	Width (of Arc Beam)	[m]
w_A	Width at Fixed End A	[m]
w_{avg}	Average Width	[m]
w_B	Width at Free End B	[m]
w_b	Wrench at Free End B (Force and Moment Vector)	[N, Nm]
$w_{eff}(\alpha)$	Effective Width at Angle α	[m]
x_s	Slider Position	[m]
Greek Symbols		
α	Angle	[rad]
α_{tot}	Total Central Angle	[rad]
β	Coefficient of Thermal Expansion	[1/K]
δx_s	Virtual Displacement of Slider	[m]
$\delta\theta_A, \delta\theta_B$	Virtual Angular Displacements	[rad]
ϕ	Phase Angle	[rad]
μ	Shear Correction Factor	[-]
ν	Poisson's Ratio	[-]
ρ	Density	[kg/m^3]
σ_{max}	Maximum Stress	[Pa]
σ_{yield}	Yield Strength	[Pa]
τ	Shear Stress	[Pa]
τ_A, τ_B	Spring Torques	[Nm]
$\theta_A, \theta_B, \theta_C$	Bar Angles	[rad]
θ_{A0}, θ_{B0}	Stress-free Bar Angles	[rad]
ω	Angular Velocity	[rad/s]
ω_n	Undamped Natural Frequency	[rad/s]
$\zeta(\xi)$	Piecewise Scaling Function (Fillet Shape Function)	[-]

1

Introduction

Aseptic pharmaceutical manufacturing stands as a cornerstone of modern healthcare, demanding uncompromising standards of sterility and cleanliness to ensure product integrity and, fundamentally, patient safety. Production environments, particularly those operating under **ISO Class 5 (Grade A)** conditions as mandated by regulations such as **EU GMP Annex 1** and FDA guidelines, are characterized by exceptionally strict requirements to minimize particulate and microbial contamination. This necessitates automation solutions that not only perform with precision and reliability but also inherently adhere to rigorous hygienic design principles.

Traditional automation components, often comprised of multi part assemblies with conventional joints, bearings, and lubricants, present significant challenges within these controlled environments. Such mechanisms can generate undesirable wear particles, harbor microbial growth in hard to clean crevices, and are inherently difficult to sterilize effectively. These issues directly increase the risk of batch contamination, compromise product quality, and hinder compliance with Good Manufacturing Practices (GMP). This drives an urgent need for innovative solutions that can meet evolving regulatory demands and improve operational efficiency without sacrificing sterility assurance.

Compliant mechanisms (CMs) offer a promising paradigm for next generation automation in aseptic manufacturing. By achieving motion through the elastic deformation of a monolithic structure, CMs inherently eliminate many of the contamination sources associated with traditional mechanisms. They require no lubricants, produce minimal to no wear debris, and their monolithic nature significantly simplifies thorough cleaning and sterilization processes. Their seamless, jointless architecture makes them ideally suited for stringent cleanroom applications where particle generation and microbial traps must be rigorously controlled.

Despite their inherent advantages, the widespread application of compliant mechanisms within the specific constraints of aseptic pharmaceutical manufacturing remains an underexplored area. Key challenges include ensuring material compatibility with aggressive cleaning agents, maintaining performance under repeated sterilization cycles, and adhering to the cleanroom design principles such as laminar airflow requirements and minimal surface roughness. This Master's thesis, conducted at the Delft University of Technology in close collaboration with **Novo Nordisk**, directly addresses this critical gap.

The **primary objective** of this research is to explore the feasibility of designing, analysing, and preliminarily validating a flexure-based compliant gripping mechanism that is inherently compatible with Grade A aseptic environments. This study focuses on the sterile and precise handling of sensitive pharmaceutical components, such as vials, cartridges, and Petri dishes.

The study systematically integrates several key aspects:

- **Defining stringent design requirements:** Based on a comprehensive literature review informed by ISO standards and EU GMP Annex 1 regulations.
- **Actuator Selection:** Identifying and selecting a cleanroom compatible Voice Coil Actuator (VCA) for its non contact, precise motion generation.
- **Mechanism Development:** Designing a compliant linear guide system (LGM) and a two-fingered gripping mechanism (GM) using advanced analytical tools like Pseudo-Rigid Body Models (PRBMs) and optimized flexure geometries, specifically incorporating a refined model for corner-filleted arc leaf flexures.
- **Hygienic Design Integration:** Incorporating an aseptic bayonet locking mechanism for modularity, tool-less changes, and ease of cleaning.
- **Validation Methodology:** Employing analytical modeling, Finite Element Analysis (FEA) for stress

and kinematic performance validation, and experimental validation of a aluminium prototype.

- **Material Transition:** Re-optimizing the design for pharmaceutical-grade materials Super Duplex Stainless Steel to ensure long-term aseptic compliance.

Ultimately, this work aims to demonstrate the viability of compliant mechanisms as a critical enabling technology for future automation in aseptic pharmaceutical manufacturing. By intrinsically fulfilling strict sterility requirements, these mechanisms hold the potential to enhance sterility assurance, significantly reduce operational complexity, and improve efficiency in advanced pharmaceutical production lines.

The remainder of this report is structured as follows: **Chapter 2** presents a comprehensive literature review on compliant mechanisms and aseptic design principles. **Chapter 3** elaborates on the systematic design process, covering the selection of actuation, the development of the compliant linear guide and gripping mechanisms, and the aseptic locking system. **Chapter 4** outlines the overall research methodology, including analytical, numerical, and experimental validation strategies. **Chapter 5** details the results obtained from the analytical models, FEA, and preliminary prototype testing. **Chapter 6** discusses the design improvements for transitioning to aseptic-grade materials. Finally, **Chapter 7** provides a reflective discussion of the findings, limitations, and future research directions, leading to the **Conclusion in Chapter 8**, summarizing the key achievements and contributions of this thesis.

2

Literature study

Compliant Mechanisms in Aseptic Pharmaceutical Manufacturing: A Systematic Review of Material Selection, Design Requirements and the State of the Art for Grade A Environments

M.C. van Ingen (4816978)
Delft University of Technology
Faculty of Mechanical Engineering
In Collaboration with Novo Nordisk
Supervision: Freek Broeren (TU Delft) & Nicolo' Vacchi (Novo Nordisk)

Abstract **- Compliant mechanisms (CMs), a relatively recent innovation in mechanical engineering, have gained significant attention due to their unique advantages over traditional rigid body mechanisms. By achieving motion through elastic deformation rather than joints, they offer advantages for high-precision industries, including zero backlash, reduced wear and simplified manufacturing. These mechanisms are already implemented in ultra-clean environments such as semiconductor manufacturing, where their monolithic design minimizes particle generation. This crucial requirement is also shared by the aseptic pharmaceutical industry, where preventing contamination is of utmost importance. However, CMs remain underutilized in this industry. This systematic review investigates how CMs can address strict regulatory demands such as the EU GMP Annex 1 and FDA guidelines in isolator-based filling lines. Through a PRISMA guided analysis of 214 studies, material selection, sterilization compatibility and airflow requirements were evaluated. The study synthesizes design principles from CMs in cryogenics, aerospace and cleanroom robotics, where frictionless actuation and fatigue resistant topologies have been proven successful. By integrating these insights with pharmaceutical grade requirements, a roadmap for designing a compliant gripper tailored to Grade A environments is proposed. Key steps include topology optimization, material validation under repeated autoclaving, and particle emission testing. The resulting guidelines for implementing CM's in aseptic production, show their potential to improve sterility while reducing maintenance complexity. Future work will focus on prototyping grippers and validating long term performance under GMP conditions.**

Index Terms **- Compliant Mechanism, Aseptic Industry, Filling Line, Regulations, Particle Generation**

2.1. Introduction

In the high stakes industry of aseptic pharmaceutical manufacturing (see Appendix 2.6) , where a single particle can compromise a multi million euro batch of medicine, the industry's reliance on conventional mechanical systems is becoming a critical vulnerability. Traditional mechanisms, which rely on sliding joints and lubricated bearings, inherently generate 0.5–5 µm particles through wear, a flaw caused by multi component designs that create micro-crevices prone to biofilm formation. Compliant mechanisms (CMs), which achieve motion through elastic deformation rather than mechanical interaction, offer an alternative [1]. These monolithic systems eliminate two primary contamination risks. Firstly, by eliminating friction which inherently reduces particle emissions. An advantage already embraced by the semiconductor industry where a single particle can damage a wafer [2], [3]. The second advantage is the removal of micro-crevices [4], [5], an inherent disadvantage of multi-component designs, that harbor sterilant-resistant microbes, an advantage that is also exploited by studies on surgical robotics

[2] and aerospace applications[6]. As regulators increase their requirements, EU GMP Annex 1 [7] now mandates continuous airborne particle monitoring with 1 CFU / m3 in Grade A zones, the need for contamination-free actuation has never been more urgent.

Despite these advantages, pharmaceutical adoption remains hindered by three barriers. First, material degradation under repeated sterilization, such as autoclaving (121°C, 15 psi) compromises fatigue life in polymers like PEEK and induces stress corrosion in metals [8]. Second, poorly optimized CM flexures disrupt unidirectional airflow (UDAF), creating turbulence that exceeds ISO 14644-1's 15% airspeed tolerance and delays particle recovery in isolators [9]. Third, regulatory uncertainty persists, as no prior study validates CM designs against Annex 1 media fill requirements or FDA 21 CFR 211.67 equipment maintenance standards [10].

This systematic review confronts these challenges through a PRISMA-guided analysis of 214 studies across robotics, aerospace, and pharmaceutical engineering. Three key innovations emerge: Optimized Topologies: Optimizing CMs not only for mechanical performance but also implementing geometry constraint like minimum radius ($>$ 3 mm) and minimum internal geometries. This will facilitate more cleanable designs and increase airflow performance. Utilizing topology optimizations is deemed to be a promising methodology of systematic implementing this in the design. GMP-Aligned Validation: A novel testing framework integrates riboflavin coverage mapping (cleanability), USP $< 788 >$ particulate counting [11], and accelerated aging to bridge the compliance gap. Actuation integration: Integration of the actuation is also uncovered as an promising way of increasing usability of CMs. As in current CM solutions the actuation generates most of the particles. Voice coil actuation has been identified as a promising solution to achieve this. The resulting roadmap positions CMs not merely as incremental upgrades, but as enablers of next-generation "zero particule" filling lines.

2.1.1. Aim

This systematic review aims to evaluate the design challenges in interoperating compliant gripping mechanisms in the aseptic industry. By combining regulations and synthesizing the state of art of cryogenic, aerospace, and clean-room design principles.

This work is structured as follows: Chapter I dissect material selection and sterilization protocols while chapter II details the PRISMA methodology and search strategy on compliant mechanisms.

2.2. Methodology

2.2.1. Search Strategy

This systematic review of the literature is structured into two distinct sections. The first chapter will examine the regulatory frameworks governing the materials and processes essential for aseptic production. The second chapter will provide an in-depth review of relevant CMs and actuations.

The search and selection process for the second chapter will follow the PRISMA guidelines for systematic reviews [12]. A detailed literature search was conducted across three key databases: Scopus, PubMed, and Web of Science. The search query was designed using a set of carefully selected keywords divided in three categories, which are listed in Table 2.1.

1. **Compliant Mechanisms**: This category encompasses terminology describing monolithic, flexure based design principles to account for variations in nomenclature across disciplines. By including synonyms, the search aims to capture the full spectrum of literature on integrated mechanical systems that achieve motion through elastic deformation.

2. **Aseptic Environment**: Due to limited literature explicitly addressing aseptic environments, this category is expanded to include applications with similar operational constraints, such as clean-room technologies, sterile processing, and cryogenic or aerospace systems. So even though they are not directly the same as the aseptic industry they can be used to gain transferable insights from adjacent industries requiring contamination control or extreme environmental isolation.

3. **Gripping Mechanism**: This category focused on mechanisms exhibiting mechanical behaviours relevant to precision gripping.

Within each category, terms were combined using the OR operator, while categories were connected using the AND operator. The decision was made to exclude the use of the NOT operator, as there were not many studies identified, so manual processing was preferred. As can be seen in table 2.1. Similarly, no filter on the document type was used as well. The results of the systematic search were stored in the reference manager Rayyan[13].

2.2.2. Selection procedure

The digital automation tool Rayyan was used to detect duplicate articles [13]. Entries identified by Rayyan were manually verified before removal. The final set of eligible studies was identified according to four eligibility criteria (EC1 to EC4), detailed in Table 2.2 These criteria were applied chronologically. Studies failing to meet these criteria were systematically excluded through a sequential screening process: first by title and abstract, then by full-text review. The decision on inclusion or exclusion was made solely by the author.

Compliant Mechanisms	Aseptic Production	Gripping Mechanisms	NOT	Document
”Compliant”	”Pharmaceutical”	”Gripper*”		
”Flexible”	”Grade A”	”End effector”		
”Monolithic”	”Sterile manufacturing”	”Handling device”		
”Origami”	”GMP”	”Manipulator”		
”Flecture”	”Biopharmaceutical”			
	”Aseptic processing”			
	”Contamination control”			
	”Cleanroom”			
	”MIR”			
	”Food”			
	Steril*			
	”Cryogenic”			

Table 2.1: Categorized key terms used to form the search strategy. Terms were combined vertically with the OR operator and horizontally with the AND operator. The slash (/) separates alternative terms or phrases combined with OR in the search string. The Not and Document area's where left empty as the search string already does not result in to many results

EC#	Description
EC1	Study uses geometry that are to complex to be of interest for this study
EC2	No compliant gripper was mentioned or designed in the study
EC3	The study uses soft robotics which can not be used in the aseptic industry
EC4	The study is to general to be of interest

Table 2.2: Eligibility criteria EC1-EC4.

2.2.3. Data extraction

The data extracted from the included articles encompassed the first author, year of publication, reference method, topic it focused on, if it included aseptic, if it was interested in particle generation, the output force of the design, the actuation methode, the design method that was used and finally the achieved range of motion. The data extraction is discussed in section 2.4.3.

2.3. Design Requirements for Mechanisms in Aseptic Pharmaceutical Production to Ensure Compliance with Regulations

Aseptic pharmaceutical production must comply with strict regulations to ensure patient safety. Therefore, the following chapter discusses the different design requirements for the mechanism within aseptic production, the design implications for CM designs and present ways to validate the design.

2.3.1. Material Criteria for Aseptic Compliance

In aseptic processing, materials must meet strict criteria to ensure safety, effectiveness, and compliance. Regulatory agencies such as the FDA and EMA have established strict guidelines specifying allowable materials for sterile pharmaceutical applications. These guidelines demand a balance between material properties such as chemical resistance, thermal stability, and particle emission risk. Based on these guidelines, the following list has been composed to create an overview of the criteria to which the materials must adhere.

- **Biocompatibility:** Materials in product contact zones must prevent leachables (e.g., plasticizers, oligomers) that could interact with drug formulations. ISO 10993-1 [14] evaluates cytotoxicity, while USP Class VI certifies non reactivity in implantation tests[15].
- **Surface Properties:** Surface roughness is another factor that is strictly specified within the regulations. Depending on the use of the specific part there are different surface roughness requirements. For example when a surface is in contact with product a surface roughness of Ra $\leq 0.8\mu\mathrm{m}$ (ASME BPE-2022) is required. This surface roughness requirement is there to minimize microbial adhesion and facilitate cleaning [16].
- **Sterilization Resistance:** As products on the line are regulurly sterilized compatibility with sterilization methods is crucial. A few common examples are autoclaving (ISO 17665:2024), gamma irradiation (ISO 11137-3:2017) or ethylene oxide (ISO 11135) [17] [18] [19].
- **Particle Emission:** As there are strict particle requirements within the Isolator lines there are regulations in place about maximum shedding during cyclic deformation, according to the USP $< 788 >$ [11] particulate limits.
- **Chemical Inertness:** The material should be resistant to cleaning agents (e.g., detergents, hydrogen

peroxide) and drug formulations so that it does not change properties, for example, by corroding.

2.3.2. Cleaning and Sterilization Methods

There are various methods available for cleaning and sterilizing of production equipment, each with their own advantages and limitations. To provide clarity, Table 2.3 presents a comparison of the most commonly used sterilization techniques. [16]

Sterilization process

The choice of an appropriate sterilization method is critical in aseptic environments and depends on several factors, including how equipment is integrated into the production line and whether it comes into direct or indirect contact with the product. These considerations dictate the washing and sterilization (W&S) requirements, influencing both the design and maintenance procedures that are used.

Format parts, which are frequently changed between production batches, typically require autoclaving before reuse. Machine parts, in contrast, are usually subjected to cleaning in place (CIP). CIP is often a manual process, where operators ensure thorough cleaning by disassembling and scrubbing parts. This method can be labor intensive and requires accessible designs with sufficiently large geometries to be cleaned manually, avoiding any complex crevices where contaminants might accumulate. However, advancements in aseptic processing have led to the development of fully integrated wash in place (WIP) and sterilize in place (SIP) systems [26], allowing entire production lines to undergo automated cleaning and sterilization simultaneously. For this review it is decided to focus in on the Autoclaving and CIP processes, due to their prevalence in the industry and the distinct design challenges they present. In many respects, CIP is a ”worst-case scenario” especially for a compliant mechanism due to its reliance on manual procedures, demanding simple geometries [27], [8], [28], [29], [30].

Design Implication for Compliant Mechanism

The chosen cleaning and sterilization method also influences the design criteria for CMs in aseptic environments. To ensure compatibility with W&S processes, key factors such as material selection, surface finish, resistance to cleaning agents, and mechanical durability must be considered. Table 2.4 provides an overview of the design considerations associated with different sterilization processes.

Validation of Sterilization

To ensure the effectiveness of sterilization methods, several verification techniques are possible. These methods provide both qualitative and quantitative assessments of the sterilization process:

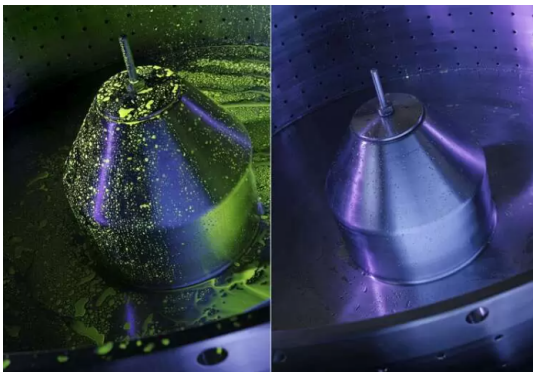

Figure 2.1: An Example of Cleaning Coverage Test Using Riboflavin to Verify Cleanbility of Design. Image from [31]

- **Biological Indicators (BIs) :** These are perhaps the most definitive form of testing. BIs consist of spores from highly resistant microorganisms (e.g., Geobacillus stearothermophilus) known to be difficult to kill. They are placed in various locations within the equipment to verify that the sterilization process achieves the desired microbial kill rate. [32] [33]
- **Chemical Indicators (CIs)** : These provide immediate, visual indications that sterilization parameters (e.g., temperature, exposure time) have been met. CIs can be used on packaging or directly on the equipment as an immediate but less comprehensive means of validation compared to BIs.[34]
- **Residual Testing :** Post cleaning tests to check for residues from cleaning agents ensure that sterility is not compromised by contaminants left on equipment surfaces. This is especially important for CIP processes where manual residue checks may be necessary.[35]
- **Microbial Monitoring :** Regular sampling and culturing procedures are conducted on surfaces after sterilization to detect any surviving microorganisms. These tests confirm the effective reduction of bioburden to acceptable levels.[36]
- **Riboflavin Coverage Test :** While not a direct sterilization verification method, this test validates washing processes by applying a UV-fluorescent riboflavin solution. Residual fluorescence under UV light identifies poorly cleaned areas, ensuring thorough contaminant removal prior to sterilization methods like autoclaving see figure 2.1[37].

In the context of the development of compliant mechanism design, sterilization verification methods such as BIs and CIs focus on validating the operational performance of sterilization equipment or processes. However, the riboflavin coverage test specifically indicates geometric challenges in compliant mechanisms such as difficult to clean flexures, fluid stagnation zones, or intricate joints that hinder washing. Therefore it was concluded that

Table 2.3: Sterilization Methods for Aseptic Applications. Data is based on literature covered in this section, relevant regulatory standards and internal SOP's of Novo Nordisk

Method	Mechanism	Materials	Compatible Temp/Pressure	Regulatory Standard	Key Considerations
Autoclaving (Steam)	Moist heat (121C, 15 psi, 15–30 min)	Stainless Steel 316L, PEEK, Ultem, Silicone	121–134C, 15–30 psi	ISO 17665:2024 [20]	- Avoid for polymers with low Tg (e.g., PU, PC). - Risk of corrosion for non-stainless metals.
Gamma Irradiation	Ionizing radiation (25–50 kGy)	PTFE, PEEK, PEHD, Polypropylene	Ambient temperature	ISO 11137-1:2025 [21]	- Causes embrittlement in some polymers (e.g., Nylon). - No residue; suitable for single-use devices.
Ethylene Oxide (EO)	Alkylation of DNA (55–60C, 40–60% humidity)	PU, PC, Nylon, Elastomers	30–60C, vacuum chamber	ISO 10993-7:2008 [22]	- Requires aeration to remove toxic residues. - Not for moisture-sensitive materials.
Hydrogen Peroxide (H_2O_2) Plasma	Oxidative radicals (Low-temperature plasma)	PTFE, PEEK, Anodized Aluminum	45–50C, low pressure	ISO 22441:2022 [23]	- Limited penetration depth. - Ideal for heat-sensitive components.
Dry Heat	High temperature (160–190C, 1–2 hrs)	Metals (e.g., 316L, Super Duplex)	160–190C, ambient pressure	ISO 20857:2010 [24]	- Suitable for moisture-sensitive metals. - Degrades most polymers.
Chemical Sterilants	Liquid disinfectants (e.g., ethanol, isopropanol)	Bronze (non-critical), Elastomers	Ambient temperature	FDA 21 CFR §178.1010 [25]	- Limited to surface sterilization. - Requires rinsing to avoid residues.

Table 2.4: Sanitization Requirements for Different Sterilization Methods. Data is based on ISO cleanability standards and internal Novo Nordisk design guidelines

Requirement	CIP	Autoclaving	VHP
Material	- VHP resistant - Chemical resistant	- Temperature resistant	- Resistant to absorption/decomposition
Radius corners	$>$ 3 mm	No minimum (preferred $>$ 3 mm)	$>$ 3 mm
Internal geometries	Accessible for manual cleaning	Accessible for water flow	–
Drainability	Self-drainable	- Self-drainable - 3 degree slope preferred	–
Surface roughness	$\leq$0.8μm	$\leq$0.8μm	$\leq$0.8μm

the riboflavin test will be the most useful for validating the cleanability during the development of a new compliant mechanism. The other validation methods should be used on a final design to get it approved for production but are less useful during initial design development.

2.3.3. Suitable Materials For Aseptic Compliant Mechanisms

In aseptic environments, the selection of materials for the mechanisms requires strict evaluation to ensure compatibility with the sterility, mechanical durability and regulatory requirements. Based on these requirements for materials as described in the section 2.3.1 a list of allowed materials has been composed, this can be seen in Appendix 2.6.4 based on this table an assessment of the materials has been generated which can be seen in Figure 2.2. From this graph, PEEK and Stainless Steel (SS) have been identified as the most promising choices for compliant mechanism applications. Therefore, they will be covered in some more detail to better understand their advantages and shortcomings.

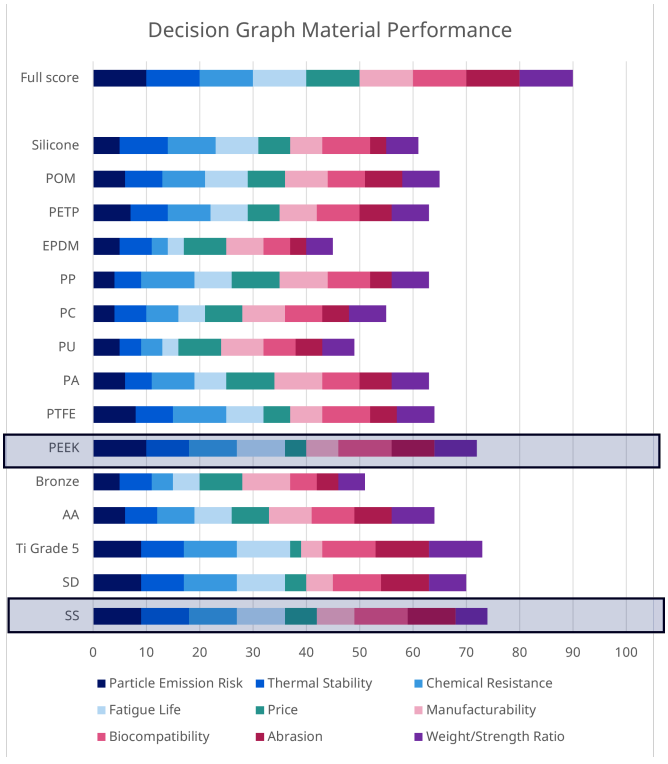

Figure 2.2: Decision graph that visualizes the material assessment for compliant mechanism within the aseptic industry. Materials where assessed on 9 different material characteristics and scored from 1-10 where 10 was the best score and 1 the worst. See Appendix G Table 2.8 for the vlue's

Polyether Ether Ketone (PEEK)

PEEK is a high-performance thermoplastic known for its exceptional mechanical properties and chemical resistance, making it a leading candidate for aseptic applications:[38], [39]

- **Properties :** PEEK has great chemical resistance, it is highly resistant to a broad spectrum of chemicals, including those involved in sterilization processes such as autoclaving and gamma irradiation. It also has great thermal Stability, it maintains performance integrity at temperatures up to 260°C and is therefore suitable for autoclave cycles. Lastly it's mechanical Strength, it offers high stiffness and strength to weight ratio, ideal for precision applications in compliant mechanisms.
- **Advantages :** Very low particle emission and excellent fatigue resistance, making it ideal for cyclic loading scenarios often encountered in compliant designs. It can be precision machined to achieve surface roughness Ra ≤0.8 µm, meeting strict cleanroom standards for minimizing contamination. [40]
- **Drawbacks :** Despite its exceptional properties, PEEK presents several limitations in aseptic compliant mechanisms. The material's high cost compared to conventional thermoplastics and metals like stainless steel can be prohibitive for large scale or budget sensitive applications. While PEEK shows a favourable strength-to-weight ratio, its load bearing capacity under sustained high stress is inferior to metals, restricting its use in ultra high stress scenarios. Additionally, PEEK is susceptible to creep under prolonged mechanical loads, which may compromise dimensional stability in precision mechanisms over time. Lastly while PEEK is one of only polymers options for autoclaving, prolonged exposure to autoclave conditions near its upper temperature limit may gradually reduce its mechanical strength over time.

Stainles Steel (316L and Similar Alloys)

SS, particularly the 316L grade, is the golden standard in aseptic environments due to its robustness and sterility:[41], [42]

- **Properties:** Firstly SS shows great corrosion resistance and as such performs well in oxidative environments and to chemical sterilants. It also has great mechanical robustness. It has excellent strength and load bearing capacity making it suitable for high stress applications.
- **Advantages :** High fatigue strength, which allows for durability in mechanisms subjected to repetitive strain. By electropolishing smooth surface finishes (Ra ≤0.8 µm) can be achieved meeting hygiene standards.
- **Drawbacks:** Susceptible to pitting and galling if not properly alloyed or treated, careful material handling and manufacturing techniques are therefore required. More complex fabrication, requiring techniques such as precision polishing and electropolishing to optimize surface properties and reduce contamination.[42]

Alternative Materials

While PEEK and SS stand out as preferred materials, alternative materials such as PTFE and titanium were considered but not selected as primary candadites for specific reasons:

- **PTFE :** Known for its excellent chemical resistance, PTFE was not chosen due to its lower mechanical strength and higher risk of deformation under load, which makes it slightly less suited for a compliant mechanisms. [43]
- **Titanium :** Offers outstanding biocompatibility and strength to weight ratio. However, the high cost and difficulties in machining make it less practical for applications requiring complex geometries or cost-efficiency.

Therefore PEEK and SS provide a balanced solution for aseptic environments and are advised to be the starting choice. However the other materials are still viable solutions when use cases ask for it.

2.3.4. Airflow requirements in aseptic production

In addition to material selection requirements in aseptic production, strict airflow regulations are in place to mitigate the risk of particle contamination. These requirements are outlined in regulatory frameworks such as ISO 14644-1 and EU GMP Annex 1 and mandate laminar unidirectional airflow (UDAF) within isolators and cleanrooms, ensuring all particles are systematically flushed from critical zones[8]. While vertical downward airflow is standard for simplicity and gravitational particle removal, horizontal airflow may be used in specific cases. As vertical downward airflow is the standard, this study will solely focus on this.

Key Airflow Criteria

- **Airspeed**: Isolators require an airspeed of 0.45–0.55 m/s (ISO 14644-1 Class 5)[9] at the HEPA filter face. Local turbulence from compliant mechanisms (e.g., flexures or hinges) must not reduce effective airspeed below 0.3 m/s in product-exposure zones.
- **Recovery Time**: Post-intervention, particle levels must return to ISO Class 5 within 15–30 seconds

(ISO 14644-3:2019) [17]. Compliant mechanisms must not obstruct airflow paths or create stagnant zones that delay this recovery.

Design Implications for Compliant Mechanisms

Compliant mechanisms, despite their jointless advantages, pose unique airflow challenges which are important to take into consideration when designing. The following list provides a very comprehensive overview of the most important concerns:

- **Turbulence Mitigation**: Uneven surfaces (e.g., actuator arms, grooves) or moving parts that disrupt smooth airflow should be avoided where possible. Use CFD simulations to ensure that turbulence stays below 20% and that airflow speed variation is within 15% (ISO 14644-1) [9].
- **Geometric Optimization**: Avoid sharp transitions; use tapered contours to guide airflow. Streamlined profiles with curved edges ($3mm$) reduce boundary layer separation and should therefore be used when possible.

Validation Protocols

- **CFD Simulations**: CFD simulations should be used to model airflow patterns, ideality including mechanism motion cycles, to identify stagnation zones or backflow.
- **Smoke Studies**: Qualitatively validate UDAF under production conditions, during operation on a (mock-up) line with the help of smoke to visualize airflow pattens and turbulence.
- **Particle Challenge Testing**: Introduce PAO/PSL spheres (0.3–5.0 µm) upstream, and then verify ≤5 $\%$ retention in mechanism crevices post-flush (ISO 14644-3) [17] .

2.4. Systematic Review of the Design Considerations for Compliant Mechanisms within the Aseptic Industry

This chapter will explore the possible areas of application, the state of the art, and finally the feasibility of CM's within the aseptic industry. The PRISMA method is used to search the literature systematically.

2.4.1. Application Possibilities Within Aseptic Production Lines

Aseptic production lines across different suppliers require similar motions and functional requirements. To identify potential applications for CM's, the various types of mechanism currently used in these lines have been analyzed. For ease of comparison, the observed motions have been categorized into three main groups:

- Linear long range actuation mechanisms
- Gripping mechanisms
- Locking mechanisms

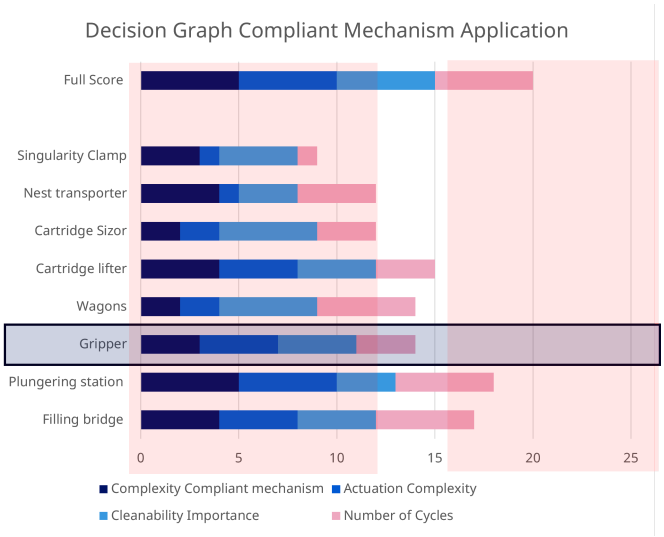

Figure 2.3: Decision graph that visualizes the application area for compliant mechanism within the aseptic industry. Actuation types where assessed on 4 different characteristics and scored from 1-5 where 5 was the best score and 1 the worst. In Red the area is shown that is out of scope for this project. And in blue the final choice is highlighted. See Appendix G Figure 2.10 for the value's

To determine the most suitable application for further research, a structured evaluation was performed using a decision matrix (see Appendix 2.6.4). This approach allowed for an objective comparison of different application areas based on relevant criteria such as complexity of the CM design, actuation complexity, cleanability importance and the number of required cycles.

Following this assessment, the study identified the compliant gripper as the most promising candidate for additional initial research. The Gripping mechanism was chosen as the areas in red where deemed ether complex or to simple for a first case study. From the remaining three application area's the Gripper was chosen as it has the most equal division of points scored for the selection criteria. This selection was based on its potential to enhance aseptic handling processes while minimizing particle generation and mechanical complexity. The next phase of this study will therefore focus on the design, feasibility, and performance evaluation of a compliant gripper for aseptic production environments.

2.4.2. State of the Art

To understand the required capabilities of compliant gripping mechanisms, it is important to understand what current aseptic options are capable of and what their respective drawbacks are. This section will provide a comprehensive overview of the state-of-the-art of aseptic gripping options. The current gripping mechanisms can be divided into four main categories: Pneumatic, Hydraulic, Vacuum and Electric grippers which can be seen in Figure 2.4

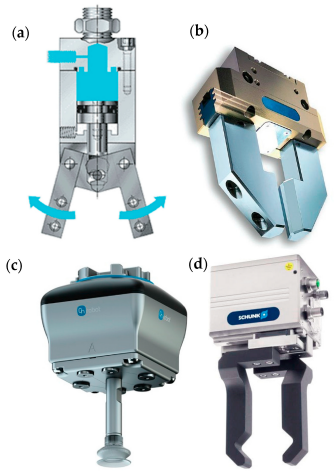

Figure 2.4: An overview of the state of the art of grippers in aseptic industry with (a) Pneumatic gripper, (b) hydraulic gripper, (c) vacuum gripper, and (d) electric gripper; image from Tanzini et al. (2023) [44]

- **Pneumatic gripper:** Actuated by compressed air, these grippers (Figure 2.4a) dominate aseptic lines due to their simplicity and low cost. However, they suffer from particle generation via exhaust air and friction in the rotational joint they also have limited positional accuracy (±0.5 mm). Hoses and valves complicate isolator sealing, while elastomer seals degrade under repeated vaporized hydrogen peroxide (VHP) sterilization. [45]
- **Hydraulic Grippers:** Systems driven by (hydraulic) fluid (Figure 2.4b) provide high gripping forces (up to 500 N) but pose significant contamination risks. Leakage of hydraulic fluid. Additionally, sterilization compatibility is poor autoclaving causes seal swelling, and gamma irradiation degrades fluid viscosity.
- **Vacuum Grippers:** Non-contact suction devices (Figure 2.4c) minimize particle shedding but are restricted to flat, non-porous surfaces. Vacuum pumps generate turbulence, disrupting unidirectional airflow (UDAF). Their inability to handle irregular geometries (e.g., syringe barrels) limits utility in multi-product facilities.
- **Electric Grippers:** Servo-driven designs (Fig. 1d) offer precision (±0.1 mm) and programmability but rely on lubricated gears and sliders. Outgassing of silicone-based lubricants exceeds ISO 14644-1 volatile organic compound (VOC) limits, and particle emissions from motor brushes necessitate frequent HEPA filter replacements. [46]

Key Limitations of Current Technologies

All conventional grippers share critical drawbacks in aseptic environments: Friction from joints/seals produces particles, exceeding Grade A limits during high-speed operation. Multi part assemblies create crevices that trap biofilms, reducing cleanability. Disassembly for cleaning in place (CIP) increases downtime and contamination risk during reassembly. These limitations show the need for compliant mechanisms monolithic, joint free designs that eliminate friction, reduce part count, and withstand aggressive sterilization.

Compliant Grippers State of the Art

There are several CM grippers for lab automation commercially available. However, the available information on these systems is very limited. In general they use gripper jaws with a parallel motion actuated mechanically or pneumatically. All the commercial available grippers that where discovered in this research where not certified according to grade A standards. Commercial solutions only mention using of an FDA-approved, food-industry-proven lubricant. So although the designs will be taken into account as they are not clean-room certified and no specific design information could be found they have not been the main focus [47], [48] [49], [50].

2.4.3. Data Extraction PRISMA Guided Search on Relevant Compliant Grippers

This section synthesizes advancements in CM design by using a PRISMA guided literature study, focusing on their application in cleanroom environments, particle generation mitigation, and adaptability to diverse handling tasks. Key studies are analyzed thematically to highlight trends, gaps, and future directions.

Design Methodologies for Contamination Mitigation

A primary focus of CM research is minimizing particle generation through monolithic, friction free designs.

Budde et al. (2024) [55] researched this approach with the CrocoGrip, an aluminium gripper tested for ISO 14644 Class 5 cleanroom particle limits [9]. Their work specifically investigated the relationship between actuation dynamics (solenoid oscillations) and particle emissions, revealing that 70% of particles originated from abrupt solenoid deactivation rather than the compliant structure itself. By integrating damping springs, they reduced oscillations but introduced mechanical complexity, highlighting a trade off between particle control and system robustness.

Mouazé and Birglen (2022) [53] introduced a bistable compliant underactuated gripper designed to minimize deformation of soft objects (e.g., fruits, tissues) using a pseudo-rigid-body model (PRBM) and point-spring model (PSM) . Their methodology prioritized computational efficiency over traditional finite element analysis (FEA), enabling rapid optimization. The gripper achieved $< 5\%$ deformation in silicone objects (simulating soft tissues) through a underactuated finger with a bistable four-bar linkage. While their focus was on deformation control rather than particle generation, the absence of sliding joints inherently reduced friction related contamination risks.

Table 2.5: Compliant Grippers Data Extraction Table of the Included studies, NM is used when the information is not mentioned

Author (Year)	Topic	Aseptics Included	Particles Included	Force	Actuation	Design Method	Motion Range	Material
Hermoza Llanos et al. (2025) [2]	Overview of Compliant Grippers	No	No	NM	Overview	Overview	NM	NM
Jahn et al. (2021) [51]	Cryogenic Mechanism	No	Yes	NM	Stepper motor	FEM	30°	TiAl6V4
Cao et al. (2024) [52]	Soft Object Gripper	No	No	10-15N	Uni-actual	NSGA-2, FEM	50-60mm	PET
Mouazé & Birglen (2022) [53]	Soft Object Gripper	No	No	2.5-3.5N	Torque/Hand	PRBM	4.6-11cm	NM
Ruiz et al. (2024)[54]	Space Gripper	No	No	10N	Tendon	NM	NM	Multi-material
Budde et al. (2024) [55]	Clean-room Gripper	Yes	Yes	6N	Solenoid/VCA	PRBM, FEM	2mm	Al
Budzyń et al. (2023) [6]	Lunar Gripper	No	No	NM	Hand	Topology Opt.	15mm	TPC
Jhan et al. (2020) [56]	Cryogenic Manipulator	No	Yes	NM	EM Coil	Topology Opt.	0.388mm	Stainless
Tanzini et al. (2024) [44]	Grade A Robotics	Yes	Yes	NM	NM	NM	NM	NM
Liu et al. (2021) [57]	Constant Force Gripper	Yes	Yes	40N	Spindle	Topology Opt.	15-30mm	TPE
Zheng et al. (2024) [58]	Soft Finger	No	No	NM	EM Coil	FEM	10-30mm	Silicon
Lofroth & Avci (2019)[59]	Micro Gripper	Yes	Yes	NM	Piezo	PRBM	154µm	Al Plate

Zheng et al. (2024) [58] expanded this approach by integrating electromagnetic actuation into a topology optimized CM. Their FEA driven design optimized for maximum bending angle (39.5° at 1.5A) while minimizing stress concentrations. Unlike Budde's [55] solenoid driven system, Zheng's electromagnetic coils enabled precise current controlled force modulation, eliminating pneumatic noise. However, reliance on silicone introduced adhesion challenges for sub 12 mm objects, mirroring limitations seen in Lofroth/Avci's [59] MEMS-gripper.

Liu et al. (2021) [57] advanced compliant mechanism design through topology optimization of a 3D-printed constant-force finger using thermoplastic elastomer (TPE). Their methodology introduced a composite objective function balancing output displacement and force regulation, achieving a near-constant gripping force of 41.9 N across a 15–30 mm input displacement range. Unlike Budde et al.'s [55] binary solenoid-driven approach, Liu's design used nonlinear large-deformation FEA to optimize elastic energy distribution, eliminating sliding joints and reducing friction-induced particle generation risks. The monolithic TPE structure, fabricated via fused deposition modeling (FDM), provided inherent compliance for delicate object handling while avoiding stress concentrations. However, the study omitted particle emission quantification during cyclic actuation, a critical gap for cleanroom applicability. Additionally, while TPE's flexibility enabled 154 µm displacement per actuator, its porosity and low glass transition temperature (−50°C) limited compatibility with autoclave sterilization.

Lofroth and Avci (2019) [**\cite {mi10050313}**] addressed micro-scale contamination by combining MEMS fabricated silicon tips with a compliant aluminium base. Their research centred on adhesion force mitigation for sub 100 µm objects, a persistent challenge in cell manipulation. However, their hybrid design (silicon + brass) introduced alignment complexities, and the silicon tips' brittleness necessitated frequent replacements, showing the need for durable, micro-scale compliant materials.

Actuation Mechanisms: Precision vs. Particle Generation

Actuation choice critically impacts CM performance in aseptic environments. Budde et al. (2024) [55] adopted solenoids for binary control, prioritizing simplicity over precision. Their work quantified the particle cost of this approach: solenoid induced emissions peaked at 1,200 particles/m³ during rapid deactivation. Lofroth and Avci, (2019) [59] used piezoelectric actuators for sub-micron precision (0.1 µm resolution), achieving closed loop control via strain-gauge feedback. Their study demonstrated successful manipulation of 6 µm silica beads in liquid environments. However, the piezoelectric system's in-

creased cost and complexity, limiting scalability.

Mouazé and Birglen (2022) [53] used nylon tendons, coated with molybdenum disulfide grease. This approach introduced porosity risks, limiting use in ISO Class 5+ environments

Zheng et al. (2024) [58] introduced a novel electromagnetic driven CM, addressing pneumatic instability and noise. Their gripper utilized current controlled coils to generate repulsive forces, achieving bending angles up to 39.5°.

Cao et al. (2024) [52] explored shape-memory polymers (SMPs) for adaptive grasping, focusing on geometric advantage (GA) optimization. Their origami-inspired gripper achieved a GA of 3.2, enabling gentle handling of ultrasoft objects like hydrogel beads. However, the SMPs' limited force output (2.22–3.52 N) restricted use in high load scenarios, and the study did not address thermal stability under autoclave conditions.

These studies collectively highlight the need for actuation systems that balance precision, force, and contamination control.

Material Selection and Sterilization Compatibility

Material biocompatibility and sterilization resilience remain underaddressed in CM research. Budzyń et al. (2023) [6] explored lunar grade Ti6Al4V for dust mitigation in extreme environments, achieving a 95% reduction in parasitic motion through topology optimization.

Ruiz et al. (2024) [54] introduced a multilayered material system for extreme thermal resilience in space debris removal, combining thermoplastic polyurethane (TPU), silicone, PTFE (Teflon), and aerogel. Their design addressed temperature swings in Low Earth Orbit, where surfaces cycled between -197°C (shadow) and 220°C (sunlight) . The PTFE external layer minimized elasticity variations, while aerogel insulation buffered internal components, maintaining operational temperatures between -96°C and 153°C . However, the study validated thermal performance (liquid nitrogen/heat gun testing), it omitted sterilization protocols critical for pharmaceutical applications (e.g., autoclave, VHP). The reliance on nylon tendons coated with molybdenum disulfide grease improved cryogenic lubrication but introduced porosity risks.

Jahn et al. (2020) [56] advanced cryogenic compatible material systems through their development of solid-state joints fabricated via selective laser melting (SLM) from Ti6Al4V titanium alloy. This material demonstrated exceptional performance at low temperatures. However, while Ti6Al4V's cryogenic stability was validated, the study did not address its compatibility with pharmaceutical sterilization protocols such as autoclaving or vaporized hydrogen peroxide (VHP), a limitation shared with Budzyń et al.'s [6] lunar-grade Ti6Al4V implementations. The electromagnetic actuator's reliance on molybdenum-disulfide-coated components introduced porosity risks similar to Ruiz et al.'s [54] nylon tendon challenges, potentially compromising ISO Class 5 compliance.

Lofroth and Avci (2019) combined silicon tips with brass backings to enhance durability, yet the brass's susceptibility to oxidation posed long-term contamination risks. Their work highlighted the need for corrosion-resistant alloys (e.g., 316L stainless steel) in CM designs but did not explore them.

Modularity and Scalability in Handling Tasks

Modular CM designs improve versatility, but introduce alignment challenges.

Cao et al. (2024) [52] introduced origami inspired grippers with shape-memory polymers, enabling formfitting grasping of irregular objects like crumpled foils. Their work emphasized reconfigurability but lacked standardized interfaces for tip replacement, a barrier for industrial adoption.

Budde et al. (2024) [55] addressed modularity with snap-fit PLA jaws, reducing replacement time to $<$ 30 seconds. However, PLA porosity retained particles after repeated use, highlighting the need for nonporous, sterilizable materials such as PEEK. They also utilized screw interfaces which limit the cleanability.

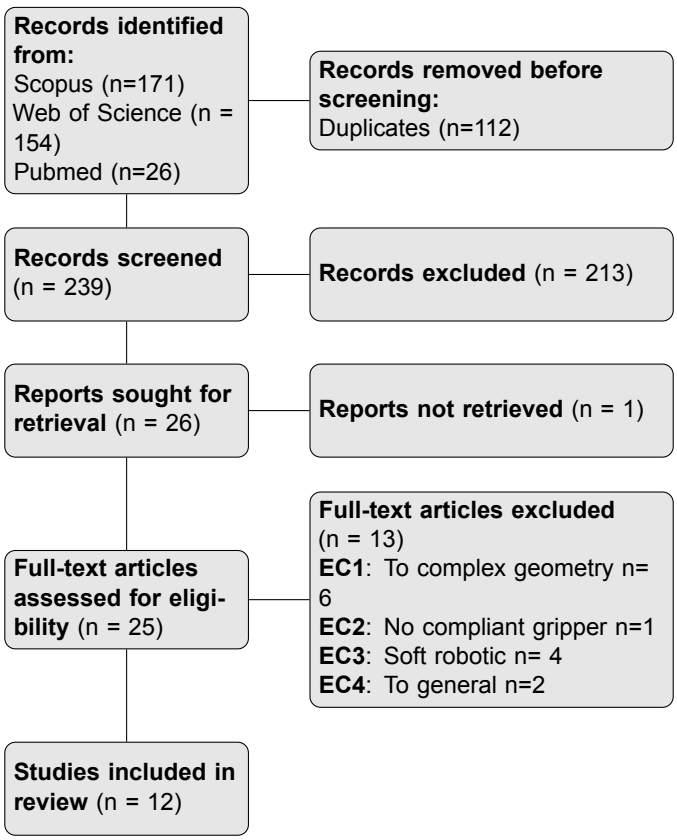

Figure 2.5: PRISMA flowchart for study selection.

2.4.4. Design Strategy

As also became apparent in the PRISMA guided literature search there are different design approaches that

can be used to design a compliant gripper. Designing the CM with the correct analytical and computational tools is critical for balancing kinematic performance, structural integrity, and contamination control. This section will therefore do a more specific deep dive in the analytical tools available and what the best option for our use case will be.

Pseudo Rigid Body Models (PRBM) and Finite Element Method (FEM) Integration. PRBM simplifies CM's into rigid body equivalents, enabling intuitive kinematic analysis. Budde et al. (2024) [55] combines PRBM with FEM to validate stress distribution in its monolithic gripper, ensuring robustness under cyclic loads. Lofroth and Avci (2019) [59] extends this approach for a surgical gripper, using PRBM for conceptual design and FEM to optimize topology for biocompatibility and sterility. The systematic review by Hermoza Llanos et al. (2025) highlights that design methodologies such as rigid-body replacement (RBR) with kinetostatic analysis enable precise motion control for tasks like vial capping, using flexure hinges to reduce particulate generation. This dual methodology ensures designs are both functionally simple and structurally reliable.

Topology optimization, distributes material efficiently according to specific input requirements, it can there for be used to reduce contamination prone surfaces. Budzyń et al. (2023) 3D printed lunar gripper combines this method with additive manufacturing, creating lightweight geometries ideal for extreme environments. For aseptic applications, topology optimization could minimize material use while ensuring cleanroom compatible geometries. Liu et al. (2021) [60] uses Topology optimization to generate a compliant gripper that has a constant force region where the force can be adjusted by changing the thickness of the finger.

Zhou et al., (2015) [61] shows that with the correct constraint on the topology optimization minium radius dimensions can be achieved. While Fernández et al. (2020), [62] shows that the design can be optimized for minimal internal geometries. Ensuring more hygienic designs. With future research this could ensure a systematic approach to find a hygienic compliant mechanism design.

The selection between PRBM-FEM and topology optimization depends on the CM's primary design focus. PRBM-FEM methodology is preferred for precision driven applications requiring specific motion paths, such as vial handling mechanisms, where kinematic predictability is critical. Topology optimization on the other hand enables systematic generation of hygienic designs by minimizing contamination-prone geometries a priority in aseptic environments.

Given this study's emphasis on Grade A compliance, topology optimization is selected. This method inherently reduces micro-crevices and optimizes airflow compatible geometries.

2.4.5. Actuation

As described in the PRISMA guided analysis of the literature, the choice of actuation method for monolithic compliant mechanisms is critical to minimizing particle generation and ensuring smooth, contamination-free operation. The selected actuation method must eliminate sliding or rotating interfaces and avoid the use of lubricants. Table 2.6 provides an analysis of various actuation technologies possibly suitable for aseptic environments, based on the reviewed papers. When selecting an actuation method, the following factors have been considered:

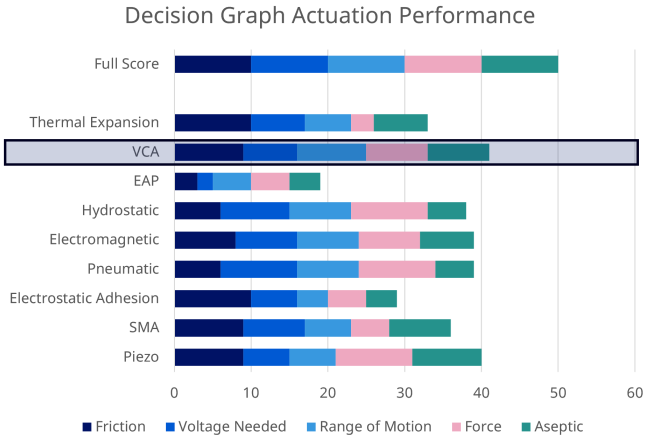

Figure 2.6: Decision graph that visualizes the actuation assessment for compliant mechanism within the aseptic industry. Actuation types where assessed on 5 different characteristics and scored from 1-10 where 10 was the best score and 1 the worst. See Appendix G table 2.9 for the values.

- **Frictionless Operation :** Methods that minimize contact between moving parts can significantly reduce particle generation. Technologies like piezoelectric motors or voice coils provide the necessary motion without traditional moving joints.
- **Precision and Control :** High precision actuation is necessary for gripping in pharmaceutical contexts. In the graph the criteria range of motion and force will take this into account.
- **Integration Complexity :** While pursuing advanced technologies, considerations should also be taken into account regarding ease of integration, scalability, and maintenance within the aseptic environment. In graph the combination of all criteria will determine this.
- **Regulatory Compliance :** Actuation methods must meet strict industry standards, ensuring that they do not introduce contaminants and that they remain stable under sterilization processes and aseptic conditions. In the graph this is covered by the criteria Aseptics.

Within this context, each actuation method presents a unique set of advantages and trade-offs in terms of efficiency, precision, and integration complexity. Therefore,

careful evaluation is necessary on a case by case basis to select the most suitable strategy for specific applications. For instance, in the case of developing a compliant gripper for handling Petri dishes, a voice coil actuator appears to be a promising option due to its capacity for smooth, precise motion and the avoidance of contamination risks while still having a suitable range of motion. The Cryogenic Voice Coil as can be seen in figure 2.7 in specifically. True that encapsulation in titanium it is composed of aseptic approved material and has less chance of sheading particles.

Figure 2.7: Voice Coil designed by JPE specificity for Cryogenic conditions. Resulting in a voice coil encapsulated in Titanium and with small heat generation characteristics $< 10W$. [63]

Analysis of Actuation Methods

- **Piezoelectric Motors :** Offer high precision and quick response times, providing frictionless operation that is ideal where micro precision is critical. However, they are limited by stroke length and require high operational voltages, which could complicate integration. [59], [64]
- **Voice Coils:** By using Lorentz force, voice coils provide seamless, contactless operation suitable for applications needing bigger displacement ranges. While they can offer smooth motion and avoid wear, they may necessitate additional considerations for cooling and electromagnetic interference (EMI) shielding.[63]
- **Magnetic Levitation (Maglev) :** Actuation through magnetic fields offers advantages such as zero contact and the elimination of lubrication needs. However, the complexity and cost associated with control systems and power requirements can be limiting factors.[65]
- **Shape Memory Alloys (SMA) :** SMAs offer compact design potential and silent operation but can suffer from slower response times. They are also often criticized for thermal hysteresis and particle shedding. Their compactness and suitability for space constrained automation offers advantages. The primary challenges heat generation and material degradation can be mitigated through thermal encapsulation (For example silicone sleeves) and high cycle life alloys like NiTiCu. [66]

2.4.6. Production Methods

The manufacturing of CM's requires careful selection of production methods to meet both functional requirements (precision, fatigue resistance) and aseptic regulatory constraints (surface roughness). Table 2.7 shows an overview of the most common production techniques, their impact on material properties, and their suitability for aseptic pharmaceutical applications. From this table it can be concluded that the decision for production technique will be highly depended on the application of the specific component and therefore a standard solution can not be recommended but should be evaluated on case basses to get the most effective solution. However from an implementation standpoint CNC Machining will be the easiest and could therefore be seen as an initial starting point when evaluating options [3].

2.4.7. Research Gap

Existing studies on compliant mechanisms (CMs), including "Achieving near-zero particle generation by simplicity of design—A compliant-mechanism-based gripper for clean-room environments" (Budde et al. (2024) [55]), validate their ability to reduce particle emissions by eliminating joints and friction. However, translating these benefits to pharmaceutical aseptic production remains under explored.

Key gaps include:

- Dynamic Performance : Pharmaceutical grippers operate at high frequencies (300+ cycles/minute) under cyclic sterilization, necessitating fatigue studies on materials like PEEK or 316L stainless steel.
- Microbial Retention : No research optimizes CM surface topologies to prevent biofilm formation in micro-crevices, despite EU GMP Annex 1's cleanability mandates.
- Airflow Compliance : ISO 14644-1 [18] mandates laminar airflow (0.45–0.55 m/s), yet no studies integrate CFD with CM motion to quantify turbulence in isolators.
- Regulatory Alignment : Current CM designs lack validation against GMP protocols, creating a disconnect between mechanical innovation and pharmaceutical compliance.

In summary, while CMs reduce particle generation, their adoption in aseptic production demands interdisciplinary research to address sterilization durability, dynamic fatigue, regulatory integration, and manufacturability bridging the gap between cleanroom principles and pharmaceutical grade compliance.

2.5. Discussion

2.5.1. Fatigue life

Although fatigue life of the different materials is discussed and the effect of sterilization methods is also taken into account it should be noted that the fatigue life behaviour

Table 2.6: Actuation Methods for Compliant Mechanisms in Aseptic Applications

Method	Principle	Force Range	Displacement	Advantages	Limitations
Piezoelectric	Voltage-induced deformation	50–1000 N	10–200 µm	- Zero friction - Sub-µm precision - Fast response	- Limited stroke - High voltage (60–150 V) - Hysteresis
Voice Coil	Lorentz force-driven motion	1–50 N	±5–20 mm	- Contactless - Smooth motion - No wear	- Requires cooling - Moderate force - EMI shielding
Maglev	Magnetic field levitation	0.1–10 N	±1–10 mm	- Zero contact - No lubrication - Scalable	- Complex control - High power - Costly
Pneumatic	Compressed air-driven	5–100 N	10–300% strain	- Low particle risk - High compliance - Simple design	- Sterile air required - Slow response - Hysteresis
SMA	Thermal phase change	0.1–5 N	2–8% strain	- Compact - Silent - Direct drive	- Slow cooling - Low efficiency - Fatigue

Table 2.7: Production Methods for Compliant Mechanisms [3]

Method	Process	Materials	Surface Roughness (Ra µm)	Advantages	Limitations
Additive Manufacturing	Layer-by-layer fabrication: - SLA - SLS - DMLS	- Polymers: PEEK - Metals: 316L stainless steel, titanium	0.5–15	- Complex geometries - Monolithic designs - Rapid prototyping	- Residual stresses - Requires post-processing (polishing) - Limited to small batches
CNC Machining	Subtractive: - Milling - Turning	- Stainless steel 316L - Aluminum - PEEK - PTFE	0.4–3.2 (polishable to ≤0.4)	- High dimensional accuracy - Biocompatible finishes - Excellent material properties	- Geometric constraints (undercuts) - Tool marks trap particles if unpolished
Injection Molding	Molten material in mirror-finish molds	- PEEK - PTFE - Medical-grade silicones	0.1–0.8	- Smooth surfaces - Scalability - No post-processing	- High tooling costs - Limited to high volumes - Low design flexibility
Laser Cutting/Etching	Precision laser ablation	- Thin stainless steel sheets - Polyimide	0.8–2.5 (deburring required)	- Fine features - Rapid prototyping - Low cost	- Thermal stress alters properties - 2.5D geometries only

of materials could be significantly effect by the combination of the rigorous sterilization and continues loading cycles. For instance, PEEK's glass transition temperature (143°C) lies close to autoclave conditions (121–134°C), potentially accelerating stress relaxation during repeated sterilization cycles. Similarly, 316L stainless steel, while robust against steam, may develop stress corrosion cracks under chloride-rich CIP agents when subjected to cyclic flexural loads. Future studies should implement accelerated aging protocols, combining 10,000+ load cycles with weekly autoclave exposure. Real time particle monitoring during these tests could correlate material degradation with USP <788> particulate thresholds, bridging mechanical failure modes to contamination risks.

2.5.2. Scalability of Additive Manufacturing

AM's layer by layer process creates micro-crevices (even post polishing) that could harbor biofilms. How does this compare to CNC machined surfaces in microbial retention studies? For large scale production, it could mean that AM's residual stresses and batch variability require 100% inspection, increasing costs.

2.5.3. Design Methodology

In this review there has mostly been looked at using a PRBM model in combination with FEM or topology optimization as design methodologies for the CM. The choice to mostly focus in on these two was made as these where used in similar CMs design synthesis covered in the PRISMA guided literature search. As such it was deemed that they where the most relevant. However there are other options available that could be used, which in the future might be interesting to research further.

2.5.4. Actuation Challenges

Choosing an appropriate actuation method for compliant mechanisms in aseptic environments is crucial to minimizing particle generation. While this study identified promis-

ing actuation technologies such as piezoelectric, maglev, and voice coil actuation, each has trade-offs in terms of power efficiency, precision, and integration complexity. Future studies should conduct experimental validations to determine the most effective actuation strategies for specific aseptic applications.

2.5.5. Material Constraints

While this study identified materials that meet regulatory requirements for aseptic environments, additional materials may be viable but were not considered within the scope of this research. Future work should explore alternative materials, to expand design possibilities while maintaining compliance with sterilization requirements.

2.5.6. Risk Mangament

While this study provides an insight in the design requirements needed to design an aseptic gripper, to get it approved for this strict industry there are a lot of risk management steps that should be followed. Due to the focus of this study on the mechanical design this was not encoperated opon but should be considered when implementing such a solution in real production lines. Especially with the risks with fatigue life of compliant mechanisms which needs to be properly verified.

2.5.7. Production Method

While a comprehensive overview of the different production methods and there subsequent advantages and disadvantages has been composed. There are still more different production methods possible and based on the design requirements of a specific mechanism it could be relevant to research literature more specifically.

2.5.8. Regulatory rules

This study mostly focusses on the European and American regulations. However based on the region a system is implemented there could be alternative or supplementary rules which should be considered.

2.6. Conclusion

This systematic review demonstrates that CMs hold great potential for aseptic pharmaceutical manufacturing, addressing critical contamination risks inherent to traditional rigid-body systems. By synthesizing insights from cryogenics, aerospace, and cleanroom robotics, this study establishes a design framework tailored to Grade A environments, where particle generation, sterilization resilience, and laminar airflow compliance are crucial.

The PRISMA-guided analysis of 214 studies shows the superiority of monolithic CM designs in eliminating friction-induced particles and biofilm-prone crevices. Material validation identifies PEEK and 316L stainless steel as optimal candidates, balancing autoclave resistance (121°C, 15 psi) with fatigue performance under cyclic loading. Topology optimization emerges as a promising methodology, allowing geometries to minimize turbulence while adhering to cleanability constraints (radii $>$ 3 mm, Ra $0.8\mu m$). Actuation integration, particularly voice coil systems, proves critical for frictionless operation, reducing emissions to $<$ 1,200 particles/m³ needed to comply with ISO 14644-1 Class 5 thresholds.

The proposed roadmap (See Appendix 2.6.4) bridges regulatory gaps by aligning CM validation with EU GMP Annex 1 and FDA 21 CFR 211.67, advocating for riboflavin coverage testing, accelerated aging protocols, and USP $<$ 788 $>$ particulate monitoring. By eliminating multi-component assemblies, CMs reduce CIP/SIP complexity, cutting maintenance downtime.

Future work must prioritize prototyping (a table with proposed design requirements can be found in Appendix H) and lifecycle testing under GMP conditions, with emphasis on dynamic fatigue behavior of PEEK flexures and long-term VHP compatibility. This research shows that CMs are not just incremental improvements but can be enablers for future ”zero-particle” pharmaceutical production, aligning mechanical innovation with patient safety.

Acknowledgements

I would like to thank dr. F.G.J. (Freek) Broeren from the department of Precision and Microsystems Engineering at TU Delft and Stienen, dr.ir. A.H.A. (Arno) from the department of Biomechatronics & Human-machine Control for their valuable feedback and guidance. I also would like to thank NVAI (Nicolo Vacchi) Advanced Mechanical Engineer at Novo Nordisk for his valuable guidance and feedback.

APPENDIX A : The Aseptic Pharmaceutical Industry

The aseptic pharmaceutical industry is a specialized sector dedicated to the production of sterile medicinal products, including injectables and vaccines, which are administered directly into the human body. Unlike non-sterile pharmaceuticals, these products cannot undergo terminal sterilization (autoclaving) after final packaging due to the sensitivity of their active ingredients, such as proteins or mRNA, to heat, radiation, or chemical agents. Therefore, aseptic manufacturing relies on the assembly of presterilized components (vials, stoppers, syringes) within controlled environments designed to prevent microbial or particle contamination during production. [36], [27]

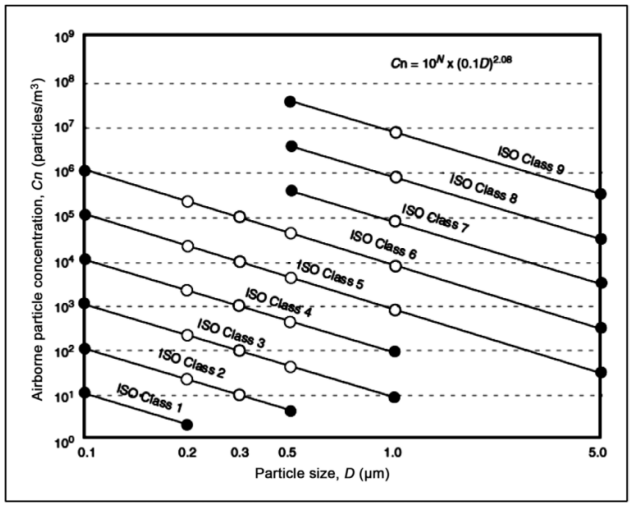

Figure 2.8: ISO class concentration limits for the clean-room, specificity ISO class 5 is relevant as that corresponds to the current concentration limit allowed for Grade A areas. Image from Prabu et al. (2017) [67]

2.6.1. Isolators

Isolators are central for current aseptic production. An isolator is a closed system engineered to maintain sterility by physically separating it from operators. Constructed from stainless steel or rigid polymers, isolators integrate advanced filtration and sterilization systems to achieve ISO Class 5 (Grade A) [9] conditions, where particle counts are limited to $3,520$ particles $(0.5m)$ per cubic meter; see Figure 2.8 for a visualization of the different ISO classes and their respective particle limits.

Isolators operate under unidirectional airflow (UDAF), where HEPA filtered air flows uniformly at 0.45–0.55 m/s to sweep contaminants away from product exposure zones. While automated decontamination methods such as vaporized hydrogen peroxide (VHP) or chlorine dioxide gas are primary sterilization tools, operators also perform supplementary cleaning via glove ports integrated into the isolator walls. Using sterile wipes soaked in cleaning agents (such as hydrogen peroxide, sodium hypochlorite), personnel manually clean surfaces, seals, and equipment within the isolator. This process adheres to strict standard operating procedures (SOPs) to prevent contamination, including:

Aseptic technique training: Operators practice glove port maneuvers in simulated environments to avoid compromising isolator integrity.

Real time particle monitoring: Sensors trigger alerts if particle counts exceed ISO Class 5 thresholds during cleaning.

Post cleaning validation : Surfaces are swabbed and tested for microbial recovery to ensure efficiency.

While robotic automation is increasingly replacing manual tasks, human intervention remains necessary for complex maintenance or localized contamination events. This hybrid approach balances the sterility benefits of isolators with the flexibility required in dynamic production environments. Material transfer occurs through rapid transfer ports (RTPs) or autoclaves, ensuring sterile components enter without breaching the system. Robotic manipulators or glove ports enable human interaction while minimizing contamination risks.

2.6.2. Regulations

Aseptic manufacturing needs to follow strict regulations to ensure patient safety a few of them are:

EU GMP Annex 1 (2022) [7]: Mandates Grade A zones for high risk operations (vial filling), continuous environmental monitoring, and validation of sterilization processes through media fills simulated production runs using microbial growth media.[8] FDA 21 CFR Parts 210/211 [30] : Requires materials in contact with sterile products to be non-reactive, non-shedding, and resistant to degradation from repeated sterilization. ISO 14644 Series [17], [18]: Defines cleanroom classifications, airflow testing protocols, and particle count thresholds.

2.6.3. Operational Challenges

The industry faces challenges, including human operator contamination risks, which remain a primary source of contamination despite protective clothing. Mechanical systems with sliding joints or lubricated parts also have the risk of generating particles during operation. In addition, materials must endure aggressive sterilization methods, such as autoclaving (121°C, 15 psi) or VHP cycles, without warping, leaching, or losing structural integrity. Validating isolator systems requires 6–12 months of rigorous testing, including smoke studies, particle monitoring, and microbial air sampling, to comply with regulatory standards.[23]

2.6.4. Summary

The aseptic pharmaceutical industry operates under strict sterility requirements to safeguard patients. Isolators, advanced filtration systems, and robotic automation collectively address contamination risks, yet challenges persist in balancing operational efficiency with regulatory compli-

ance. This shows the necessity for continuous innovation in materials, processes, and infrastructure to meet evolving demands of sterile drug production.

APPENDIX B : Terms

- ASME - American Society of Mechanical Engineers
- BPE - Bioprocessing Equipment (ASME BPE standard)
- CFD - Computational Fluid Dynamics
- CIP - Clean In Place
- COP - Clean Out of Place
- EC - Eligibility Criteria (e.g., EC1-EC4)
- EMA - European Medicines Agency
- EU GMP - European Union Good Manufacturing Practice
- FDA - Food and Drug Administration
- HEPA - High-Efficiency Particulate Air filter
- ISO - International Organization for Standardization
- PAO - Polyalphaolefin (used in particle testing)
- PEEK - Polyether Ether Ketone
- PEG - Polyethylene Glycol (used in smoke studies)
- PRISMA - Preferred Reporting Items for Systematic Reviews and Meta-Analyses
- PSL - Polystyrene Latex
- PTFE - Polytetrafluoroethylene
- RA - Roughness Average
- SIP - Sterilize In Place
- UDAF - Unidirectional Airflow
- USP - United States Pharmacopeia
- W&S - Wash and Sterilization
- WIP - Wash In Place
- AM - Additive Manufacturing
- BI - Biological Indicators
- CAD - Computer Aided Design
- CFU - Colony Forming Unit
- CI - Chemical Indicators
- CM - Compliant Mechanism
- CNC - Computer Numerical Control
- DMLS - Direct Metal Laser Sintering
- EAP - Electroactive Polymer
- EMI - Electromagnetic Interference
- EO - Ethylene Oxide
- EPDM - Ethylene Propylene Diene Monomer
- FEA - Finite Element Analysis
- GA - Geometric Advantage
- MEMS - Micro-Electro-Mechanical Systems
- MIR - Minimum Invasive Robotics
- PA - Polyamide
- PC - Polycarbonate
- PETP - Polyethylene Terephthalate
- POM - Polyoxymethylene
- PP - Polypropylene
- PRBM - Pseudo-Rigid Body Model
- PSM - Point-Spring Model
- PU - Polyurethane
- RBR - Rigid-Body Replacement
- RTP - Rapid Transfer Ports
- SLA - Stereolithography
- SLS - Selective Laser Sintering
- SMA - Shape Memory Alloys
- SMP - Shape-Memory Polymers
- SOP - Standard Operating Procedures
- SS - Stainless Steel
- UV - Ultraviolet
- VCA - Voice Coil Actuator
- VHP - Vaporized Hydrogen Peroxide
- VOC - Volatile Organic Compounds

APPENDIX C: Planning

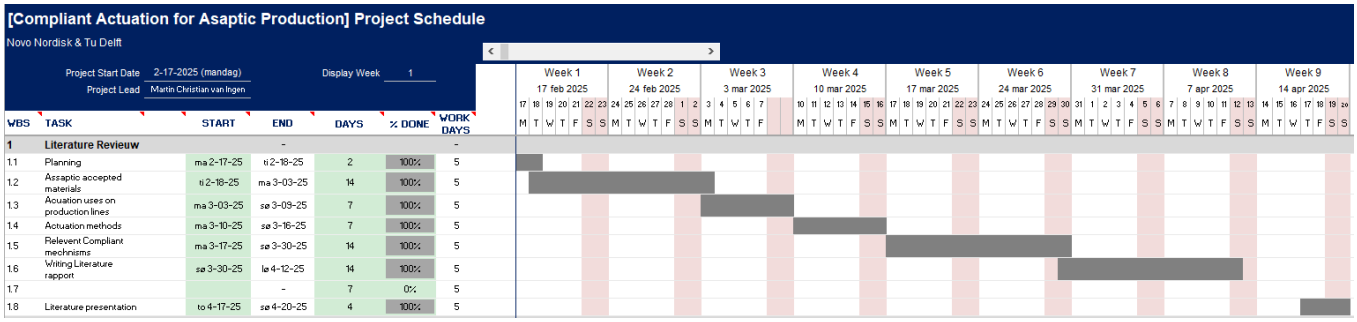

WBS	TASK	START	END	DAYS	% DONE	WORK DAYS
1	Literature Revieuw		-			-
1.1	Planning	ma 2-17-25	ti 2-18-25	2	100%	5
1.2	Asaptic accepted materials	ti 2-18-25	ma 3-03-25	14	100%	5
1.3	Acuation uses on production lines	ma 3-03-25	sø 3-09-25	7	100%	5
1.4	Actuation methods	ma 3-10-25	sø 3-16-25	7	100%	5
1.5	Relevent Compliant mechnisms	ma 3-17-25	sø 3-30-25	14	100%	5
1.6	Writing Literature rapport	sø 3-30-25	lø 4-12-25	14	100%	5
1.7			-	7	0%	5
1.8	Literature presentation	to 4-17-25	sø 4-20-25	4	100%	5

Figure 2.9: Planning for the Literature Study

APPENDIX D: Application Possibilities Compliant Mechanisms

This appendix shows the different application possibilities for compliant mechanisms that are there in the aseptic industry filling lines. The application possibilities are divided in the three different groups.

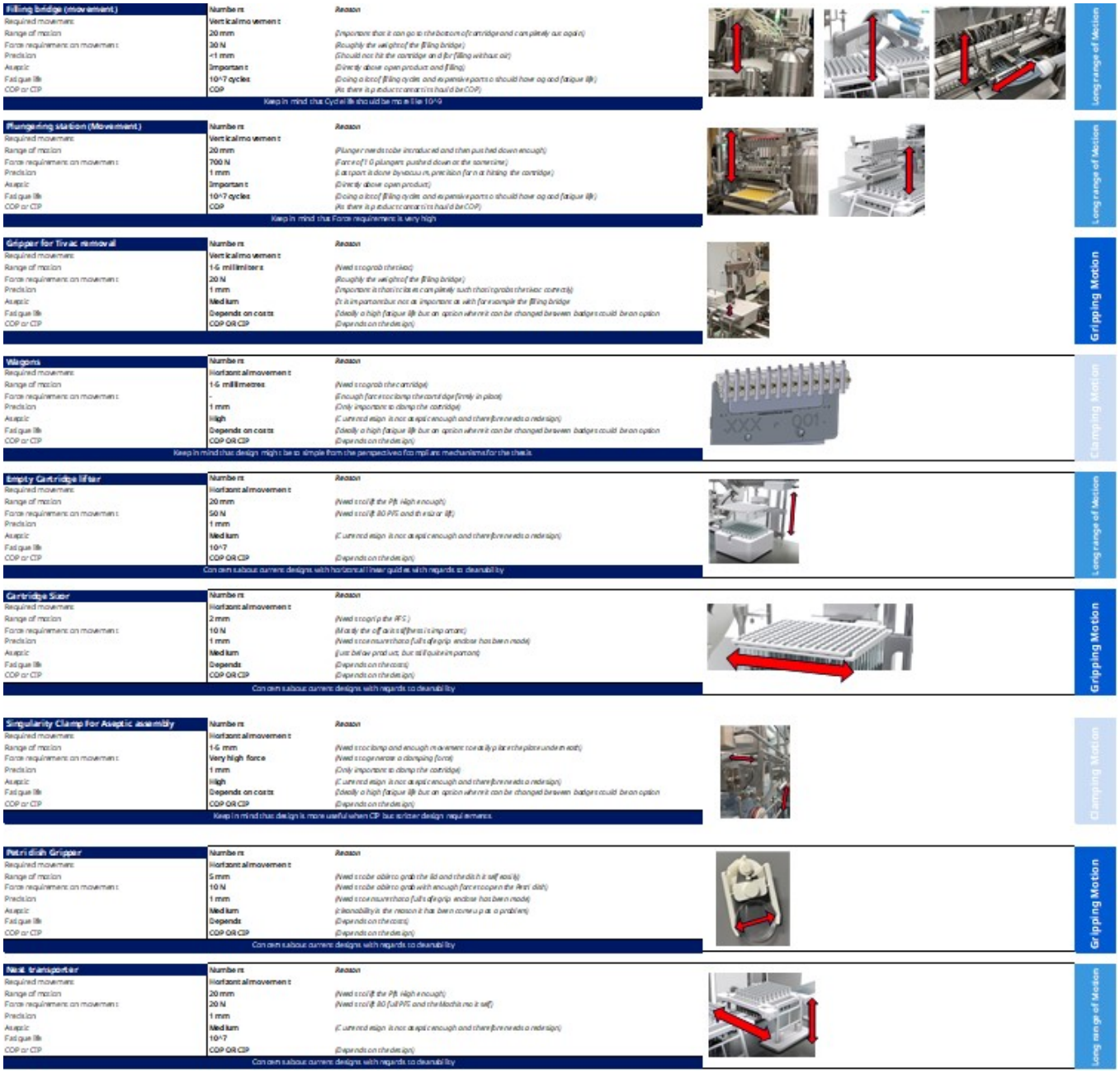

Figure 2.10: Revieuwd application possibilities for compliant mechanisms in lines at Novo Nordisk

APPENDIX E: Material Table

This table has been composed based on the requirements that materials are subjected to as described in section 2.3.1. The materials that are covered in this table are based on materials internally approved in Novo Nordisk as well as materials commonly used in the Industry. [41], [68], [69], [38], [43], [70], [71], [72]

Material	Biocompatibility Certification	Particle Emission Risk	Thermal Stability	Chemical Resistance	Sterilization Methods	Mechanical Notes	Key Restrictions
Stainless Steel 316L (EN 1.4404)	ISO 5832-1:2024, USP Class VI	Low (if polished)	Stable to 400°C	High (resists acids, bases, solvents)	Autoclave, Gamma, CIP, VHP	High fatigue strength, rigid	Avoid abrasive cleaning (risk of pitting)
Super Duplex (EN 1.4410/SAF2507)	ASTM A182, NACE MR0175	Low	Stable to 300°C	Exceptional (chloride resistance)	Autoclave, Gamma	High strength, corrosion resistant	Cost prohibitive for small mechanisms
Titanium Grade 5	ISO 5832-3 (surgical implants), ISO 10993-1, ASTM F136	Low (if polished)	Stable to 300°C (continuous), 600°C (short-term)	Excellent (chlorides, saline, oxidizing acids); Poor (reducing acids like HCl)	Autoclave, Gamma, VHP, EtO, IPA	High strength to weight ratio, fatigue resistant	Galvanic pairs (e.g., with steel)
Anodized Aluminium (AW5083/6082)	ISO 7583, FDA 21 CFR §177.1460	Moderate (anodized layer)	Stable to 150°C	Moderate (sensitive to strong bases)	Chemical (H_2O_2), EO	Lightweight, moderate strength	Not for fluid contact; anodization degrades with steam
Bronze (Non-External)	ASTM B584, FDA 21 CFR §175.300	High (if uncoated)	Stable to 230°C	Poor (oxidizes in moisture)	Chemical wipe (ethanol)	High wear resistance	Restricted to internal, dry areas; copper leaching risk
PEEK	ISO 10993-1, USP Class VI	Very Low	Stable to 250°C (short term)	Excellent (except chlorine)	Autoclave, Gamma, EO, VHP	High stiffness, low creep	Avoid chlorine-based cleaners
PTFE (Teflon)	USP Class VI, FDA 21 CFR §177.1550	Low	Stable to 260°C	Exceptional (inert)	Gamma, EO	Low friction, cold flow issues	Avoid high-stress dynamic applications
Nylon (PA)	FDA 21 CFR §177.1500, ISO 10993-10	Moderate (hygroscopic)	Stable to 100°C	Moderate (hydrolysis risk)	EO, Chemical	Flexible, wear-resistant	Avoid humid environments; absorbs moisture
PU (Polyurethane)	USP Class VI, ISO 10993-3	Moderate (degradation)	Stable to 80°C	Poor (UV/ozone degradation)	EO, H_2O_2 Plasma	Highly flexible, variable hardness	Medical grade only; avoid prolonged UV exposure
PC (Polycarbonate)	FDA 21 CFR §177.1580, ISO 10993-1	Low	Stable to 135°C	Moderate (sensitive to alkalis)	Gamma, EO	Impact resistant, transparent	Stress cracks with alkalis
PP (Polypropylene)	USP Class VI, FDA 21 CFR §177.1520	Low	Stable to 100°C	High (chemically inert)	EO, Autoclave (limited)	Low cost, lightweight	Poor fatigue resistance; not for cyclic loading
EPDM	FDA 21 CFR §177.2600, ISO 10993-1	Moderate (porous surface)	Stable to 120°C	Poor (hydrocarbons, oils)	Peroxide based chemicals	Elastic, good sealing properties	Limited to static seals; avoid dynamic friction

APPENDIX F: Flow chart

To make it easier to understand the connection between the different parts of the material covered in this literature review a flow chart has been composed. This flow chart should be used as guidance to understand the main steps in developing a compliant mechanism in the aseptic environment but should not be seen as a stand alone document.

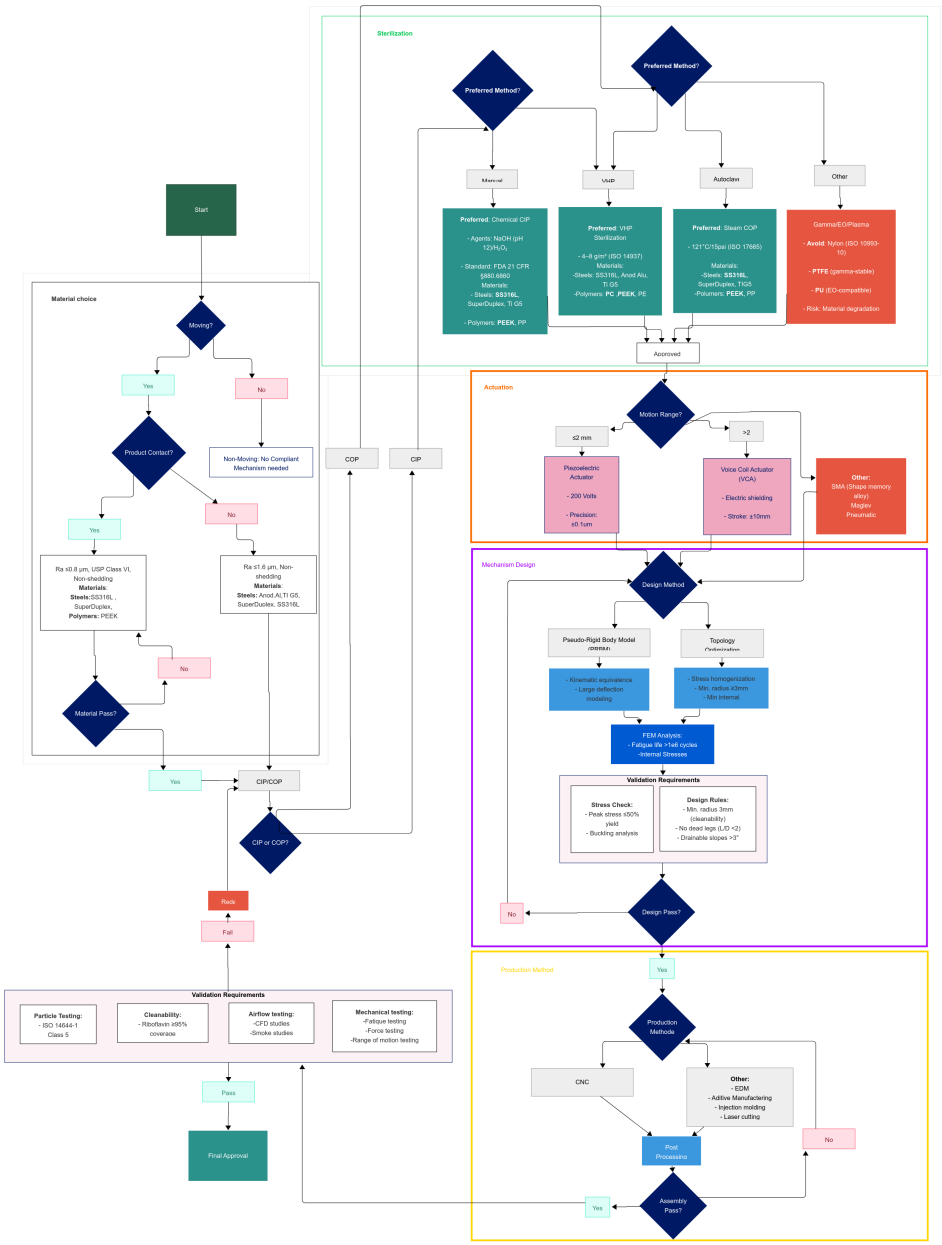

Figure 2.11: Flow chart visualizing the different steps that need to be followed to synthesis a compliant gripper of an grade A environment

APPENDIX G: Scoring Tables for the Selection Procedures

Table 2.8: Material Properties for Aseptic Applications. This table is used to make the decision graph for the material selection. The table has been made based on the information gathered in section 2.3.1 and Appendix E

Material	Particle Risk	Thermal	Chemical	Fatigue	Cost	Manufact.	Bio-compat.	Abrasion	W/S Ratio
SS	9	9	9	9	6	7	10	9	6
SD	9	8	10	9	4	5	9	9	7
Ti Grade 5	9	8	10	10	2	4	10	10	10
AA	6	6	7	7	7	8	8	7	8
Bronze	5	6	4	5	8	9	5	4	5
PEEK	10	8	9	9	4	6	10	8	8
PTFE	8	7	10	7	5	6	9	5	7
PA	6	5	8	6	9	9	7	6	7
PU	5	4	4	3	8	8	6	5	6
PC	4	6	6	5	7	8	7	5	7
PP	4	5	10	7	9	9	8	4	7
EPDM	5	6	3	3	8	7	5	3	5
PETP	7	7	8	7	6	7	8	6	7
POM	6	7	8	8	7	8	7	7	7
Silicone	5	9	9	8	6	6	9	3	6

Table 2.9: Actuation Mechanism Properties for Aseptic Applications. This table is used to make the decision graph for the actuation selection. The table has been made based on the information gathered in section 2.4.3, 2.4.5

Name	Friction	Voltage	Motion Range	Force	Aseptic	Cycles
Piezo	9	6	6	10	9	9
SMA	9	8	6	5	8	7
Electrostatic Adhesion	10	6	4	5	4	8
Pneumatic	6	10	8	10	5	9
Electromagnetic	8	8	8	8	7	9
Hydrostatic	6	9	8	10	5	9
EAP	3	2	5	5	4	6
VCA	9	7	9	8	8	10
Thermal Expansion	10	7	6	3	7	6

Table 2.10: Compliant mechanisms scoring table. The scores are based on the data from Appendix D. The dark gray column ” Complexity Compliant mechanism” is composed of the three dark gray columns on the right

Application Area	Complexity Compliant mechanism	Actuation Complexity	Cleanability Importance	Number of Cycles
Filling bridge (movement)	4	4	4	5
Plungering station (Movement)	5	5	3	5
Gripper for Tivac removal	3	4	4	3
Wagons	2	2	5	4
Empty Cartridge lifter	4	4	4	3
Cartridge Sizor	2	2	5	3
Nest transporter	4	1	3	4
Singularity Clamp For Aseptic assembly	3	1	4	1

Force	Movement range	Precision	Complexity Compliant mechanism
3	4	5	4
5	4	3	5
3	1	5	3
1	1	3	2
2	4	2	4
1	2	3	2
4	4	3	4
5	2	2	3

APPENDIX H: Design Requirements Compliant Gripper Aseptic Industry

This table shows the design requirements for a compliant gripper in aseptic production based on the information discussed in this paper. For each requirement a short description is given and if the requirement is a wish or a demand.

Table 2.11: Design Requirements for Aseptic Handling System

Requirement	Value	Description	Demand/Wish
Aseptic class	Grade A/ISO 5	Required air quality in isolator-based filling lines per regulations	D
Maximum Dimension	250×250×250 mm	Rough size estimation based on robotic handling arm	W
Maximum Weight	5 kg	Operator handling limit (lower preferred)	D
Force per finger	6 N	Required force for petri dish handling	W
VHP resistance	30%	Steam-in-Place cleaning requirement	D
Interface	Linear input	Force compatibility with VCA actuator	D
Cycles	$> 10^7$	Minimum industry-standard lifecycle	W
Cycle time	5 s	Minimum interesting duration (faster preferred)	W
Heat resistance	>120C	Autoclaving sterilization requirement	D

3

Design Process

The design process of the compliant flexure based gripping mechanism for application in a Grade A aseptic environment followed a systematic, iterative approach. This section describes the progression from the initial concept development to the final optimized design, highlighting key design decisions, challenges, and methods used. The design process was divided into distinct phases: initial evaluation and problem framing, actuator selection, development of a linear guide support system, design and modelling of the gripping mechanism, and development of an aseptic compatible bayonet lock for modularity and cleanability.

3.1. Initial Evaluation and Problem Framing

The study began in chapter 2 with the identification of the fundamental requirements and constraints based on specifications for Grade A aseptic environments as outlined in EU GPM ANNEX 1 (2022) [7]. These environments require ultra-clean operation where contamination risks from particle generation and surface residues must be minimized. With this in mind, the primary functional goal of the mechanism was defined as **enabling a secure, precise grip** on small, sensitive components while **preserving sterility and cleanliness**.

3.1.1. Design Requirements Compliant Gripper

The requirements were broken down into primary and secondary objectives:

Primary Objectives:

1. Develop a gripping mechanism that applies sufficient force to securely hold objects between 5-10 mm in size (e.g. cartridges, vials, and Petri dish, etc.).
2. Eliminate traditional rigid-body joints to prevent sources of contamination, such as lubricant usage or wear-induced particles.
3. Retain operational performance in harsh sterilization conditions such as autoclaving or exposure to aggressive cleaning agents.

Secondary Objectives:

1. Ensure Compatibility with Clean-In-Place (CIP) or Clean-Out-of-Place (COP) procedures.
2. Minimize overall size and weight for integration with industrial robotics.
3. Reduce number of parts and complexity to enhance manufacturability and reliability.

3.1.2. Design Phases and Building Blocks

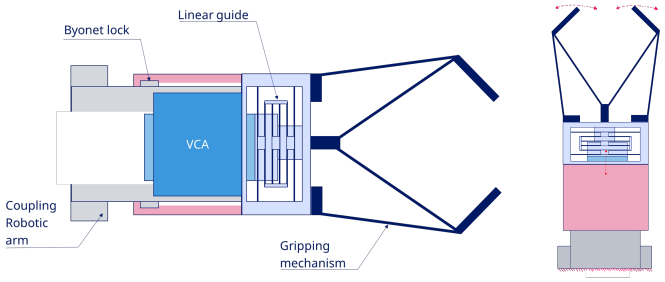

Figure 3.1: Design of the full Compliant gripper mechanism with the different building blocks indicated.

The design phase was divided into a set of building blocks, each of which was introduced to meet a specific functional requirement or regulatory constraint for the operation in Grade A aseptic environments, the different building blocks can be seen in figure 3.1 . After the problem framing, these blocks defined the design progress.

At the core sits the actuator module. Its role is fundamental: it supplies the primary, controllable input motion and force that the compliant mechanism must be designed around. In an aseptic setting the actuator cannot be chosen on performance alone; it must avoid sliding seals, lubricants and other features that generate particles or create crevices that trap contaminants. The actuator establishes the boundary conditions such as stroke, peak force and design envelope that constrain design decision.

Closely coupled to the actuator is the linearguide mod-

ule. A voice coil or similar contact free actuator produces excellent axial motion but is vulnerable to off-axis deflection of the moving elements. The linear guide's purpose is to protect the actuator and ensure repeatable translation: it constrains radial and rotational degrees of freedom so that the moving coil or magnet cannot contact stationary parts, which would create wear debris or upset positioning.

The compliant gripper converts the actuator's central displacement into the controlled jaw motion needed to handle vials, cartridges and Petri dishes. This block exists to eliminate conventional joints and bearings that are difficult to clean, instead using monolithic flexures to transform and amplify motion. The gripper must therefore satisfy kinematic, force and cleanability requirements simultaneously: it must produce the required tip travel with low parasitic deflection, minimise stress concentrations that compromise lifespan, and avoid small cavities or discontinuities that would violate washability rules.

To enable rapid wash and sterilize cycles and safe tool changes, a modular locking sub-block provides a hygienic means of securing the mechanism. The locking concept must deliver constraint in all six degrees of freedom while avoiding sliding, threaded, or hinged interfaces that generate wear or trap contaminants.

3.2. Actuator Selection and Constraints Analysis

3.2.1. Actuation System Overview

One of the critical aspects of the design was the selection of the actuator to drive the gripping mechanism. The actuator had to meet the following criteria:

1. **Cleanliness:** Suitable for aseptic environments, avoiding risks of particle emissions or lubricant dependencies.
2. **Precision:** Ability to generate small, repeatable, and controllable displacements.
3. **Compactness:** Minimal size to allow ease of integration within robotic manipulators operating in confined cleanroom spaces.
4. **Output:** Force-to-displacement ratio to activate the gripper throughout its full range of motion.

3.2.2. Selection Process

In the literature study 2 several actuation methods were evaluated. The main candidates identified were:

- **Pneumatic Actuators:** Rejected due to the potential for contamination from leaks and increased system complexity (e.g., tubing and valve controls). [45]
- **Piezoelectric Actuators:** Found to lack sufficient range of motion and would require amplification mechanisms, increasing design complexity.[59], [64]
- **Voice Coil Actuators (VCA):** Selected for their inherent advantages: non-contact force generation, high precision, compact form factor, and suitability for particle-free environments.[65]

Based on the evaluation, it was determined to use a voice coil actuator for the actuation of the system.

3.2.3. Actuator Constraints

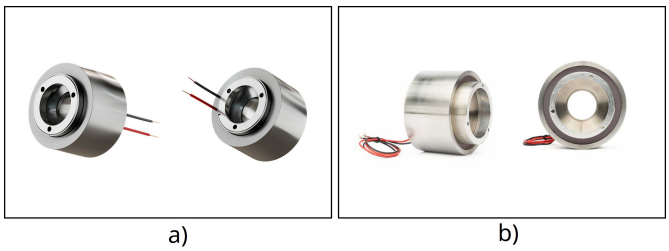

Figure 3.2: a) Shows the fully vacuum compatible version of VCA 5536 actuator by Magnetic Innovation, b) shows the same 5536 VCA actuator but not validated for vacuum use. Image from source [73]

based on the gripping mechanism's specifications the VCA minimum required operating parameters were determined to be the following:

- **Stroke:** Required a minimum displacement of 4 mm to grip objects within the target size range (5–10 mm).
- **Force:** Output force of at least 80 N was defined to ensure sufficient actuation force to deform the mechanism.
- **Envelope Dimensions:** Actuator dimensions were constrained to $< 100 \times 70 \times 70$ mm to meet size requirements.

After extensive research, the Vacum Actuator 5536 from the company Magnetic Innovation [73] was chosen see figure 3.2. For the full overview see Appendix D. This specific VCA was chosen as it offers the same certified model for cleanroom applications made of aseptically approved materials with the correct performance characteristics. For the prototype, the cheaper option that is not approved by vacuum was chosen; see Figure 3.2 b, as it has the same characteristics and dimensions. The only characteristics which are significantly different can be seen in figure 3.3. These are axial and radial passive attraction force between coil and moving magnet as a result of ferromagnetic steel being present in the design. As a result the axial force needs to be overcome when installing and disassembling and should thus be account for (this should not cause to significant issues as it is 40 N at each peak so within operator limits). The radial force needs to be accounted for in the positioning of the moving magnet as when this is deflected slightly a force will pull it towards the coil. However as the radial gap is only 0.5 mm this is 5 N at most and therefore should not cause problems.

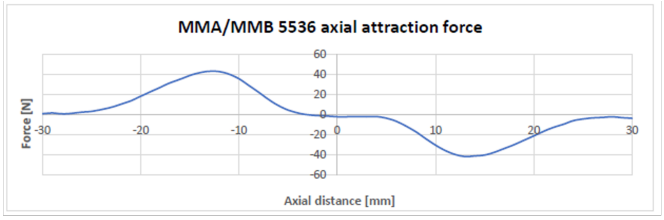

a)

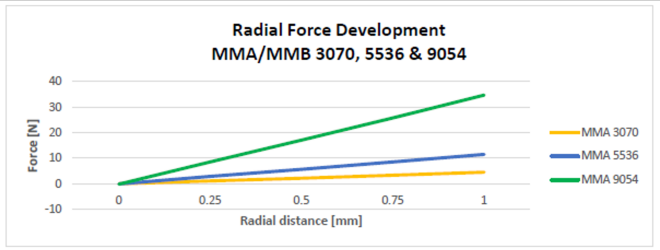

b)

Figure 3.3: a) Shows the passive axial force vs distance of the 5536 VCA actuator, b) shows radial of multiple VCA actuator including the chosen 5536 version. Graphs as supplied by MagneticInnovation[73].

3.2.4. Actuation Strategy: Passive Gripping with Active Release

The selection of the Voice Coil Actuator (VCA) and the strict requirements of aseptic manufacturing led to a passive actuation strategy for gripping with active opening and release. This approach is inspired by successful designs in [55] and addresses several critical operational considerations:

1. **Energy Efficiency and Thermal Management:** VCAs, while precise and contamination free, generate heat when continuously powered. By designing the gripper's neutral (unactuated) position to be slightly smaller than the object to be gripped, it maintains a secure grip passively, leveraging the compliance of the mechanism to generate the necessary gripping force. This eliminates the need for continuous actuation power during the gripping phase, significantly reducing heat generation and power consumption.
2. **Robustness Against Power Failure:** In a critical aseptic environment, maintaining control over pharmaceutical components is crucial. A passively gripping mechanism ensures that objects are not dropped in the event of a power outage, enhancing overall system safety and product integrity.
3. **Optimized for Repetitive Tasks:** Pharmaceutical isolator lines often involve repetitive handling of specific, well-defined objects (e.g., vials, cartridges, Petri dishes). This allows for precise optimization of the compliant mechanism's geometry such that its unactuated state provides the exact required gripping force, minimizing active control complexity.
4. **Operator Safety:** Unlike environments with human interaction, the enclosed nature of an isolator reduces direct safety concerns for personnel regarding a continuously forceful gripper. The primary goal shifts to product safety and process reliability.

While the primary gripping action is passive, the VCA is actively engaged to open the gripper, release objects, or to provide active force augmentation during gripping if higher or adjustable forces are temporarily required. This hybrid approach capitalizes on the VCA's precision for dynamic movements while optimizing for efficiency and reliability.

3.3. Development of the Linear Guide System

With the choice for a VCA as the actuation source for the mechanism, more requirements are added to the design of the compliant mechanism (CM). The resulting requirements are:

- The actuator provides a maximum input displacement of ± 4 mm, corresponding to a stroke range of 8 mm [73].
- Total VCA has a maximum of 140 N of actuation force [73]. However, the design should be designed for a maximum of 100 N, preferable even less to allow for some safety margin.
- The CM should support the permanent magnet and resist parasitic motion. such that there is no contact with the coil.
- The LGM should be as compact as possible.

These requirements make it almost inevitable to use a linear guide mechanism (LGM) in combination to the gripping mechanism (GM) such that the coil will be correctly supported. The compliant LGM will serves as a critical element in the overall GM, providing precise translational motion along the actuation (z) direction. The secondary function of the LGM is to resist off-axis deformation and ensure rotational stability, which are both critical for maintaining overall alignment during operation and ensuring no contact is made.

The design is influenced by principles described in key works, including:

- **A Long-Stroke Nanopositioning Stage With Annular Flexure Guides by Yang et al. (2021) [74]**: Provided the mathematical framework for analytical stiffness modeling using Castigliano's theorem and the two-port mechanical network method.
- **Design of a Cylindrical Compliant Linear Guide with Decoupling Parallelogram Mechanisms by Liu et al. (2022)[75]** : Inspiration for fully decoupled flexure-based guiding systems with symmetry to eliminate undesirable parasitic errors.
- **A 2-DOF nano-positioning scanner with novel compound decoupling-guiding mechanism by Wang et al. (2021) [76]** : Provided insights into

range-of-motion management with compound compliant mechanisms using additional sets of parallel leaf springs to improve stiffness and manage stress.

- **Flexure Systems based on a Symmetric Diaphragm Flexure by Awtar et al. (2005) [77]** : Investigates symmetric diaphragm designs using folded-beam pairs and curved-beam models to guide the design of monolithic, laser-cut linear guides with low parasitic rotation and tunable stiffness.

The design draws heavily from these works while adapting and improving upon their key ideas. Notably:

- An set of leaf flexures was removed (original 4 stacks reduced to 3 stacks) to balance rotational stiffness and ensure a large range of motion while maintaining the stress below the material yield strength.
- A minimum flexure thickness of 0.5 mm was imposed to satisfy the constraints of manufacturability given the limitations of 5-axis CNC machining. Increasing it from the requirement of 0.3 mm in [74]
- The double compound mechanism was extended to include a third flexure to form a Triple compound FPM to distribute the stresses more such that the yield stress is not exceeded. See figure 3.5

3.3.1. Structure of the Linear Guide System

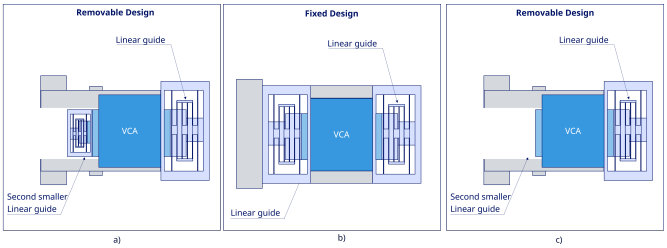

Figure 3.4: a) Double-sided LGM removable, b) Fixed double-sided LGM, c) Single-sided LGM

Different configurations for the LGM were initially considered. For instance, designs featuring two LGMs on both sides, as demonstrated in Yang et al. (2021) [74], offer robust support. However, such configurations introduce small, intricate geometries that are difficult to properly sterilize via manual Clean-In-Place (CIP). While Vaporized Hydrogen Peroxide (VHP) sterilization might be possible depending on the final design, it is not always sufficient for the strictest Grade A environments. This often leads to the need for removal possibility such that autoclaving is possible. Consequently, more complex multi-sided support structures were deemed impractical. This led to the evaluation of two primary design options: a linear guide with a big and small LGM on either side, and a single-sided LGM support see figure 3.4. Ultimately, the single-sided LGM support was chosen due to its inherent simplicity and ease of cleanability. This decision was further supported by the off-axis to axial stiffness ratios and the relatively small mass of the moving VCA components, suggesting that sufficient stability could be achieved with this simpler configuration.

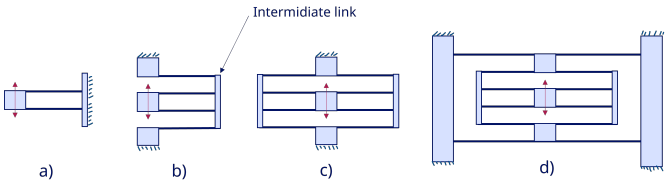

Figure 3.5: a) Conventional FPM, b) Compound FPM, c) Double compound FPM, d) Tripple compound FPM .Image Inspired by [74].

The LGM employs a flexure based design, specifically using symmetric parallel flexure guide mechanisms. Inspired by the curved double-compound flexure parallelogram mechanism (FPM) in [74] and the concept of decoupling parallelograms described in [76], this architecture achieves:

1. A high stiffness-to-compliance ratio for improved positioning precision.
2. Effective decoupling of translational motion in the z-direction from parasitic motion.
3. A compact form factor for better integration with the VCA.

The chosen final structure consists of three double-compound FPM stacks in parallel (rather than four) to address the smaller radius and prevent the flexures from being undesirably thin. To accomplish this without exceeding the material yield stress of Al-7075, the system was configured with three FPM stacks and an extra set of leaf flexures, inspired by the work presented in [76], where additional parallel elastic members were introduced to control stress distribution and ensure durability. For the optimized flexure design, Z was calculated to ensure $\sigma_{\text{max}} < \sigma_{\text{yield}}$ (503 MPa for Al-7075).

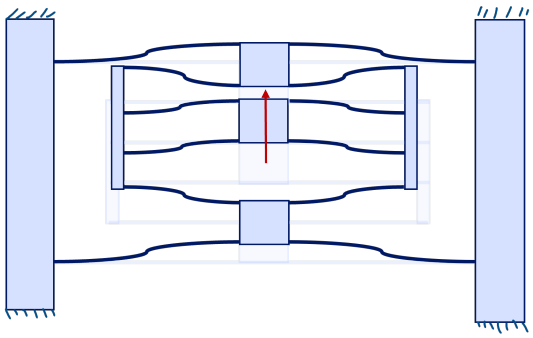

Figure 3.7: Deformation mode of the FPM

The deformation mode of a single FPM set for a axial load in z -direction can be seen in figure 3.7.

Effect of Fillets on Stiffness

Yang et al. (2021) [74] analytical model neglected fillets at flexure ends. These corner fillets improve cleanability and reduce local stress concentrations, but they also shorten the effective compliant span of each arc leaf and therefore increase stiffness. The magnitude of this trade-off depends on geometric ratios such as fillet radius to flexure thickness (R/h), fillet radius to arc length (R/Larc). Figure 3.8 compares the linear guide mechanism with and without fillets: the radiused transitions on the left visibly reduce the effective compliant length relative to the sharp baseline on the right. If fillets are ignored, analytical predictions and FEA can under estimate stiffness and over estimate peak stress relative to real life.

Li et al. (2021) [78] studied the effect of fillets on leaf flexures show the significance of fillet effects. They found that neglecting fillets produced compliance prediction errors up to 30–76 % in certain load cases, whereas models that include fillets match nonlinear FEA within about 3.5 % and experiments within about 10 %. They also found that peak stresses were reduced by roughly 33% at equal deflection compared to sharproot baselines [78].

The Li model depends on angle dependent integrals that grow strongly with span; even modest radii therefore yield a noticeable increase in motion stiffness once the shortened span is used in the element compliance.

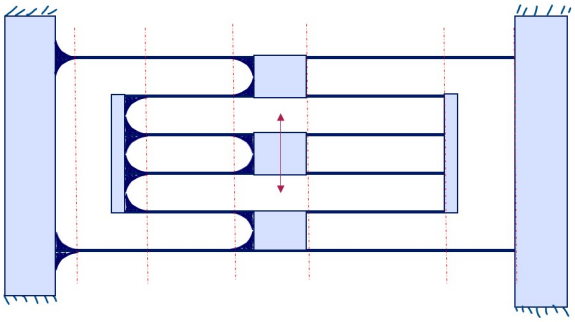

Figure 3.8: Visualization of effect of Fillets on leaf flectures ends on the effective length

3.3.2. Initial Numerical Validation

A 3D-printed prototype was tested to verify the motion behaviour. Because printed polymer properties are highly sensitive to process parameters (material grade, print speed, temperature, layer orientation, infill, and post-processing), the measured stiffness is not expected to match the model exactly. The print served only to confirm motion behaviour, clearances, and absence of parasitic binding. The force–displacement curve from analytical model and the 3D-print test are shown in Figure 3.9.

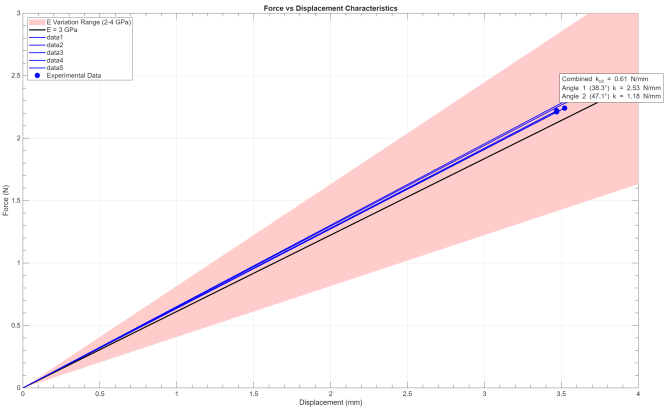

Figure 3.9: A test to verify the motion behaviour of the LGM by use of a 3D print and the Instron tensile testing machine [79]

3.4. Gripping Mechanism Design

The design of the gripping mechanism (GM) is fundamentally constrained by the requirements of the selected VCA and the subsequent designed LGM. This compliance based GM must provide precise and reliable motion to ensure safe handling of pharmaceutical components (e.g. vials, Petri-dish and cartridges) in aseptic environments. It should fulfil this while minimizing particle generation and meeting cleanability standards. In designing the GM, several functional and geometric constraints were identified, and different configurations were explored to determine the most suitable solution.

The GM must integrate seamlessly with the fixed geometry of the LGM and VCA. The design was informed by three key constraints. First, the mechanism must attach to fixed points located at an outer radius of 40 mm such that it can be mounted on the designed LGM. Second, it must accommodate a centralized input motion applied by the VCA at the centre, with a total stroke range of ± 4 mm (8 mm total input). Third, the mechanism must effectively translate this small, centralized input into a sufficient gripping motion at the output tips, which will interact with the objects being handled.

3.4.1. Evaluating Potential GM Configurations

To determine the optimal solution for the GM, various conceptual designs were modelled and analysed, each inspired by established linkage systems and the principles of the CM. The focus was on ensuring a balance between simplicity, manufacturability, and compliance with aseptic requirements while prioritizing precision and robustness.

The first consideration was related to the overall type of GM, specifically whether a two-fingered mechanism or a multi-fingered mechanism would be more suitable. While multi-fingered grippers provide greater adaptability for irregular or variable sized objects, they were deemed less suitable for this application due to their increased complexity and the challenges associated with cleaning and sterilization post-assembly. In contrast, a two-fingered mechanism is simpler, easier to clean, and more

tailored to the well defined geometries of objects commonly handled in aseptic pharmaceutical environments, such as Petri dishes or vials. As such, the two-fingered design was selected as the basis for further evaluation.

Finally, consideration was given to the use of a bi-stable mechanism. A bi-stable mechanism operates by snapping between two predefined states (open) and (closed) without requiring continuous actuation force, which would save energy during operation. While advantageous in terms of energy efficiency, this design was ultimately rejected due to its unsuitability for handling sensitive objects such as syringes and vials. The rapid snapping behaviour introduced the potential for damage to delicate pharmaceutical components, making it less desirable in this application [53].

Several specific configurations of two-fingered mechanisms were then considered to analyse their suitability. To better understand their motion behaviour and evaluate their performance, a motion generator (MotionGen [80]) for linkage systems was used to simulate and visualize their kinematics. Among the configurations considered, the following were evaluated extensively.

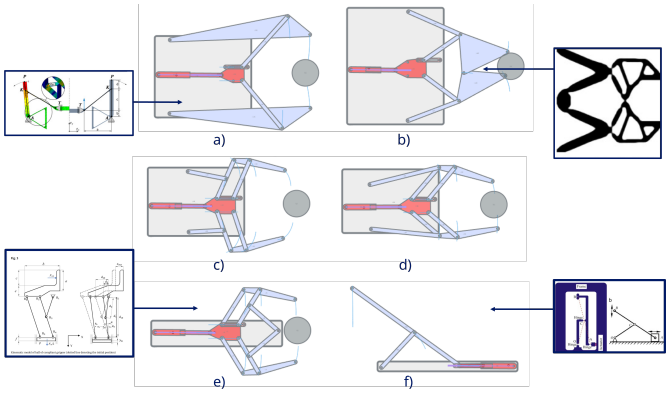

Figure 3.10: a) Simple 2 fingered design, b) Topology optimized inspired design, c) Different orientation of outward deflection resistant design d) Third option of outward deflection resistant design e)Double parallel linear path mechanism, f) Linear path generator)

- Linear-trajectory generators: predictable tip paths but sensitive to lateral deflection under asymmetric loads. Inspired by Zhu et al. (2020) [5].
- Outward-deflection-resistant linkages: improved lateral stability at the expense of geometric complexity and potential cleaning limitations. Zhu et al. (2020)[5].
- Topology-optimized linkages: mechanically efficient but possible drawback for cleaning due to intricate geometries and small cavities. And very high local stresses in one node hinges.[81]
- Simple two fingered design: Simple two finger design with only 3 hinge points, Inspired by the Budde et al. (2024) study [55].

After the analysis of these configurations, the symmetric flexure-based GM was selected as the basis for further development. Its design offered a balance of simplicity, precision, and compliance with aseptic handling requirements while minimizing complexity and ensuring modularity.

3.4.2. Optimization of the GM

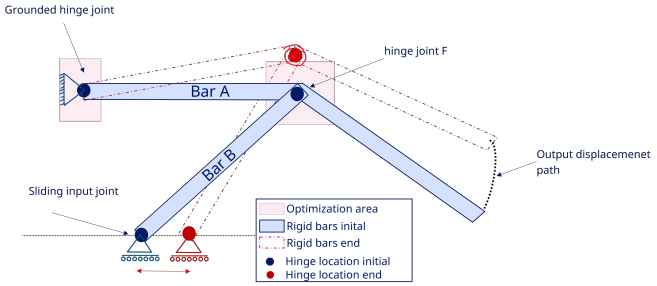

Figure 3.11: Design optimization of chosen design, by optimizing the hinge joint locations

The selected design was subsequently optimized to improve motion efficiency, maximize input-to-output displacement, and ensure uniform stress distribution across the structure. This optimization focused on the strategic placement of joints to fine-tune both the force amplification and the kinematic motion profile.

The first step in the optimization process involved identifying the variables that could be modified. In this design, each joint could be adjusted slightly in position to influence the overall motion behaviour and stress distribution. However, the degree of freedom for joint placement varied depending on functional constraints. For example, the sliding input joint was limited by the requirement to remain close to the x-axis to maintain symmetry and alignment with the VCA actuator. Similarly, the ground joint was constrained by its attachment to the linear guide system. In contrast, the final intermediate joint had greater flexibility for positional adjustment.

Using a simulation-based approach, the kinematic behaviour of the gripper was modelled for various joint configurations. Two key outputs were calculated for each configuration: the input-to-output displacement ratio and the angular deflections of each joint. The input-to-output displacement ratio provided insight into the efficiency of motion transfer, while the angular deflections highlighted potential points of high stress contributing to fatigue. This iterative optimization process aimed to balance these objectives.

The results of the simulations were visualized using Pareto plots, which allowed for identifying configurations that achieved an optimal balance between motion efficiency and stress minimization. Functional constraints, such as maintaining sufficient stiffness and avoiding excessive angular rotation at the joints, were used to limit the solution space. See Appendix B for the mathlab code used.

Chosen point: Ground Y = 5.0; F = (9.0, 5.8). This point is chosen based on the Pareto-knee behavior: The

Pareto plot shows a distinct knee at this region. Up to the knee, displacement ratio improves with relatively modest increases in angular deflection; past the knee, the curve steepens, small increases in amplification require disproportionately large increases in joint rotation. Given the primary objective to minimize angular deflection (to reduce hinge moments, stress concentration and fatigue) while obtaining high motion amplification, the knee represents the optimal compromise. Selecting a point beyond the knee would yield marginal gains in displacement ratio at the cost of substantially higher joint angles and associated risks (reduced stiffness, higher bearing loads, shorter life, and more demanding control).

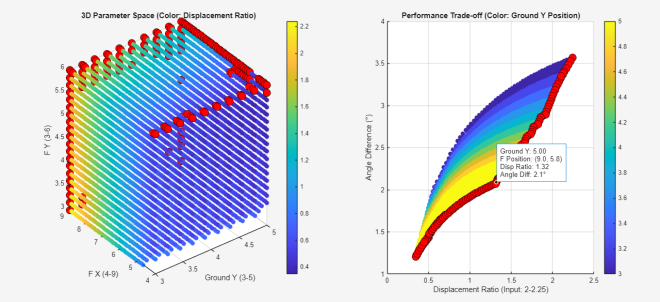

Figure 3.12: Pareto plot optimum for different joint locations with there respective input-output displacement relation and the angle difference.

3.5. Rotational locking mechanism

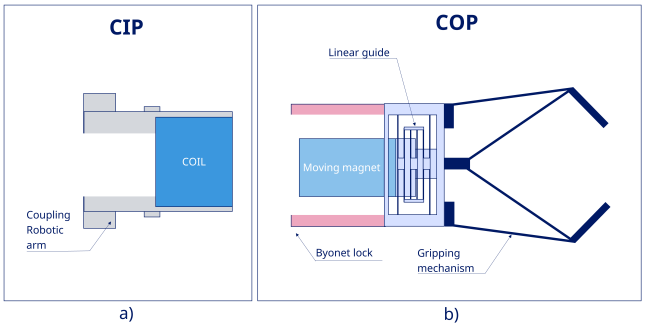

Figure 3.13: Design divided up in a) Clean in place parts b) clean out of place parts

For modular tooling in isolators, such as this mechanism, an aseptic locking mechanism is essential to enable rapid Wash and Sterilize (W&S) changeovers while maintaining Grade A/ISO 5 conditions [7] [16]. Threaded fasteners (screws) are increasingly discouraged because thread roots and blind pockets act as micro-crevices and “dead legs,” compromising cleanability during CIP [7]. Consequently, the locking concept should ideally be monolithic, hinge-less, and provide constraint of all six degrees of freedom (DOF), while remaining easy to engage using glove ports and compatible with CIP/SIP and autoclaving. In figure 3.13 the CIP and COP parts that need to be connected with this locking mechanism are visualized.

Design requirements derived from aseptic regulations and hygienic design

- Constraining in 6-DOF.
- sterility by design: Minium radius (R ≥ 3 mm), minimal internal cavities, and self-drainable surfaces (preferred slope ≥ 3°), with surface roughness Ra ≤ 0.8 µm. See literature report section 2.3.2.
- No hinges or lubricated joints.
- W&S compatibility: Access for flow paths and wiping during CIP; avoidance of dead legs (lengths greater than 3× the internal diameter) and stagnant zones and use of autoclave/VHP resistance materials see literature rapport section 2.3.2..

Options in literature and aseptic constraints

- Screws: Provide axial retention and anti-rotation via friction and thread geometry but create thread roots and blind holes that are difficult to clean, violate dead-leg guidance; therefore, they are being phased out for Grade A tooling.
- Bayonet/quarter-turn locks: Offer quick engagement. However, conventional bayonets use sliding contact across slots, which can create wear particles unless surfaces are fully polished and radiused; slot geometry must avoid sharp corners and must drain.
- Kinematic couplings: Three V-grooves mating with three ribs or spherical elements provide deterministic 6-DOF constraint with minimal contact area and repeatable positioning. Classical ball-vee designs introduce multi-part elements and cavities that can trap fluids; hygienic variants with shallow vee grooves and flush ribs in monolithic parts mitigate these risks if radiused and polished [82].
- Compliant snap-fits: Circumferential or tabbed snap features provide hinge-less, elastic engagement. Properly designed snaps can deliver axial retention and torsional detents without sliding joints. Stress concentrations must be verified for fatigue and sterilization effects [83] [84] .

Selected locking concept: compliant kinematic snap-bayonet To satisfy 6-DOF constraint, tool-less engagement, and aseptic geometry, we propose a hybrid concept combining a bayonet lock with a monolithic compliant snap for retention and anti-rotation.

Retention and anti-rotation: A circumferential compliant snap fit that deflects elastically over a broad, radiused shoulder. Once seated, provide torsional resistance. Release is achieved by a simple axial tool that elastically lifts the tabs, avoiding hinges and minimizing sliding. Drainability and flow access: All pockets are sloped ≥ 3° and opened to the exterior to prevent fluid stagnation during CIP and to meet dead-leg guidance; no blind threaded features or undercuts are present.

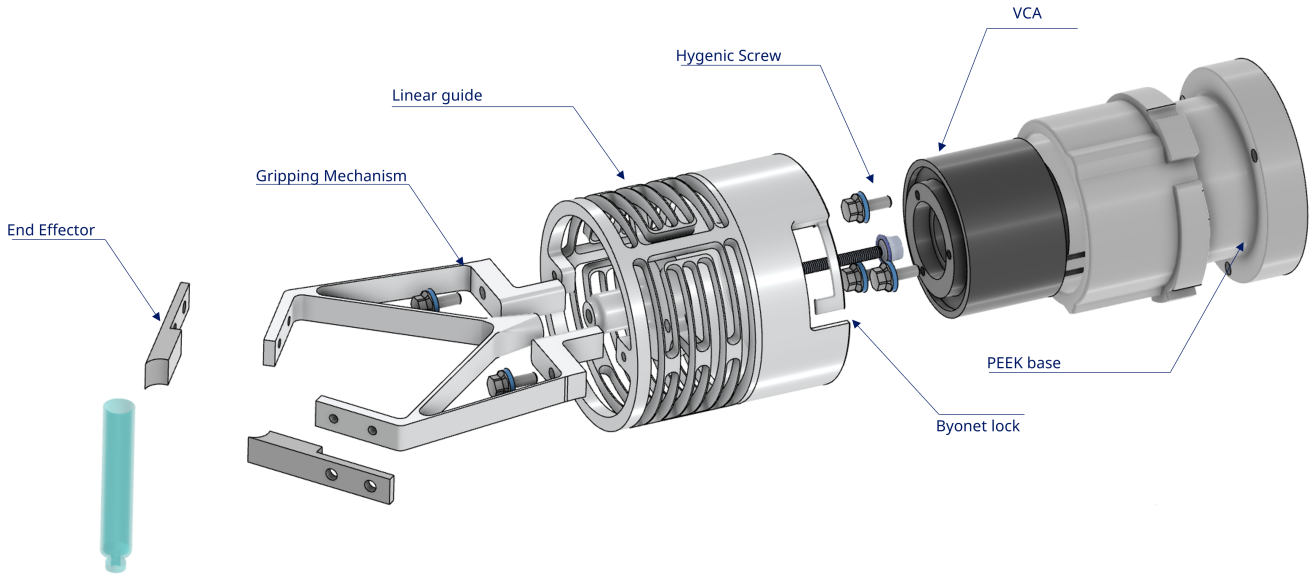

Figure 3.14: Exploded vieuw of the Final design as it has been orded for further analasys

4

Research Methodology

This chapter covers the methodologies, analytical models, numerical techniques, and experimental procedures used to investigate and validate the compliant mechanisms described in Chapter 3. It outlines how the designs were analysed, optimized, and prepared for validation.

4.1. Overall Research Approach

This research used an iterative design and validation approach. Following the design requirements (Chapter 3), literature insights (Chapter 2) and finally the conceptual designs for the linear guide mechanism (LGM) and gripping mechanism (GM) as they were formulated in Chapter 3. These designs were analyzed and optimized using analytical modeling and Finite Element Analysis (FEA) for component- and system-level evaluation. Design iterations were refined based on these analyses, prioritizing kinematic performance, stress distribution, and cleanroom compatibility. Lastly, an experimental validation will be performed.

4.2. Analytical Stiffness Modelling

Analytical modelling provides the theoretical framework for predicting the mechanical behaviour of compliant elements and mechanisms. These models are crucial for initial design sizing, rapid parameter optimization, and benchmarking numerical simulations, offering fundamental insights without relying on computationally intensive Finite Element Analysis (FEA).

4.2.1. Analytical Modelling of Corner-Filleted Arc Leaf Flexures for Linear Guiding Mechanisms

To characterize the flexural elements within the Linear Guiding Mechanism (LGM), an analytical model for Corner-Filleted Arc Leaf Flexures (CFLFs) was developed. This model integrates geometric and mechanical effects of corner fillets and linear width tapering, features implemented in the design for stress management and cleanability.

The core of this approach applies Castigliano's second theorem to quantify flexure deformation. The total elastic strain energy (V_e) for an arc beam, integrating axial, shear, bending, and torsional components, is computed along its neutral axis. Variable cross-sectional properties, resulting from tapering and fillets, necessitate numerical integration for accurate compliance calculation.

This model integrates and extends methodologies from two key research works:

1. **Yang et al. (2021/2022) [74]**: Provides the baseline arc beam compliance model, derived using Castigliano's theorem, for standard arc flexures. They validated this formulation against FEA and experiments for annular flexure guides, and assembled element-level models using a two-port mechanical network.

2. **Li et al. (2021) [78]**: Introduces the concept of stress-reducing corner fillets and quantifies their effect on compliance for straight leaf springs.

The presented model extends these approaches by:

- Incorporating the geometric and mechanical effects of corner fillets within an arc beam context.
- Allowing for linear width tapering along the arc length.
- Implementing an asymmetric fillet distribution.

4.2.2. Geometric Definitions and Cross-Sectional Properties for CFLFs

Arc Beam Geometry

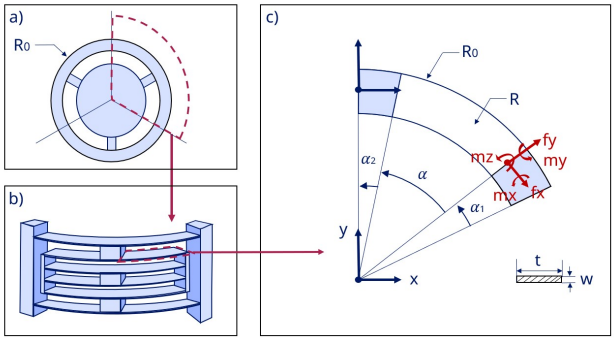

Figure 4.1: a) Full LGM configuration, b) One triple compound FPM, c)Single arced leaf flexure paramatrizaiton

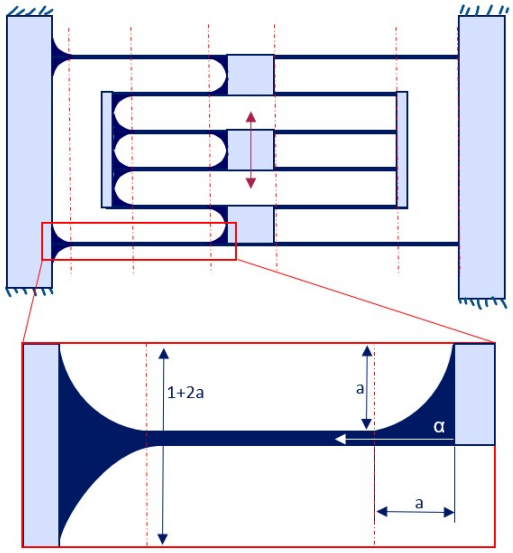

Figure 4.2: LGM with fillets and there effect on arc length

A single arc beam element is defined by its median radius R, spanning a central angle α_{tot} from the free end B ($\alpha = 0$) to the fixed end A ($\alpha = \alpha_{\text{tot}}$). Its dimensions include a width w (which may vary along the arc), a constant thickness t, and corner fillet radii r applied at both ends. The differential arc length is $ds = R\,d\alpha$.

Critical Fillet Orientation and Asymmetric Configuration

A adaptation from Li et al. [78] for arc beams in configurations such as the LGM stage [74] is the reorientation of the corner fillets. While the original formulation assumed fillets affect the *thickness*, for arc flexures in LGM-type mechanisms, the fillets are configured to modify the effective width.

The fillet distribution is asymmetric along the beam length to match the design of the LGM. At the fixed end (point A, $\alpha = \alpha_{\text{tot}}$), fillets are applied on *both sides* of the width. At the free end (point B, $\alpha = 0$), a fillet is applied on only *one side* of the width.

The normalized fillet parameters are:

$$a = \frac{r}{w_{\text{avg}}}, \quad b = \frac{L}{w_{\text{avg}}} \tag{4.1}$$

where $L = R \cdot \alpha_{\text{tot}}$ is the total arc length and $w_{\text{avg}} = (w_A + w_B)/2$ is the average width.

Baseline Cross-Sectional Properties

For a standard rectangular cross-section of width w and thickness t, the section properties are:

$$A = w \cdot t \quad \text{(Cross-sectional area)}$$

$$I_y = \frac{w^3 t}{12} \quad \text{(Bending about } y\text{-axis)}$$

$$I_z = \frac{w t^3}{12} \quad \text{(Bending about } z\text{-axis)}$$

$$I_p = w^3 t \left(\frac{1}{3} - 0.21\frac{w}{t} + 0.0175\left(\frac{w}{t}\right)^5\right) \quad \text{(Torsional constant)}$$

Fillet and Taper Shape Functions

The local effective width of the beam, $w_{\text{eff}}(\alpha)$, is influenced by both a linear width taper and the corner fillets.

Width Taper Function The width $w(\alpha)$ varies linearly from w_B at the free end to w_A at the fixed end:

$$w(\alpha) = w_B + (w_A - w_B) \cdot \frac{\alpha}{\alpha_{\text{tot}}} \tag{4.2}$$

Corner Fillet Shape Function The fillet effect is captured by a piecewise scaling function $\zeta(\xi)$, where $\xi = R\alpha/w_{\text{avg}}$ is the normalized arc coordinate. The function accounts for the asymmetric fillet configuration: bilateral fillets at the fixed end and a unilateral fillet at the free end:

$$\zeta(\xi) = \begin{cases} 2\left(a - \sqrt{\max(a^2 - (a-\xi)^2, 0)}\right) + 1 & 0 \le \xi < a \quad \text{(Fixed end, } \alpha = \alpha_{\text{tot}}\text{)} \\ 1 & a \le \xi \le b - a \quad \text{(Mid-section)} \\ \left(a - \sqrt{\max(a^2 - (\xi - b + a)^2, 0)}\right) + 1 & b - a < \xi \le b \quad \text{(Free end, } \alpha = 0\text{)} \end{cases} \tag{4.3}$$

The coefficient difference reflects the fillet configuration:

- **Fixed end** ($0 \le \xi < a$): Coefficient of **2** yields maximum $\zeta_{\text{max}} = 1 + 2a$ (bilateral fillets).

- **Free end** ($b - a < \xi \leq b$): Coefficient of **1** yields maximum $\zeta_{\text{max}} = 1 + a$ (unilateral fillet).
- **Mid-section** ($a \leq \xi \leq b - a$): $\zeta = 1$ (no fillet effect).

Modified Cross-Sectional Properties

Combining the taper $w(\alpha)$ and fillet $\zeta(\alpha)$ functions, the effective width at any point is $w_{\text{eff}}(\alpha) = w(\alpha) \cdot \zeta(\alpha)$. The section properties then become functions of α:

$$\begin{aligned} A(\alpha) &= w_{\text{eff}}(\alpha) \cdot t \\ I_y(\alpha) &= \frac{[w_{\text{eff}}(\alpha)]^3 \cdot t}{12} \\ I_z(\alpha) &= \frac{w_{\text{eff}}(\alpha) \cdot t^3}{12} \\ I_p(\alpha) &= [w_{\text{eff}}(\alpha)]^3 \cdot t \cdot \left(\frac{1}{3} - 0.21 \frac{w_{\text{eff}}(\alpha)}{t} \right. \\ &\quad \left. + 0.0175 \left(\frac{w_{\text{eff}}(\alpha)}{t} \right)^5 \right) \end{aligned} \tag{4.4}$$

4.2.3. Compliance Matrix Derivation via Castigliano's Theorem

The compliance of the arc flexure is derived using Castigliano's second theorem, which states that the displacement corresponding to a force is the partial derivative of the total strain energy with respect to that force. The total elastic strain energy V_e integrates elemental energy densities along the beam's neutral axis ($s = R\alpha$):

$$\mathsf{V}_e = \int_0^{\alpha_{\text{tot}}} \left[\frac{f_{x,P}^2(\alpha)}{2EA(\alpha)} + \frac{\mu f_{y,P}^2(\alpha)}{2GA(\alpha)} + \frac{\mu f_{z,P}^2(\alpha)}{2GA(\alpha)} + \frac{m_{x,P}^2(\alpha)}{2GI_p(\alpha)} + \frac{m_{y,P}^2(\alpha)}{2EI_y(\alpha)} + \frac{m_{z,P}^2(\alpha)}{2EI_z(\alpha)} \right] R \, d\alpha$$

Here, E is Young's modulus, $G = E/(2(1+\nu))$ is the shear modulus (ν being Poisson's ratio), and $\mu = 6/5$ is the shear correction factor for a rectangular cross-section. The terms $f_{i,P}$ and $m_{i,P}$ represent the local internal force and moment components at angle α.

Local Force-Moment Relations

The end wrench and twist at the free end B are described by:

$$\mathbf{w}_b = [f_{bx},\ f_{by},\ f_{bz},\ m_{bx},\ m_{by},\ m_{bz}]^T \tag{4.5}$$

$$\mathbf{t}_b = [\theta_{bx},\ \theta_{by},\ \theta_{bz},\ u_{bx},\ u_{by},\ u_{bz}]^T \tag{4.6}$$

The local internal forces and moments ($f_{i,P}(\alpha), m_{i,P}(\alpha)$) at an angle α are determined by the external loads ($\mathbf{w}_b$) applied at the free end. These relations involve trigonometric terms that account for the coordinate transformation from the end frame to the local frame at α, as well as varying moment arms. For example:

$$m_z(\alpha) = M_z + F_y \cdot R(1 - \cos\alpha) - F_x \cdot R\sin\alpha \tag{4.7}$$

$$m_x(\alpha) = M_x + F_z \cdot R\sin\alpha + M_y \cdot \sin\alpha \tag{4.8}$$

The full set of local force and moment expressions are obtained through static equilibrium.

Compliance Matrix Formulation

Applying Castigliano's second theorem to the strain energy formulation, end deflections are obtained through partial derivatives:

$$\theta_{bx} = \frac{\partial V_e}{\partial m_{bx}}, \quad u_{bz} = \frac{\partial V_e}{\partial f_{bz}}, \quad \text{etc.} \tag{4.9}$$

This yields the symmetric compliance matrix $\mathbf{C}$ which relates the applied end loads $\mathbf{w}_b$ to the resulting end deflections $\mathbf{t}_b$ through $\mathbf{t}_b = \mathbf{C} \cdot \mathbf{w}_b$. Each entry C_{ij} of the compliance matrix is obtained by taking the second partial derivative of the total strain energy:

$$C_{ij} = \frac{\partial^2 V_e}{\partial w_i \partial w_j} \tag{4.10}$$

Substituting the strain energy expression (Eq. (4.2.3)) and the local force/moment relations, each C_{ij} is expressed as an integral of the form:

$$\frac{R}{\text{Material Property}} \int_0^{\alpha_{\text{tot}}} \frac{\text{[Trigonometric Weight]}(\alpha)}{\text{[Section Property]}(\alpha)} d\alpha \tag{4.11}$$

These integrals are categorized into specific "J-terms" based on the material property (E, G) and section property (A, I_y, I_z, I_p) they involve, and the trigonometric weighting function.

For example, a few representative compliance terms are:

$$C_{u_x f_x} = \frac{R}{E} J_{A,1} + \frac{R^3}{E} J_{I_z,2} + \frac{\mu R}{G} J_{A,3}$$

$$C_{u_z m_x} = C_{\theta_x f_z} = \frac{R^2}{E} J_{I_y,3} - \frac{R^2}{G} J_{I_p,7}$$

The full 6×6 compliance matrix $\mathbf{C}$ exhibits a specific sparse structure due to the geometric symmetries and decoupling assumptions of the arc flexure. This matrix was determined in Yang et al. (2021) [74] and is as follows:

$$\mathbf{C}_a = \begin{bmatrix} C_{u_x f_x} & C_{u_x f_y} & 0 & 0 & 0 & C_{u_x m_z} \\ C_{u_y f_x} & C_{u_y f_y} & 0 & 0 & 0 & C_{u_y m_z} \\ 0 & 0 & C_{u_z f_z} & C_{u_z m_x} & C_{u_z m_y} & 0 \\ 0 & 0 & C_{\theta_x f_z} & C_{\theta_x m_x} & C_{\theta_x m_y} & 0 \\ 0 & 0 & C_{\theta_y f_z} & C_{\theta_y m_x} & C_{\theta_y m_y} & 0 \\ C_{\theta_z f_x} & C_{\theta_z f_y} & 0 & 0 & 0 & C_{\theta_z m_z} \end{bmatrix} \tag{4.12}$$

The positions of zeros indicate decoupled degrees of freedom within this model. Closed-form components derive from dimensionless integrals over α, capturing axial-torsion-bending couplings inherent to curved geometries. For a more detailed deep dive and how to implement the two-port network to include the intermediate links, see Yang et al. (2021) [74].

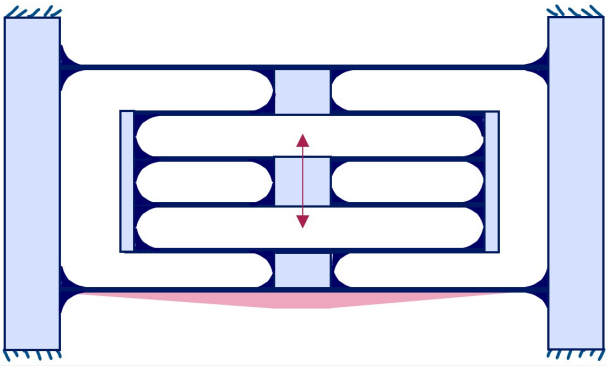

Figure 4.3: LGM in the final modelled configuration with fillets and taper in pink

4.2.4. Numerical Integration Strategies

Constant vs. Variable Properties

In cases of constant width ($w_A = w_B = w$) and no fillets ($r = 0$), the section properties (A, I_y, I_z, I_p) are constant and can be factored out of the J-term integrals. This allows for analytical evaluation of the remaining integrals.

However, when width tapering or fillets are present, the section properties $A(\alpha), I_y(\alpha), I_z(\alpha), I_p(\alpha)$ vary along the arc and must remain within the integral. For example, for $J_{A,1}$:

$$J_{A,1} = \int_0^{\alpha_{\text{tot}}} \frac{\cos^2 \alpha}{w(\alpha) \cdot t \cdot \zeta(\alpha)} d\alpha \tag{4.13}$$

In such cases, these integrals typically require numerical integration.

4.2.5. Axial Stiffness Extraction

The axial stiffness is extracted by enforcing an axial-only end displacement. This involves solving the inverse compliance relationship:

$$\mathbf{t}_b = [0\ 0\ 0\ 0\ 0\ \Delta z]^T \Rightarrow \mathbf{w}_b = \mathbf{C}_a^{-1}\mathbf{t}_b \tag{4.14}$$

The axial stiffness is obtained through first solving the linear system $\mathbf{C}_a\mathbf{w}_b = \mathbf{t}_b$, followed by extracting the third component (axial force component f_{bz}) of the wrench vector ($\mathbf{w}_b$). Finally, stiffness is computed as $k_z = f_{bz}/\Delta z$. When the fillets and taper are neglected for simplicity sake this would result in the explicit stiffness expression:

$$\begin{aligned} k_z = \frac{C_{\theta_x m_x} C_{\theta_y m_y} - C_{\theta_y m_x} C_{\theta_x m_y}}{\left(C_{\theta_x m_x} C_{\theta_y m_y} - C_{\theta_y m_x} C_{\theta_x m_y}\right) C_{u_z f_z}} \\ + C_{u_z m_x}\left(C_{\theta_y f_z} C_{\theta_x m_y} - C_{\theta_x f_z} C_{\theta_y m_y}\right) \\ + C_{u_z m_y}\left(C_{\theta_x f_z} C_{\theta_y m_x} - C_{\theta_y f_z} C_{\theta_x m_x}\right) \end{aligned} \tag{4.15}$$

Physical Interpretation The axial stiffness depends not only on the direct compliance $C_{u_z f_z}$ but also on several coupling terms:

- $C_{u_z m_x}$ and $C_{u_z m_y}$: Axial displacement induced by bending moments.
- $C_{\theta_x f_z}$ and $C_{\theta_y f_z}$: Rotational compliance due to axial force.
- Cross terms between bending compliances $C_{\theta_i m_j}$.

The curved geometry creates mechanical coupling between axial displacement and parasitic bending/torsional moments. Even when enforcing pure axial translation, the flexure's curvature generates secondary moments that must be constrained. The derived stiffness expression quantifies this behavior through off-diagonal compliance terms.

4.2.6. Stiffness Configuration of the FPM

The stiffness of the full stack is determined by calculating the series-parallel combinations. Each FPM structure contains several leaf flexures connected both in parallel and series configurations. The combined stiffness for series flexures is:

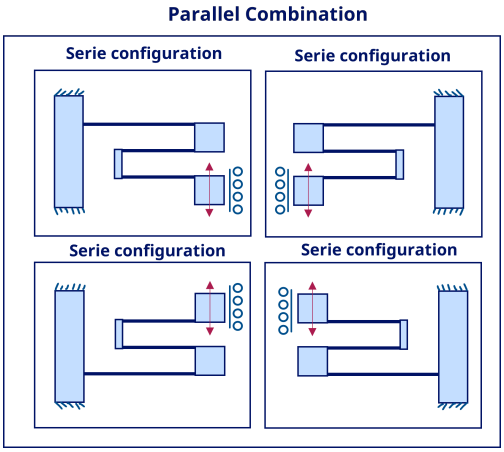

Figure 4.4: A visualization of one FPM stack divided into its series and parallel combinations of arced leaf flexures

$$k_{\text{series}} = \frac{1}{\frac{1}{k_{\text{short}}} + \frac{1}{k_{\text{short}}} + \frac{1}{k_{\text{long}}}}.$$

By combining the four parallel configurations, the effective stiffness of the FPM system is computed:

$$k_{\text{FPM}} = l_p \cdot k_{\text{series}},$$

where l_p is the number of parallel flexures. Finally, the stiffness of the overall linear guide is:

$$k_{\text{total}} = n \cdot k_{\text{FPM}},$$

where n is the number of FPM stacks.

4.3. Pseudo-Rigid Body Model (PRBM) for Gripper Design

For the compliant gripping mechanism (GM)'s five-bar configuration (Section 3.4), the Pseudo-Rigid Body Model (PRBM) offers an effective and computationally efficient alternative to non-linear FEA for initial kinematic

analysis. THe PRBM methode simplifies large deflection compliant mechanisms by replacing compliant segments with rigid links connected by equivalent torsional springs at characteristic pivots [85]. This method provided a clear understanding of motion amplification and force transmission while accounting for the elasticity of flexural elements in our specific gripper design.

4.3.1. PRBM Formulation

The symmetric five-bar gripper (Section 3.4.1) was translated into this PRBM, defining rigid links and pivots derived from the gripper's CAD model. In this formulation, each compliant bar is represented by a single torsional spring at its characteristic pivot, rendering the kinematic system determinate. Distributed flexibility is concentrated in these torsional springs, using standard PRBM constants (γ, K_Θ) and flexure material properties (Young's modulus, area moment of inertia, length). Spring torques are directly proportional to angular deflections from stress-free configurations. This simplification of using only one spring for each flexure is based on an initial quick FEA analyses. The observed deformation behaviour showed that due to the two flexures being connected at the end they behave like a fixed-pinned and guided-pinned flecture.

Input force (F_{in}) was computed directly via the principle of virtual work, relating spring torques and angular sensitivities. Angular sensitivities (e.g., $\partial\theta_A/\partial x_s$ and $\partial\theta_B/\partial x_s$) were obtained by implicitly differentiating a reduced 2×2 Jacobian system derived from loop closure equations. Mechanism stiffness ($K_{mech}(x_s)$) was subsequently derived as the force derivative with respect to slider position. This approach, mathematically equivalent to energy-based methods, provides an efficient analytical reformulation for calculating input force.

4.3.2. Kinematic Constraints

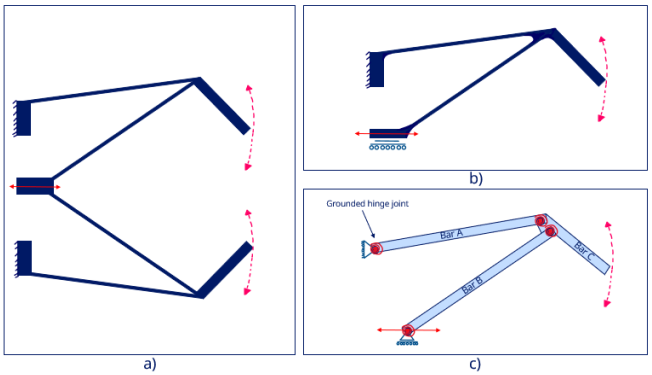

Figure 4.5: A visualization of the compliant gripper mechanism, a) the full GM, b) On side the GM, c) the initial PRBM

With one spring per bar, the system is kinematically determinate. The loop closure equations (Eqs. (4.16) and (4.17)) uniquely define the bar angles θ_A, θ_B, and θ_C for any given slider position x_s. No redundant constraints exist, and the configuration is fully specified once x_s is prescribed.

Let (G_{Ax}, G_{Ay}) be the coordinates of ground pivot A, y_0 be the y-coordinate of the slider, l_a, l_b, l_c be the lengths of Bar A, Bar B, and the Coupler, respectively, and x_s be the slider's x-position. The loop closure equations for the mechanism are derived from the vector loop describing the mechanism's geometry:

$$(x_s + l_b \cos\theta_B) - (G_{Ax} + l_a \cos\theta_A) - l_c \cos\theta_C = 0 \tag{4.16}$$

$$(y_0 + l_b \sin\theta_B) - (G_{Ay} + l_a \sin\theta_A) - l_c \sin\theta_C = 0 \tag{4.17}$$

These relationships are obtained by numerically solving the nonlinear loop closure equations at each slider position.

The angular positions are thus explicit functions of slider position:

$$\theta_A = \theta_A(x_s), \quad \theta_B = \theta_B(x_s), \quad \theta_C = \theta_C(x_s) \tag{4.18}$$

These relationships are obtained by numerically solving the nonlinear loop closure equations at each slider position.

4.3.3. Spring Torques and Angular Deflections

The PRBM torsional springs at the characteristic pivots of Bar A and Bar B generate restoring torques proportional to their angular deflections from the stress-free configuration:

$$\tau_A = K_A(\theta_A - \theta_{A0}) \tag{4.19}$$

$$\tau_B = K_B(\theta_B - \theta_{B0}) \tag{4.20}$$

where K_A and K_B are the torsional stiffnesses calculated depending on the boundary conditions. These torques represent the internal elastic moments that resist angular deformation of the compliant segments.

The general form for the torsional spring stiffness for a flexible segment modeled as a PRBM flexural pivot is:

$$K = \gamma K_\Theta \frac{EI}{L} \tag{4.21}$$

where E is Young's modulus, I is the area moment of inertia of the compliant segment's cross-section, L is the length of the compliant segment, γ is the characteristic radius factor, and K_Θ is the stiffness coefficient.

For specific boundary conditions, the factors γ and K_Θ take on common values:

- **Fixed-Hinged Flexural Pivot:**

$$\gamma_A = 0.5, K_\theta = 2.65 \tag{4.22}$$

- **Guided-Hinged Flexural Pivot**

$$\gamma_B = 0.85, K_\theta = 2.65 \tag{4.23}$$

4.3.4. Direct Force Calculation via Virtual Work

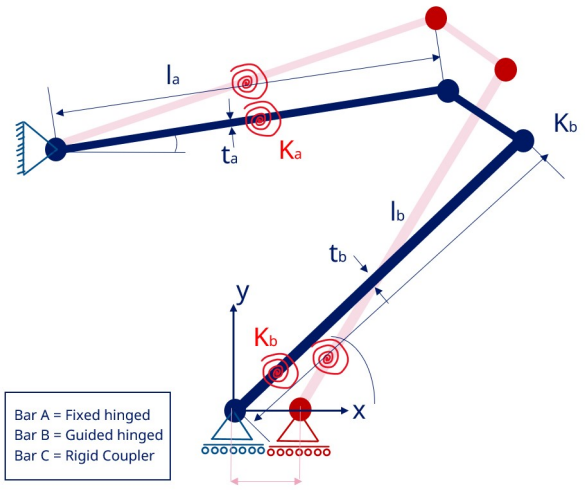

Figure 4.6: A visualization of the PRBM for the compliant gripper mechanism

The principle of virtual work provides a method for computing the input force without resorting to numerical differentiation of the total energy. Consider a virtual displacement δx_s of the slider. This displacement induces corresponding virtual angular displacements $\delta\theta_A$ and $\delta\theta_B$ through the kinematic coupling of the mechanism see figure 4.6

The virtual work performed by the input force F_{in} must equal the virtual work performed against the spring torques:

$$F_{\text{in}} \cdot \delta x_s = \tau_A \cdot \delta\theta_A + \tau_B \cdot \delta\theta_B \tag{4.24}$$

Dividing both sides by δx_s and taking the limit yields:

$$F_{\text{in}}(x_s) = \tau_A \frac{\partial\theta_A}{\partial x_s} + \tau_B \frac{\partial\theta_B}{\partial x_s} \tag{4.25}$$

Substituting the torque expressions from Eqs. (4.19) and (4.20):

$$F_{\text{in}}(x_s) = K_A(\theta_A - \theta_{A0})\frac{\partial\theta_A}{\partial x_s} + K_B(\theta_B - \theta_{B0})\frac{\partial\theta_B}{\partial x_s} \tag{4.26}$$

For the symmetric mechanism with mirrored top and bottom chains, the total input force is:

$$F_{\text{in,total}}(x_s) = 2\left[K_A(\theta_A - \theta_{A0})\frac{\partial\theta_A}{\partial x_s} + K_B(\theta_B - \theta_{B0})\frac{\partial\theta_B}{\partial x_s}\right] \tag{4.27}$$

4.3.5. Reduced Jacobian for Angular Sensitivities

The angular sensitivities $\partial\theta_A/\partial x_s$ and $\partial\theta_B/\partial x_s$ required in Eq. (4.27) are obtained from implicit differentiation of the loop closure equations. Since the coupler angle θ_C is kinematically dependent but does not contribute to the elastic energy (the coupler is rigid), a reduced 2×2 Jacobian system can be employed:

$$\mathbf{J}_{\text{kin}}^{2\times2}\begin{bmatrix}\partial\theta_A/\partial x_s \\ \partial\theta_B/\partial x_s\end{bmatrix} = \begin{bmatrix}-1 \\ 0\end{bmatrix} \tag{4.28}$$

where the reduced Jacobian matrix is:

$$\mathbf{J}_{\text{kin}}^{2\times2} = \begin{bmatrix}l_a \sin\theta_A & -l_b \sin\theta_B \\ -l_a \cos\theta_A & l_b \cos\theta_B\end{bmatrix} \tag{4.29}$$

The right-hand side $[-1, 0]^T$ arises from differentiating the loop closure equations with respect to x_s, recognizing that $\partial x_s/\partial x_s = 1$ and the slider is constrained to move horizontally ($\partial y_0/\partial x_s = 0$).

Solving this linear system:

$$\begin{bmatrix}\partial\theta_A/\partial x_s \\ \partial\theta_B/\partial x_s\end{bmatrix} = \left(\mathbf{J}_{\text{kin}}^{2\times2}\right)^{-1}\begin{bmatrix}-1 \\ 0\end{bmatrix} \tag{4.30}$$

This approach avoids finite-difference approximations, providing exact analytical sensitivities at each configuration.

4.3.6. Equivalence to Energy-Based Methods

It is important to note that Eq. (4.27) is mathematically identical to the force obtained by differentiating the total strain energy (Eq. (4.31)) with respect to x_s using the chain rule:

$$F_{\text{in}} = \frac{\partial U_{\text{total}}}{\partial x_s} = \frac{\partial U_{\text{total}}}{\partial\theta_A}\frac{\partial\theta_A}{\partial x_s} + \frac{\partial U_{\text{total}}}{\partial\theta_B}\frac{\partial\theta_B}{\partial x_s}$$

Here, the total strain energy U_{total} for the symmetric mechanism is given by:

$$U_{\text{total}}(x_s) = K_A(\theta_A(x_s) - \theta_{A0})^2 + K_B(\theta_B(x_s) - \theta_{B0})^2 \tag{4.31}$$

Recognizing that $\partial U_{\text{total}}/\partial\theta_i = 2\tau_i$ (from Eq. (4.31)), this reduces to Eq. (4.27).

4.4. Numerical Simulation (Finite Element Analysis - FEA)

Besides analytical models, Finite Element Analysis (FEA) is used to provide an more detailed assessment of the compliant mechanisms, providing insights into stress concentrations, displacement behaviour, under various loading conditions. FEA was critical for verifying performance and optimizing geometries. All FEA simulations were conducted using CATIA 3DX FEA. Standard isotropic elastic properties for Aluminium 7075-T6 (E = 71.7 GPa, ν = 0.33) were used, with non-linear geometry settings for large deformations.

4.4.1. Meshing and Convergence Studies

Mesh convergence studies needs to be performed on all critical components, varying element size and local refinements, and monitoring maximum von Mises stress and

total displacement. Convergence was typically achieved when output parameters didn't change significantly between successive refinements. Quadratic tetrahedral elements will be used.[86]

4.4.2. Analysis Types

FEA characterized the mechanisms via:

- **Static Structural Analysis:** Primary analysis for stress, strain, and displacement under VCA loads, enabling non-linear geometry for large deformations.
- **Modal Analysis:** Identified natural frequencies and mode shapes, crucial for dynamic stability and avoiding resonance.
- **Fatigue Analysis (Preliminary Considerations):** FEA-based fatigue analyses, using stress results and material fatigue properties, estimated theoretical fatigue lives under cyclic loading.

For the fatigue analyses the following data will be used. As it is determined to ideally have a calculated fatique life of at least a million cycles resulting in the following maximum Von Misses stresses.

- PEEK, max Von Misses stress < 26 MPa [87].
- Superduplex (SAF2507), max Von Misses stress < 430 MPa [88].
- Alumnium 7075, max Von Misses stress < 180 MPa [89].
- StainlessSteel (316L), max Von Misses stress < 200 MPa [90].

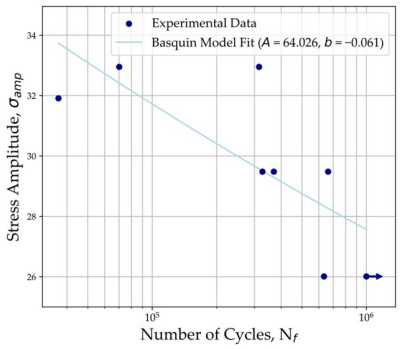

Figure 4.7: SN-curve plot for PEEK[87]

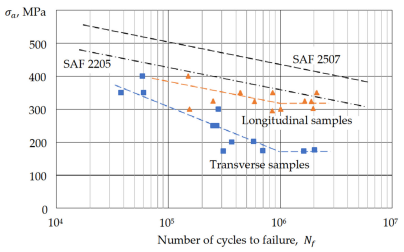

Figure 4.8: SN-curve plot for SAF2570[88]

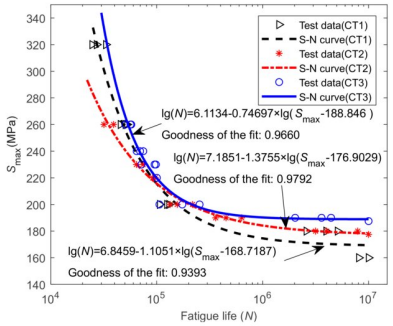

Figure 4.9: SN-curve plot for AL7075[89]

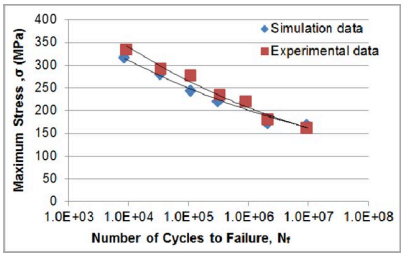

Figure 4.10: SN-curve plot for SS316L [90]

4.5. Experimental Validation Methods

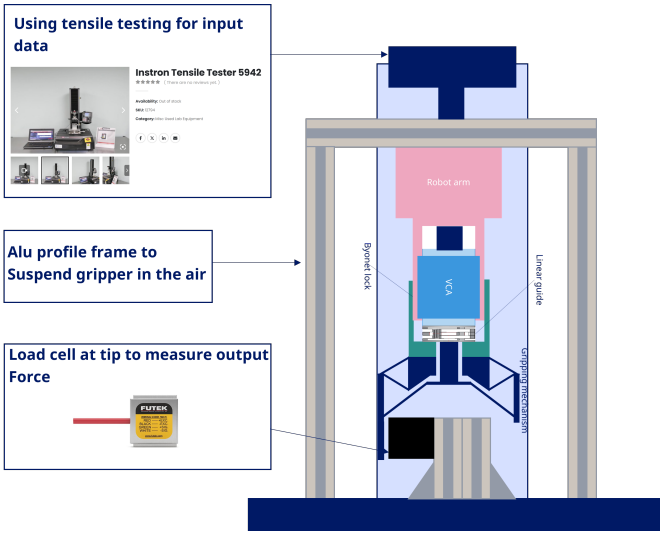

Figure 4.11: Test setup for Validation used to quantify the behaviour of the AL7075 prototype

Preliminary experimental considerations and methods were established to bridge the gap between theoretical predictions and real-world performance, addressing critical aseptic manufacturing requirements.

4.6. Experimental Validation Methods

To validate that the analytical and numerical models accurately represent the physical behaviour of the compliant mechanism, and to assess the actual performance of the design in terms of force and motion, a prototype will be fabricated and tested. These experimental methods are designed to bridge the gap between theoretical pre-

dictions and real-world performance, addressing critical aseptic manufacturing requirements.

4.6.1. Test Setups and Procedures

The prototype will be tested using a combination of precision instrumentation and visual analysis techniques:

1. **Force-Displacement Characterization (Instron Tensile Testing Machine):** A universal Instron tensile testing machine (*e.g.*, Model 5969, equipped with a $500\,\mathrm{N}$ load cell) will be employed to acquire accurate force-displacement curves. This will be performed on:
    - Individual building blocks: The Linear Guide Mechanism (LGM) and the Gripping Mechanism (GM) will be characterized independently to validate their isolated stiffness and kinematic response against model predictions.
    - The complete integrated system: Testing the full assembly will provide data on overall system compliance and the interaction between components.

    This method allows for precise control of displacement or force input and direct measurement of the corresponding output, providing quantitative data for model validation.
2. **Gripping Force Measurement:** To specifically quantify the gripping force generated by the end effector, a dedicated load cell (e.g., a $30\,\mathrm{N}$ FUTEK load cell) will be placed between at one of the gripper tips. This setup will enable the measurement of:
    - **Passive Gripping Force:** The force exerted by the gripper when no external actuation force is applied (due to its pre-loaded compliant design).
    - **Active Gripping Force:** The maximum force achievable when the Voice Coil Actuator (VCA) is actively engaged. This will validate the design's ability to provide sufficient and potentially variable gripping force for target objects.
3. **Motion Behaviour Analysis (Video Tracking):** To visually verify and quantify the precise kinematic behaviour of the compliant mechanism, a video analysis technique will be utilized.
    - **Setup:** A high-resolution camera will be positioned to capture the motion of the prototype. A grid will be placed directly behind the mechanism to serve as a reference.
    - **Tracking:** Small, distinctly coloured (*e.g.*, orange) 3D-printed markers will be placed at known, critical locations on the prototype (e.g., input from LGM and gripper tips).
    - **Data Extraction:** Custom Python code, leveraging computer vision libraries, will be used to automatically track the displacement of these markers across recorded video frames. This will allow for the measurement of input-to-output displacement ratios and path[91].

4.6.2. Riboflavin Coverage Test Protocol

Cleanability validation is crucial for aseptic environments. This will involve a riboflavin coverage and removal test on the prototype[37]. The protocol includes:

1. **Application:** A UV-fluorescent riboflavin solution will be uniformly applied to all surfaces of the prototype, including intricate flexure roots and features of the bayonet lock, simulating a worst-case contamination scenario.
2. **Cleaning Cycle:** The prototype will then undergo a standardized cleaning cycle, in Novo Nordisk it is common to use a worst case scenario where the prototype is washed for 10 seconds instead of the normal hour cycle with the same settings.
3. **Inspection and Quantification:** Following the cleaning cycle, the prototype will be inspected under UV light. Residual fluorescence will identify any areas where the riboflavin was not thoroughly removed, indicating potential "hard-to-clean" spots. Image analysis software will quantify the remaining coverage, guiding design refinements for enhanced cleanability.

4.6.3. Material Considerations for Prototyping

Initial functional prototypes were fabricated from Aluminum 7075-T6 for its excellent machinability, high stiffness to weight ratio, and cost effectiveness for demonstrating mechanical principles. It is crucial to acknowledge that while this material facilitates rapid prototyping and validation of kinematic and dynamic behaviours, it is not suitable for end use in aseptic pharmaceutical environments. For production, materials such as PEEK or 316L Stainless Steel are specified due to their chemical inertness, biocompatibility, and sterilization compatibility (as discussed in section 7.6.1). The prototype material validates the design principles, not the final product performance under aseptic conditions.

5 Results

This chapter presents the key findings derived from the analytical models, numerical simulations (Finite Element Analysis), and experimental tests outlined in chapter 4. The results are organized to first discuss the performance of individual sub-mechanisms (e.g., the linear guide mechanism (LGM) and the gripping mechanism (GM)) before presenting observations on the integrated system. Data are presented in the context of the design requirements established in chapter 3.

5.1. Linear Guide Mechanism (LGM) Performance

The linear guide mechanism (LGM) is designed to provide precise axial motion for the Voice Coil Actuator (VCA) while resisting parasitic off-axis deflections. Its performance was evaluated through analytical modelling, Finite Element Analysis and tests.

5.1.1. Analytical Model Results

This section shows the results of the analytical model, as described in chapter 4. The effect of features like fillets and taper significantly influences the predicted stiffness.

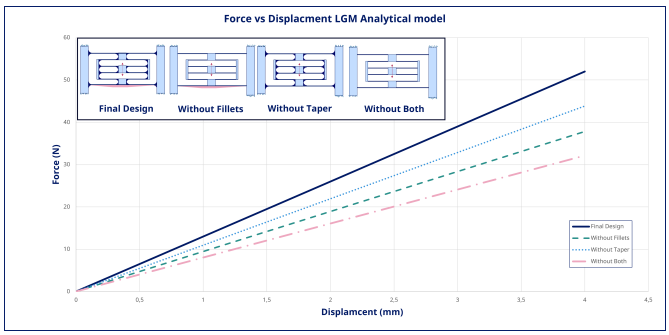

Figure 5.1: Resulting force displacement plot for the analytical model of the LGM with fillets and taper and without

The stiffness values for different configurations are:

- Final design (with fillets and taper): $13.00\,\mathrm{N/mm}$
- Without fillets: $9.54\,\mathrm{N/mm}$
- Without taper: $10.96\,\mathrm{N/mm}$
- Without both: $8.03\,\mathrm{N/mm}$

As visible in figure 5.1, ignoring fillets alone results in a $26.6\,\%$ underestimation of stiffness ($13.00\,\mathrm{N/mm}$ vs. $9.54\,\mathrm{N/mm}$), while ignoring taper results in a $15.8\,\%$ underestimation ($13.00\,\mathrm{N/mm}$ vs. $10.96\,\mathrm{N/mm}$). Ignoring both leads to a substantial $38.3\,\%$ underestimation of stiffness ($13.00\,\mathrm{N/mm}$ vs. $8.03\,\mathrm{N/mm}$).

5.1.2. FEA Results

Mesh Convergence

A mesh convergence study for the LGM confirmed that both the maximum von Mises stress and the total displacement converged to stable values when the local mesh size in critical flexure regions was refined to $0.2\,\mathrm{mm}$ or finer. Coarser meshes, particularly those close to the LGM's thickness, under predicted both stress and displacement, as visualized in figure 5.2 for different mesh densities and figure 5.3 for the convergence plots. The red areas in figure 5.2 highlight regions where mesh size is close to the geometry size and as a result under predicts.

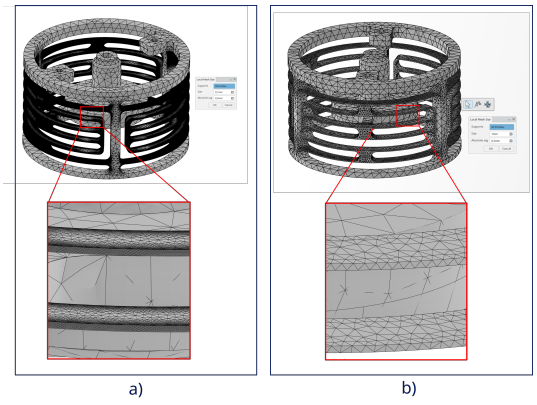

Figure 5.2: Visualization of local Mesh and the effect of different local mesh size with a) 0.1 mm local mesh size and b) 1 mm local mesh size

Stiffness and Displacement Characteristics

The FEA resuts in an axial motion stiffness for the LGM of approximately $13.45\,\mathrm{N/mm}$. This value shows a difference of only $3.46\,\%$ compared to the analytical model's prediction of $13.00\,\mathrm{N/mm}$ for the final design. The FEA also produced similar trends to the analytical model when comparing the effects of neglecting fillets and taper, which can be seen in Table 5.1.

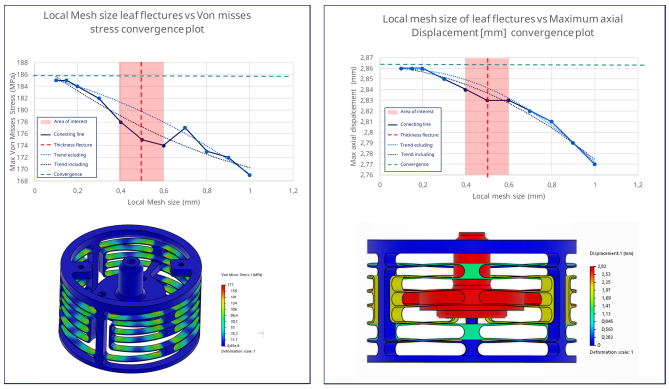

Figure 5.3: Convergence plot for LGM a) Von Misses stress convergence b) Axial displacement convergence

Eigenmode Analysis

This section presents a comparison between a simplified analytical model and the detailed FEA results for the eigenmodes of the LGM.

Analytical Natural Frequency Prediction For an initial assessment, the LGM's primary axial motion can be approximated as a Single-Degree-of-Freedom (SDOF) system. The undamped natural frequency (ω_n) and natural frequency (f_n) are given by:

$$\omega_n = \sqrt{\frac{k}{m}}, \quad f_n = \frac{1}{2\pi}\sqrt{\frac{k}{m}} \tag{5.1}$$

Based on the final analytical stiffness for the LGM, and considering an effective moving mass (m) of $0.04\,\mathrm{kg}$ (as determined in the design phase for the moving VCA magnet and attached components, visualized in figure 5.4), the parameters are:

- Axial Stiffness, $k = 13.00\,\mathrm{N/mm} = 13 \times 10^3$ N/m
- Effective Moving Mass, $m = 0.042\,\mathrm{kg}$

Substituting these values into Equation 5.1, the analytical prediction for the natural frequency of the LGM is:

$$\omega_n = \sqrt{\frac{13{,}000\ \text{N/m}}{0.042\ \text{kg}}} = \sqrt{325{,}000} \approx 556.8\ \text{rad/s}$$

$$f_n = \frac{556.8\ \text{rad/s}}{2\pi} \approx 88.6\ \text{Hz}$$

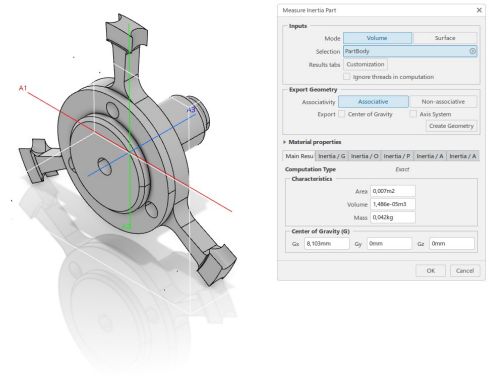

Figure 5.4: Moving mass of the LGM determined in CATIA for analytical eigen mode

Numerical Modal Analysis (FEA)

The FEA model of the LGM, fixed at its base, yielded the following first few natural frequencies and corresponding mode shapes (visualized in figure 5.5):

- **Mode 1 (Axial Translation):** $f_1 = 84.196\,\mathrm{Hz}$. This mode corresponds to the desired translational motion along the actuator's axis (z-direction).
- **Modes 2–3 (Off-axis/Lateral Flexure):** $f_2 \approx 314.542\,\mathrm{Hz}$ and $f_3 \approx 314.883\,\mathrm{Hz}$. These modes represent parasitic lateral or rotational deflections, demonstrating the LGM's stiffness in directions perpendicular to the primary axial motion.

Comparison eigenmodes LGM Comparing the analytical prediction for the fundamental axial natural frequency ($f_n = 88.6\,\mathrm{Hz}$) with the FEA-derived first axial mode ($f_1 = 84.196\,\mathrm{Hz}$), a difference of approximately $5.2\,\%$ is observed, with the analytical model yielding a slightly higher frequency. This difference is within typical engineering tolerances and is primarily attributed to the SDOF model's simplification of distributed mass, localized compliances, and support flexibility, which are fully captured by the FEA.

The ratio between the axial mode ($84.196\,\mathrm{Hz}$) and the higher-frequency off-axis/lateral modes (approximately $315\,\mathrm{Hz}$) is approximately 3.7 times higher.

This minor difference is well within typical engineering tolerances and can be attributed to several factors inherent in the simplification of the analytical SDOF model.

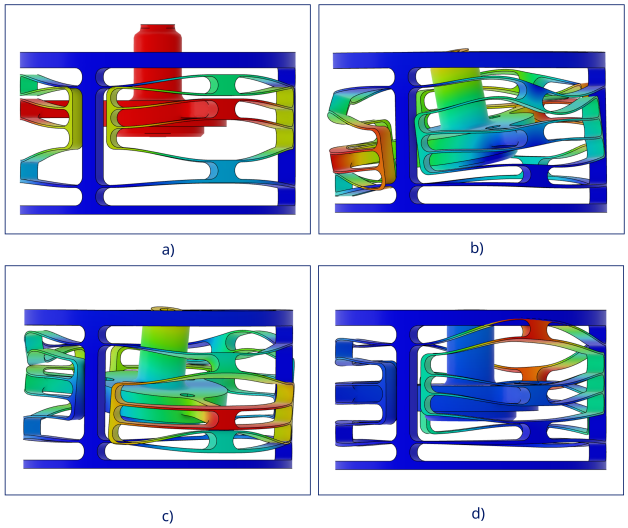

Figure 5.5: The eigenmodes found trough a FEA simulation of the full mechanism. a) first mode 84.196 Hz b) second mode 314.542 Hz c) Third mode 314.542 Hz d) Fourth mode 412.199 Hz

Peak Stress Distribution

The FEA showed localized stress concentrations within the arc leaf flexures. The peak von Mises stress observed reached $282\,\mathrm{MPa}$ for the maximum single sided $4\,\mathrm{mm}$ motion range. The yield strength of the chosen Aluminum 7075-T6 is $503\,\mathrm{MPa}$, resulting in a safety factor of approximately 1.78. Peak stress concentrations were particularly visible on the inner curves of the leafflexures. A investigation in the origin of this stress concentration revealed that this is at least partly due to the limitations in how the large fillets are modelled in CATIA; as seen in figure 5.7, the fillet's geometry does not perfectly follow the arc curvature, especially on the inside. Ideally, a variable radius fillet would be employed to maintain parallelism with the arc's centreline, mitigating these localized stress risers more effectively.

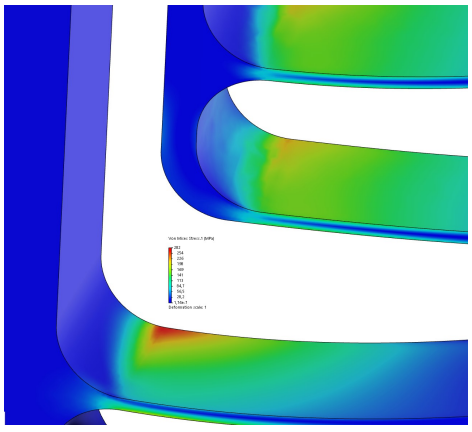

Figure 5.6: Peak stress for LGM at 4.3 mm displacement for AL7075

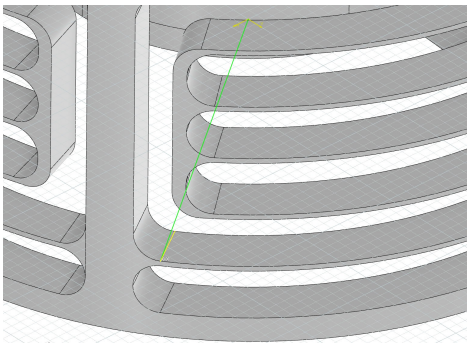

Figure 5.7: Detailed view of how the fillet doesn't follow the arc correctly

5.1.3. Motion Behaviour LGM

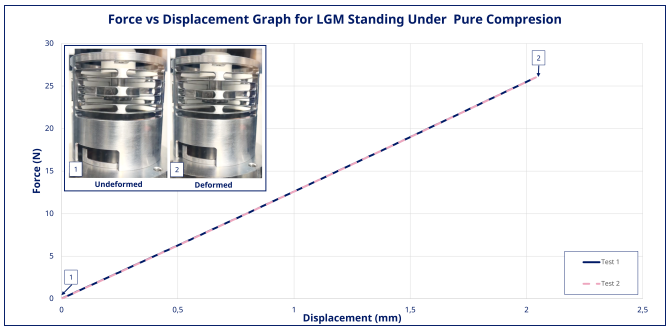

Figure 5.8: Instron Tensile Testing Motion Behaviour Graph for LGM standing

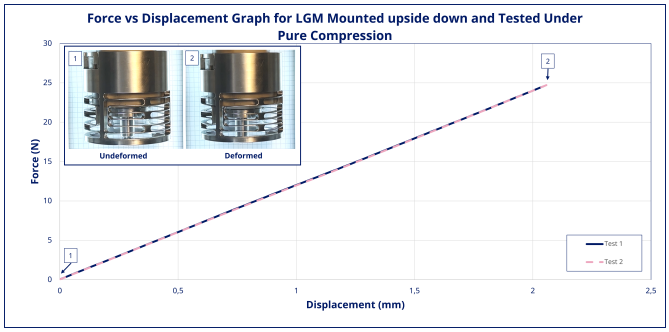

Figure 5.9: Instron Tensile Testing Motion Behaviour Graph for LGM hanging

The LGM prototype demonstrated smooth and accurate axial translation. During manufacturing, some machining differences occurred, including an accidental taper in the bottom leaf flexure set not present in the original CAD model. To assess if this asymmetry influenced performance, the prototype was tested both standing (figure 5.8) and suspended (figure 5.9). No noticeable difference in force-displacement behaviour or parasitic motion was observed between these two orientations. The force-displacement tests yielded a curve exhibiting linear elastic behaviour. As shown in the comparison (figure **??**), the FEA and analytical models closely matched the prototype's behaviour. The prototype, while showing similar behaviour, was slightly less stiff. This slight deviation is attributable to several factors: the prototype's mea-

sured dimensions, which deviated slightly from the initial CAD and were used to adjust the models, and potential changes in material characteristics due to heat generated during the CNC machining process (figure 5.11), despite efforts to mitigate this with cooling.

FEA vs Analytical vs Tests Verification LGM

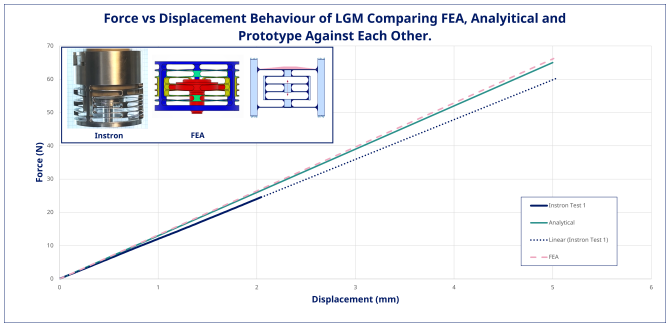

Figure 5.10: Force displacement curves of the LGM for the prototype tests, the FEA results and the analytical model

Table 5.1: LGM Mechanism performance of Analytical, FEA and tests against each other. With the measurement data for 4 and 5 mm being extrapolated data indicated with a *. The percentage in the last row is determined of the force at 5 mm and in blue the final models are highlighted

LGM Mechanism	F (N) 2.4mm	F (N) 4mm	F (N) 5mm	Error %
Measurement	41.4	50.0*	62.5*	-
Analytical model	31.2	52.0	65.0	4
Analytical (No Fillets)	22.7	37.8	47.0	-25
Analytical (No Taper)	26.3	43.8	54.8	-12
Analytical (No both)	19.3	32.1	40.2	-36
FEA model	31.7	52.9	66.1	6
FEA (No Fillets)	22.8	38.1	47.6	-24
FEA (No Taper)	26.0	43.4	54.3	-13
FEA (No both)	19.0	31.8	39.9	-36

Figure 5.11: CNC production of the LGM prototype out of AL7075

5.2. End Effector Mechanism (Gripper) Performance

The gripping mechanism (GM) was evaluated through FEA and prototype testing to observe its operational characteristics, focusing on optimized flexure geometry and motion generation.

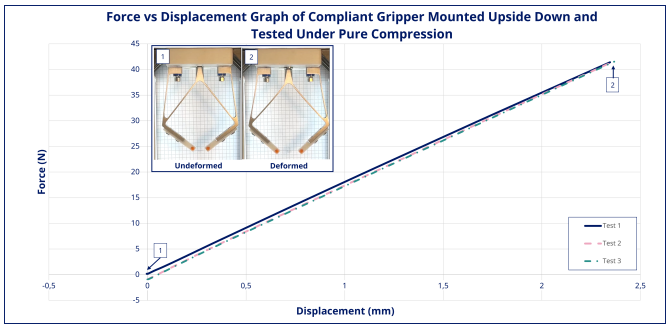

Figure 5.12: Instron Tensile Testing Motion Behaviour Graph Gripping Mechanism

5.2.1. FEA Results: Convergence Gripping Mechanism

The mesh settings for the GM FEA where also refined by doing a convergence study.The Von Mises stress, being highly sensitive to localized stress concentrations, requires finer mesh elements to converge accurately, especially near fillet radii. In contrast, the tip displacement showed less change even with coarser local meshes, while stress values continued to refine until a mesh size of $0.2\,\mathrm{mm}$ was reached.

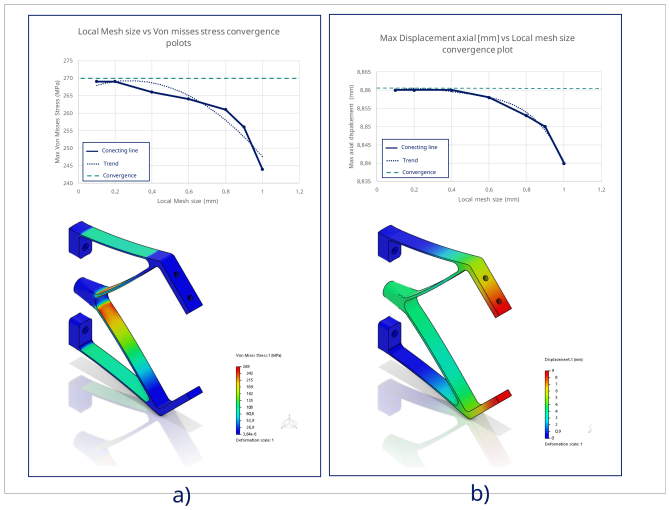

Figure 5.13: Convergence plot for GM a) Von Misses stress convergence b) Axial displacement convergence

Peak stress

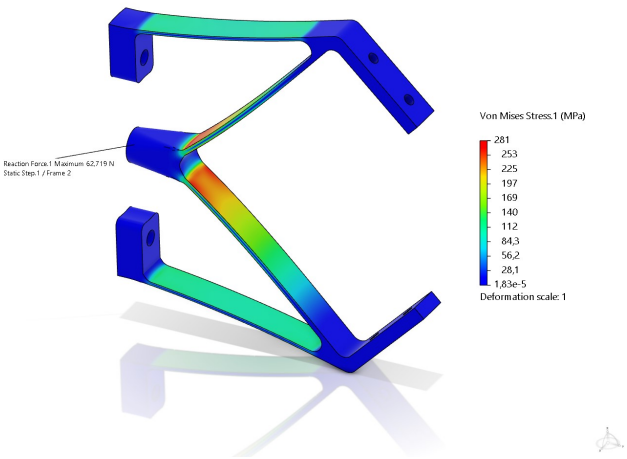

Figure 5.14: Peak stress gripper for an input displacement of 4 mm

The Peak Von Misses stress in the gripping mechanism is 281 MPa. The yield strength of the chosen Aluminium 7075-T6 is $503\,\mathrm{MPa}$, resulting in a safety factor of approximately 1.78 As a result the safety margin is 1.79. However it it can also be seen that the stresses are mostly located at the root of the flexures at the input. Ideally this stress would be more equally distributed over the two leaf flexures.

Input-to-Output Displacement Ratio

The optimized compliant gripper mechanism, with an input displacement of $\pm 4\,\mathrm{mm}$ from the VCA, resulted in a total grip motion of approximately $7.5\,\mathrm{mm}$ at the output tips. figure 5.15 visualizes the open and closed positions.

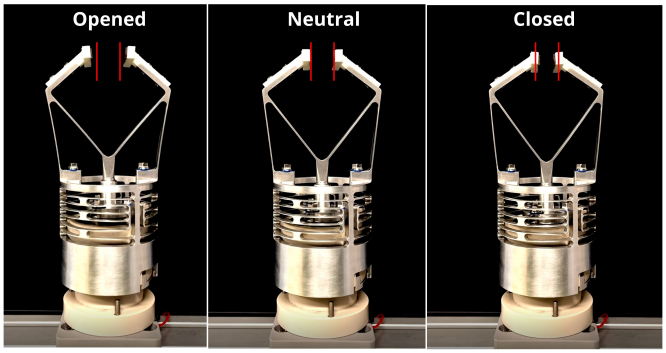

Figure 5.15: Picture of the gripping mechanism in its open, closed and neutral positions, showing total grip motion.

When the FEA, Analytical and physical tests results are visualized against each other as can be seen in figure 5.16. The analytical model and FEA model seem to follow the same kind of curve just slightly offset from each other, a 12 $\%$ difference between them as can be seen in 5.2. The FEA model seems to predict the performance quite well up to 2 mm compared to the physical test data. As the data after that is extrapolated it is hard to draw conclusions on the those results.

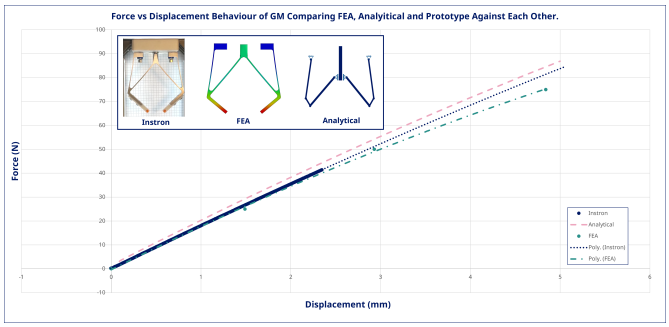

Figure 5.16: Force displacement curves of the gripper mechanism with the Test data of the prototype, FEA results and the analytical model

Table 5.2: Gripping Mechanism performance of Analytical, FEA and tests against each other. With the measurement data for 4 and 5 mm being extrapolated data indicated with a *. The percentage in the last row is determined of the force at 5 mm

Gripping Mech.	F (N) 2.4mm	F (N) 4mm	F (N) 5mm	Error %
Measurement	41.4	68.4*	83.8*	-
Analytical model	44.3	71.3	86.9	4
FEA Model	40.9	64.3	77.2	-8

5.3. Rotational Locking System

As the primary focus of this study is on the compliant LGM and gripping mechanism, the rotational locking system was only limited investigated. A Finite Element Analysis (FEA) model was performed to confirm that the design concept was sound and met its functional requirements, specifically concerning internal stresses. This initial design was not optimized but rather served as a proof-of-concept to ensure the feasibility of an aseptic, tool-less bayonet-style lock for modularity. The Internal peak von misses stress resulting from the FEA model for the required displacement is 225 MPa (see figure 5.17) compared to the Yield stress of Aluminum 7075-T6 which is 503 MPa would result in a safety margin of 2.24.

5.3.1. Handling Byonet lock

The bayonet lock performed well overall. When engaged, it constrained all six degrees of freedom with negligible play. A small plateau was observed in the force–displacement curve when transitioning from tension to compression (Figure 5.18). This □0.1 mm flat region is believed to be the clearance take-up/backlash in the lock interface. Under VCA actuation, this effect did not cause any visible issues.

The primary shortcoming encountered was during engagement. The magnetic attraction between the moving magnet and the coil occurred at a larger separation than anticipated from the supplier data, making it difficult to mate the two halves smoothly without unintended pull in.

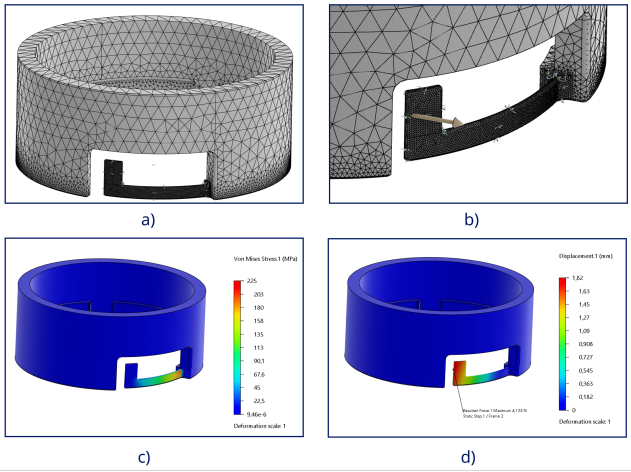

Figure 5.17: Results for the FEA analysis for the rotating locking design. a) The local fine mesh, b) the force displacement of the tip, c) the Von Misses stress d) the displacement

5.4. Complete System Performance

The performance of the fully integrated compliant gripping system, including the VCA, LGM, GM, and aseptic locking mechanism, was evaluated through FEA simulations and prototype testing. Experimental testing of the full prototype under active VCA actuation provided insights into the system's dynamic response and force output. As shown in figure 5.19, the graph illustrates the relationship between input force from the VCA and the resulting gripping force.

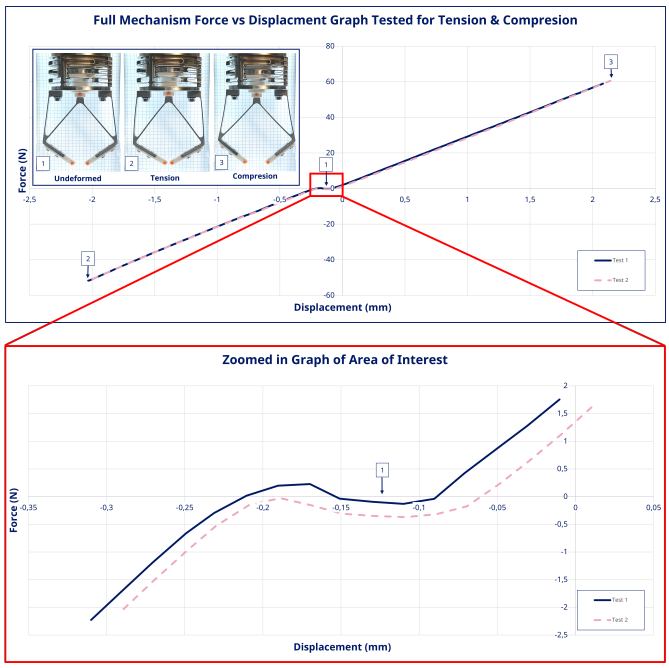

Figure 5.18: Instron Tensile Testing Motion Behaviour Graph Full Mechanism Under Compresion and Tension

5.4.1. Active Gripping

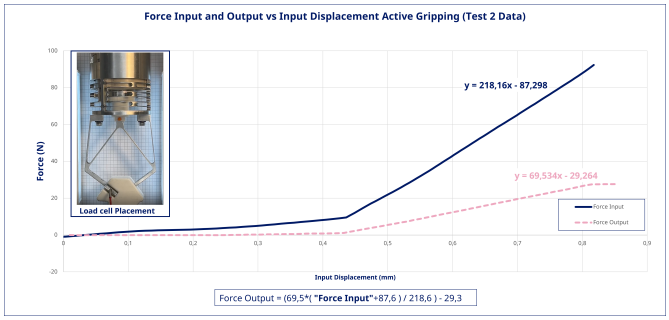

Figure 5.19: Graph with the active gripping results for Instron actuated prototype. With the force input and the force output plotted and the formula connecting them

The active gripping mode, although not the intended operating strategy, is useful for characterization. Figure 5.19 shows the system actuated by the Instron tensile testing machine, which allows both the input force (at the actuator interface) and the output gripping force (at the finger tip load cell) to be measured synchronously and plotted against time and against each other. This enables derivation of a simple calibration relationship between input and output forces.

Within the tested range, the maximum measured gripping force per finger was approximately 30 N, which is consistent with the FEA predictions for the same input conditions. For the VCA actuated test the maximum force was around 16 N. This lower value is the result of the actuator not delivering more force after 5 A (see figure 5.20 which was a controller issue (indicated in red).

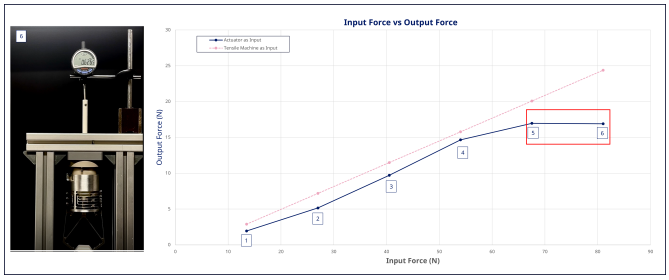

Figure 5.20: Graph with the active gripping results for Instron actuated prototype. And the VCA actuated prototype. The number represent the amount of Amps with which the actuator was powered

5.4.2. Passive Gripping

The passive gripping strategy, where the gripping force is maintained by the mechanism's preloaded compliance, was validated experimentally. Figure 5.21 compares the passive gripping response of the VCA-actuated prototype, the FEA model, and the Instron-actuated prototype. Across all three methods, the force–displacement behaviour is well approximated by a linear relation with a common slope (stiffness) of approximately 8.35 N/mm. This consistency indicates that the passive mode is dominated by the compliant architecture and is largely independent of the actuation method. This calibrated stiff-

ness can be used to design to set the required opening (preload) for future applications.

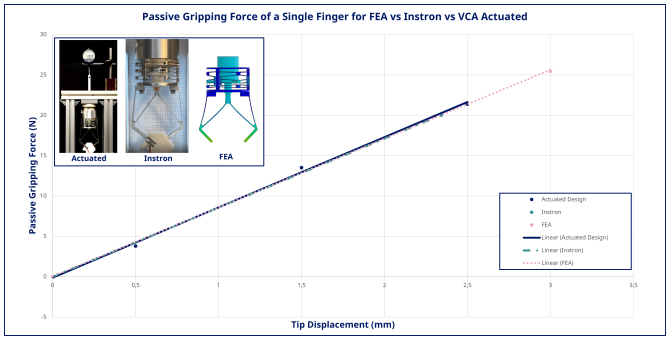

Figure 5.21: Graph with the passive gripping results for VCA actuated prototype, FEA model and Intron actuated prototype are compared

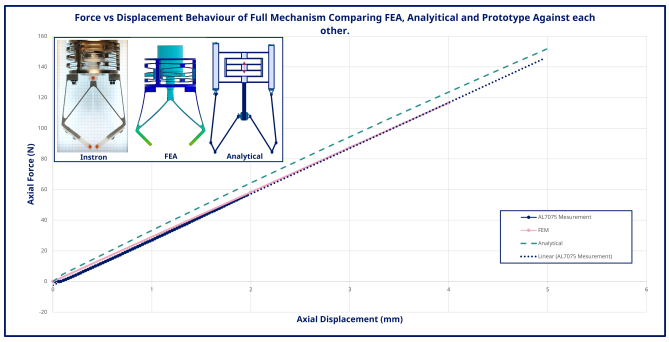

Figure 5.22: Force Displacement Graph Full Mechanism comparing the different models

Overall Displacement

The force-displacement characteristics of the full mechanism under compression and tension can be seen in figure 5.22. This graph illustrates the overall stiffness of the full compliant system. A comparison of the force-displacement behaviour across different models (analytical, FEA, and prototype) for the full mechanism is provided in figure 5.22. The prototype resisted radial and rotational deflections when an axial force was applied. No significant binding or unintended contact between components was observed during actuation.

Table 5.3: Complete Mechanism performance of Analytical, FEA and tests against each other. With the measurement data for 4 and 5 mm being extrapolated data indicated with a *. The percentage in the last row is determined of the force at 5 mm

Complete Mech.	F (N) 2mm	F (N) 4mm	F (N) 5mm	Error %
Measurement	56.63	113.3*	141.6*	-
Analytical model	64.40	123.64	151.88	7.3
FEA Model	58.29	116.52	141.00	-0.4

System-Wide Stress Distribution

Analyzing the complete assembly's stress distribution under maximum operational load showed all components remained within their elastic limits. Peak stresses were located within the flexural hinges of the LGM and GM. Interfaces.

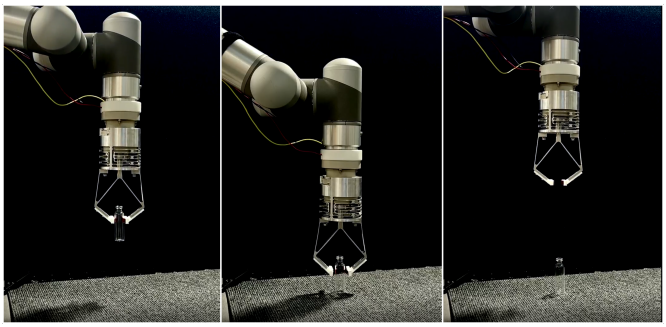

Figure 5.23: Test with the gripper mounted on a robotic arm and gripping an cartridge

System Eigenmodes

The final modal analysis on the complete assembly resulted in the lowest frequency mode corresponding to the intended axial motion, demonstrating the system's overall dynamic characteristics. The first four eigenmodes are shown in figure 5.24: a) first mode ($62.38\,\mathrm{Hz}$), b) second mode ($121.98\,\mathrm{Hz}$), c) third mode ($205.85\,\mathrm{Hz}$), and d) fourth mode ($261.96\,\mathrm{Hz}$). which indicates a ratio of 2 between first and second mode.

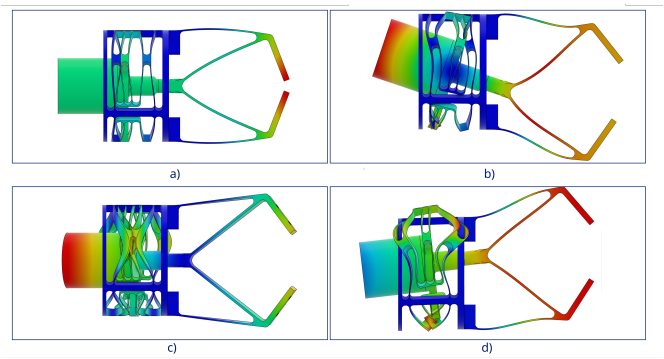

Figure 5.24: The eigenmodes found trough a FEA simulation of the full mechanism. a) first mode 62.38 Hz b) second mode 121.98 Hz c) Third mode 205.85 Hz d) Fourth mode 261.96 Hz

Motion Tracking

Motion tracking with high contrast markers (orange dots) against a calibrated background grid was used to validate the end effector kinematics across the operating range (Figure 5.25; same actuation sequence as Figure 5.18). Figure 5.26 compares the tracked input displacement with the Instron actuator displacement for the same time points and reveals a systematic deviation. The discrepancy is attributable to camera perspective, pixel mm calibration error, and slight marker placement offsets relative to the true input reference. Consequently, the motion□tracking data should be considered qualitative/relative rather than metrically exact.

Despite the scale offset, the tracked trajectories exhibit the same functional shape as the Instron measurements, and the tip displacement–force relationship aligns

well with the FEA model over the tested range. Additionally, the forward and reverse paths nearly overlap, indicating minimal hysteresis in operation.

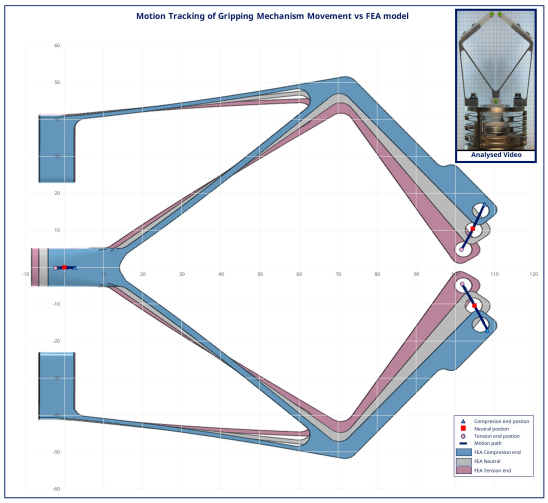

Figure 5.25: Motion tracking to validate the motion behaviour of the end effector the FEA results shown behind the plotted displacement was for a +- 2 mm input

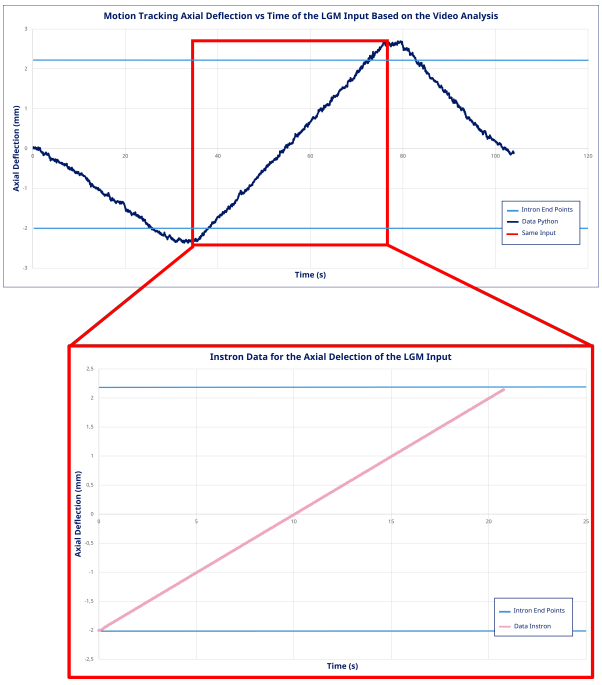

Figure 5.26: The displacement vs time curve of the input of the LGM from the Instron and the Python analysed video against each other

5.5. Cleanability Assessment: Riboflavin Test Considerations

A conceptual assessment of the design's cleanability was initially performed through visual inspection of the CAD model and 3D-printed prototypes, in collaboration with internal specialists at Novo Nordisk. Key features like open, radiused surfaces and the absence of "dead legs" in the compliant bayonet lock suggested that fluid stagnation would be prevented, thereby allowing rinsing and sterilization. The general conclusion from this preliminary meeting was that the design concept appeared promising, with no initial concerns identified regarding its cleanability from a design perspective.

To perform a more rigorous cleanability assessment, the proposed riboflavin test protocol (Section 4.6.2) was performed out on the AL7075 prototype. The results from this coverage test were largely promising. As visualized in figure 5.27 and detailed with comments in Appendix F.0.1, the main finding was that the inherent design of the compliant mechanism itself did not pose major cleanability risks. Most observed residual riboflavin was concentrated on the outer surfaces of the design, primarily as an effect of the prototype's orientation within the wash cycle, rather than due to inherent design flaws.

However, the assessment identified a few specific areas requiring further attention:

- **Mounting Interface between GM and LGM:** The current design incorporates a $90°$ corner at the mounting interface between the Gripping Mechanism and the Linear Guide Mechanism. In the initial riboflavin tests, some residue collected in this corner. Suggesting a need for radius optimization or a redesigned interface
- **Vertical LGM Testing (Bayonet Lock Feature):** During vertical testing of the LGM, some riboflavin residue was observed on an internal surface close to one of the features of the bayonet lock. While partially attributable to the orientation during the wash cycle, this area was identified as potentially more challenging to clean effectively due to its geometry.
- **Water Retention between Leaf Flexures:** When the LGM was positioned vertically, water retention was observed between the leaf flexures after the wash cycle. This phenomenon is primarily caused by the tight geometry and surface tension. While not deemed an immediate concern, a different orientation during washing or minor adjustments to flexure spacing could mitigate this issue.

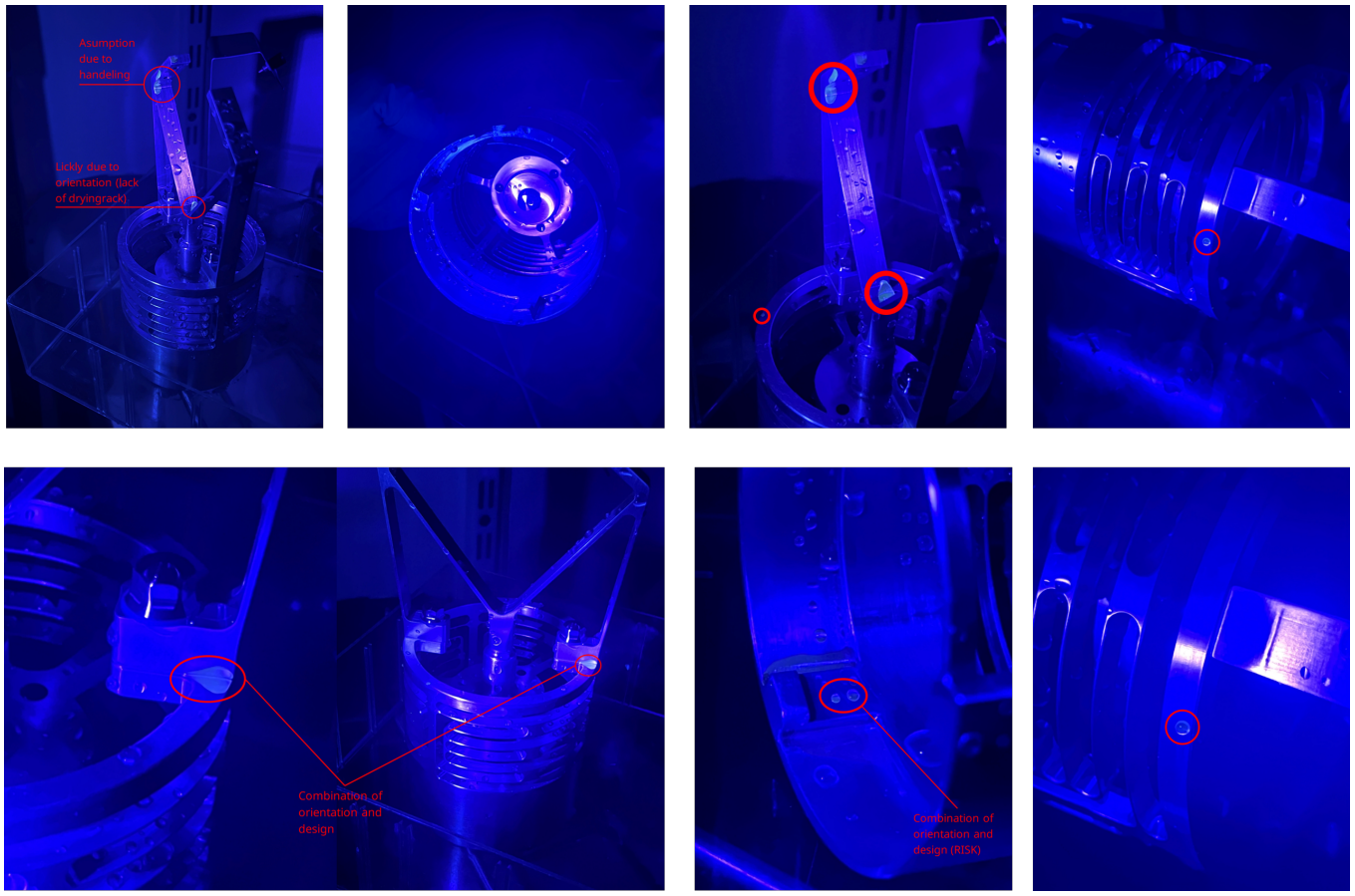

Figure 5.27: Results of the riboflavin coverage test for better visual see appendix F.0.1

6

Design Improvements: Transition to Aseptic-Grade Materials

Following the successful feasibility assessment of the compliant mechanism using the Aluminium 7075 prototype (Chapters 3 and 5), the next phase will focus on translating this design into materials suitable for Grade A aseptic pharmaceutical manufacturing. The Al7075 prototype, while excellent for demonstrating mechanical principles and initial validation, is inherently unsuitable for long-term use in sterile environments due to its limited chemical inertness, susceptibility to corrosion from aggressive cleaning agents, and poor performance under repeated sterilization cycles such as autoclaving (as highlighted in Section 2.3.3).

This section details the design improvements undertaken to transition the mechanism to aseptic-compatible materials, specifically Super Duplex, while preserving the validated kinematic performance of the Al7075 prototype. The goal was to achieve full compliance with the hygienic design principles and material criteria established in Chapter 2.

6.1. Material Selection and Justification for Aseptic Deployment

Based on the comprehensive material assessment (Section 2.3.3, Figure 2.2, and Appendix E), Super Duplex was selected as the primary material for the linear guide mechanism (LGM) and critical structural components due to its exceptional corrosion resistance, high mechanical strength, and superior fatigue life.

6.2. Geometric Re-optimization for Aseptic-Grade Materials

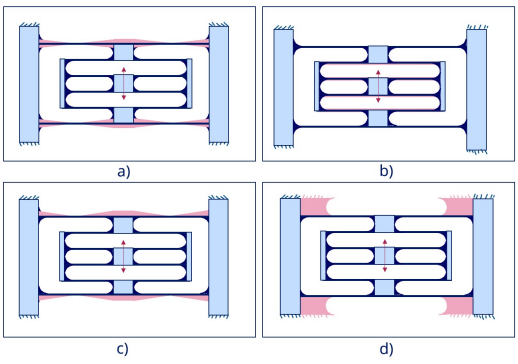

Figure 6.1: Options to get equal stress between flexures. a)Both long flexures tapered at the top and bottom b) increase thickness of the short flexures C) Taper the outside of the long flexures d) Decrease the length of the long flexures

The transition to Super Duplex (SD) or 316L stainless steel(SS) necessitated a geometric re-optimization of the entire compliant mechanism. These materials have a significantly higher Young's moduli compared to Al7075 (e.g., Super Duplex 200 GPa, 316L SS 193 GPa vs. Al7075 71.7 GPa). Directly replicating the Al7075 flexure dimensions would result in a mechanism with drastically increased stiffness and reduced range of motion, far exceeding the VCA's actuation capabilities.

The primary objective was to ensure the re-designed mechanism exhibited equivalent force-displacement characteristics and kinematic response (e.g., input-to-output displacement ratio, parasitic motion) as the Al7075 prototype. This was achieved through iterative Finite Element Analysis (FEA) by adjusting critical flexure dimensions (thickness, length, and width profiles). Flexure Geometry Adjustments: To adjust for the higher material stiffness, the flexural elements within both the LGM and GM were made thinner than their Al7075 counterparts. This approach maintained the desired compliance while keeping maximum von Mises stresses within acceptable limits for the chosen stainless steel alloys, well below their respective yield strengths and suitable for long fa-

tigue life.

Stress Redistribution: The effectiveness of tapered flexures and optimized fillets (Section 3.4.4) became even more critical with these higher-strength materials. The design refinements previously observed to reduce peak von Mises stresses by approximately 35% in Al7075 were maintained and further optimized. This ensured that, despite the greater material stiffness, localized stress concentrations were mitigated, promoting long fatigue life essential for continuous operation in pharmaceutical production.

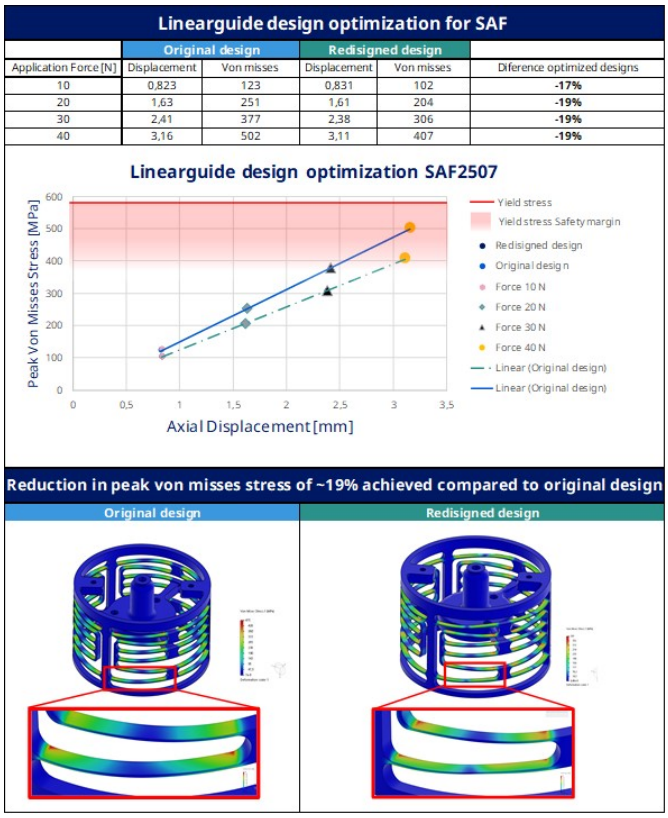

Figure 6.2: Design adjustment for Super Duplex LGM

6.2.1. Geometry of the Leaf Flexures of the GM

The initial design of the GM had leaf flexures with a uniform cross section between the hinge points. However, FEA simulations revealed significant localized stress concentrations at **Joint A**. This observation was expected based on the design geometry, as Joint A undergoes the highest angular displacement.

Localized stress concentrations will impact the fatigue performance and reliability of compliant mechanisms due to material yielding or potential fracture under cyclic loading. Therefore it was investigated how the flexure geometry could be changed to reduce stress concentrations while maintaining the performance of the mechanism.

Optimization of Leaf Flexure Geometry

To minimize localized stresses, the geometry of the leaf flexures was refined. While flexures with a uniform cross section are simpler to manufacture, they produce uneven stress distributions under large rotational angles, with stress peaks occurring at the fixed ends.

A review of literature on flexure geometry optimization revealed two promising methods to address this issue:

1. Introducing **tapers** along the width or thickness of the flexures to redistribute stresses more evenly along the entire flexure length.[92] [83]
2. Implementing **fillets** or curved transitions between the flexures and adjoining components to reduce sharp geometric discontinuities.[83]

The reviewed studies [83] suggested incorporating tapered profiles for the flexures, as this approach minimizes stress concentrations by varying the cross-sectional dimensions to achieve more uniform stress gradients. Meanwhile, adding fillets at connection points further mitigates peak stresses. It was found that ratios of

$$\frac{R}{h} = 0.6 \tag{6.1}$$

yields the best results. Bigger ratio's don't change the stress distribution significantly. As in the case of our design there are also aseptic requirements, it is decided to encompass a larger fillet. This, however, is therefore not an parameter that has a lot of use optimizing further as changing the geometry further will not result in a significant better stress distribution.

Implementation of Optimized Geometry

The optimized flexure geometry introduced a taper along the width of the leaf flexures, with the cross section narrowing toward the central portion of the member. This gradient reduces stiffness at the flexure's center while ensuring higher stiffness at the attachment ends, thereby redistributing stresses more evenly.

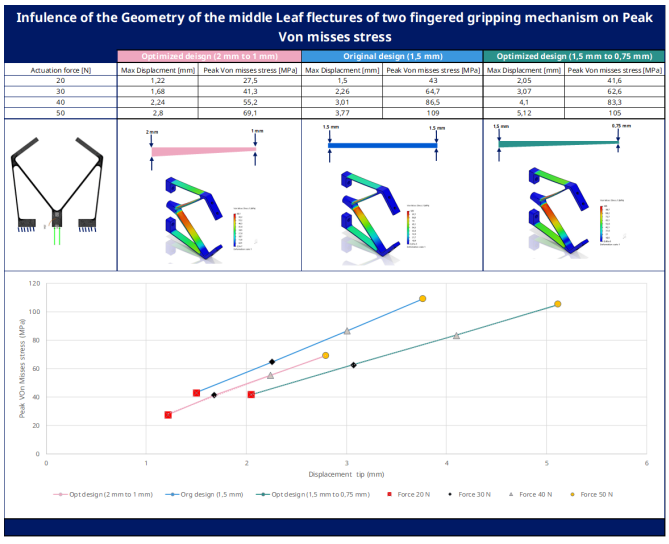

Figure 6.3: Optimization of the gripper design, simulations with the AL7075 material

Results and FEA Validation

The modified tapered flexure geometry was simulated using FEA to evaluate its effect on stress distribution and overall mechanical performance. The key observations are summarized below:

- **Stress Reduction at Joint A:** The introduction of the tapered flexure resulted in a substantial reduction in localized stress at Joint A. Peak von Mises stresses decreased by approximately 27% compared to the initial uniform design.
- **Input-to-Output Efficiency:** The displacement efficiency of the gripper mechanism was preserved, as the updated geometry maintained effective transfer of input motion to output gripping motion with minimal deviations from the original kinematic path.

6.2.2. Complete Compliant Mechanism Performance with Super Duplex (SD)

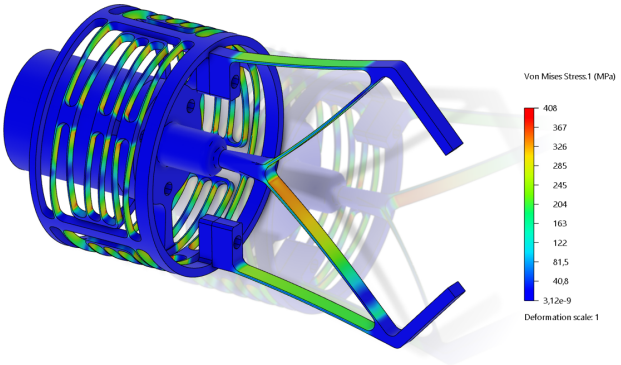

Figure 6.4: Optimised compliant gripper design Von Misses Stress plot for 80N of application force for SAF2507

Following the geometric re-optimization for Super Duplex (SD, SAF2507) stainless steel, a Finite Element Analysis (FEA) simulation was performed on the complete compliant gripping mechanism. An input force of 80 N, applied to the moving magnet of the Voice Coil Actuator (VCA), generated an input displacement of 4 mm. This resulted in an output gripping motion of **7.15 mm** at the gripper tips, which is consistent with the kinematic response observed for the AL7075 prototype (9.5 mm gripping motion from 4 mm input. Demonstrating that the re-optimized geometry effectively maintains the desired kinematic performance despite the significant change in material stiffness.

For the internal stresses, a peak von Mises stress of **403 MPa** was observed within the LGM flexures under maximum operational load. While this is higher than the 282 MPa recorded for the AL7075 prototype (which has a yield strength of 503 MPa, as seen in Section 5.1.2), it remains below the specified yield strength of **580 MPa** for the chosen Super Duplex alloy. This yields a safety factor of approximately **1.44** (580 MPa$/403$ MPa ≈ 1.439).

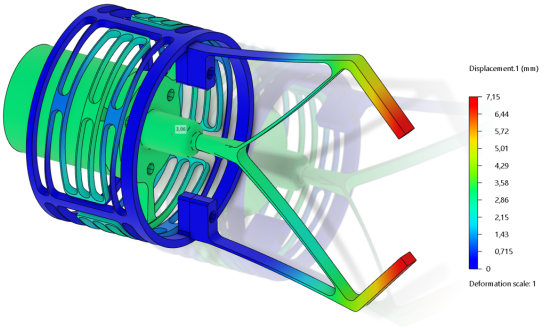

Figure 6.5: Optimised compliant gripper design displacement plot for 80N of application force for SAF2507

The eigenmode analysis for the Super Duplex system revealed the following natural frequencies and corresponding mode shapes:

- **Mode 1: 36.855 Hz**, primarily corresponding to the axial translation of the mechanism, which is its intended operational mode.
- **Mode 2: 71.131 Hz**, representing the first parasitic rotational deflection.
- **Mode 3: 106.724 Hz**.
- **Mode 4: 174.536 Hz**.

The ratio between the first two modes (Mode 2 / Mode 1) is approximately **1.93** (71.131 Hz$/36.855$ Hz ≈ 1.930). This ratio is comparable to the **1.95** ratio observed in the AL7075 prototype (121.98 Hz / 62.38 Hz, as detailed in Section 5.4). This consistent dynamic separation between the primary axial motion and critical parasitic modes is essential for ensuring dynamic stability, preventing resonance during high frequency operation.

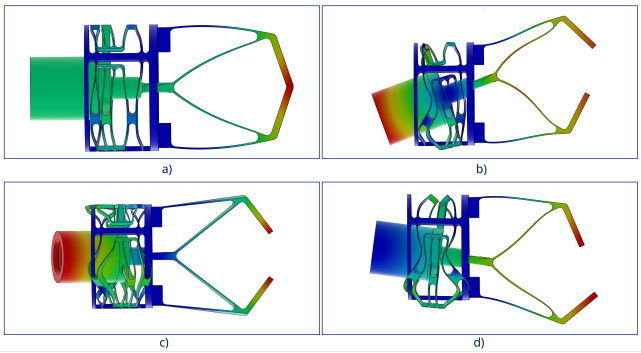

Figure 6.6: Optimised compliant gripper design eigenmodes for 80N of application force for SAF2507, a) first eigen mode 36.855 Hz, b) second eigenmode 71.131 Hz, c) third eigenmode 106.724 Hz, fourth eigenmode 174.536 Hz

7 Discussion

This chapter reflects on the study's results, contextualizing them within existing literature, highlighting the challenges overcome, and outlining the practical implications for the proposed compliant mechanism. The presented study explored the feasibility of implementing a compliant mechanism designed for integration into aseptic production environments, a critical challenge in modern pharmaceutical manufacturing. While the findings indicate considerable potential for these mechanisms, several limitations, opportunities for improvement, and crucial directions for future research have been identified.

7.1. Overview of Key Findings

This feasibility study demonstrated the potential of compliant mechanisms for particle elimination in sterile environments, directly addressing the goal of enhanced sterility assurance. The design, analysis, and validation confirmed the viability of a flexure-based gripping mechanism specifically tailored for Grade A cleanrooms.

Key findings supporting this conclusion include:

- **Validated Mechanical Performance:** The developed gripper demonstrated more then the required gripping force. Generating up to 25 N when passive gripping at each finger with a stiffness of 8.35 N/mm. And generating up to 16 N for the active gripping at 5A while powered by the VCA while possibly able of actively gripping with 30N as shown with Instron test. It also shows precise displacement range ($9.25\,\mathrm{mm}$ output motion from $4\,\mathrm{mm}$ VCA input) for sensitive pharmaceutical components, confirmed by analytical models, FEA, and prototype testing.
- **Inherent Contamination Control:** The monolithic, jointless architecture inherently eliminates typical sources of contamination like wear particles, lubricants, and microbial harbering points, fulfilling a core requirement for aseptic environments.
- **Design for Aseptic Compatibility:** Successful integration of crucial hygienic features, such as radiused surfaces, self-draining geometries, and an aseptic bayonet lock, significantly enhances cleanability and modularity. Preliminary riboflavin tests supported the design's cleanability (Section 5.5).
- **Material Transferability:** The design proved adaptable to pharmaceutical-grade materials (Super Duplex and $316\,\mathrm{L}$ Stainless Steel), with FEA confirming operation well within elastic limits ($403\,\mathrm{MPa}$ peak stress in SD LGM vs. $580\,\mathrm{MPa}$ yield strength, providing a safety factor of 1.44).

These results collectively validate the feasibility of compliant flexural systems as a viable alternative to conventional gripping mechanisms in Grade A pharmaceutical environments.

7.2. Comparison with Existing Technologies

The compliant gripping mechanism developed in this study offers a compelling alternative to existing automation technologies in aseptic pharmaceutical manufacturing, directly addressing critical shortcomings identified in the literature review.

Compared to conventional grippers (pneumatic, hydraulic, electric):

- The voice coil-actuated compliant gripper fundamentally eliminates the contamination risks associated with moving seals, tubing, exhaust air (pneumatic), fluid leakage (hydraulic), or lubricated gears and sliders (electric). This provides particle-free, precise motion without requiring external air supplies.
- The monolithic, jointless design simplifies isolator integration and significantly reduces complexity and points of failure, which are inherent issues in multi-component traditional grippers.

Compared to other compliant mechanisms described

in literature:

- This work's contribution lies in its holistic approach to integrating material compatibility, sterilization resilience, and rigorous hygienic design principles explicitly for Grade A pharmaceutical manufacturing, a niche often overlooked in broader CM research.
- The design prioritizes cleanability from the start, distinguishing it from some highly complex or topology-optimized CMs (e.g., [60]) that might pose challenges in aseptic cleaning.
- The aseptic bayonet lock significantly enhances modularity and ease of maintenance, a practical advantage over multi-part compliant systems or those using threaded fasteners.

This research therefore establishes an integrated design methodology that bridges the gap between mechanical innovation and the stringent cleanroom compatibility criteria essential for pharmaceutical production.

7.3. Interpretation of Results

7.3.1. Material Behaviour and Mechanical Performance

The high agreement (only a 1.7% difference) between analytical models and FEA results for the LGM's stiffness validates the accuracy of the refined flexure models, particularly their ability to account for the stiffness increasing effects of corner fillets and tapers [78]. This modelling precision is valuable, not only confirming the design but also offering advantages for rapid design iteration and optimization more efficiently than solely relying on extensive FEA.

While the LGM's stiffness ratio between motion direciton and offaxis directions is lower than some designs optimized purely for maximum stiffness (e.g., [74]), this represents a deliberate design trade-off. The selection of a $0.5\,\mathrm{mm}$ minimum flexure thickness and the inclusion of an additional set of leaf flexures were driven by considerations for manufacturability via 5-axis CNC, robust stress distribution, and enhanced cleanroom compatibility by avoiding overly delicate features. As the mechanism's dynamic analysis confirmed sufficient stiffness for the VCA's $0.4\,\mathrm{kg}$ moving mass, with no significant parasitic deflections or binding observed in simulations.

For the Gripping Mechanism, the implementation of tapered flexures yielded a substantial $35\,\%$ reduction in peak von Mises stresses. This stress redistribution is critical for maximizing fatigue life, addressing a key concern for reliable operation in repetitive industrial tasks. The successful re-optimization for Super Duplex material, maintaining kinematic performance while achieving a 1.44 safety factor, further validates the design principles' transferability across materials with significantly different mechanical properties.

7.3.2. Cleanroom Compliance and Design Philosophy

The 'sterility by design' approach, central in this work, prioritizes the elimination of contamination sources at the conceptual stage. The monolithic structure and absence of traditional joints fundamentally prevent particle generation and microbial harborage, a principle further reinforced by the non-contact operation of the VCA.

Conceptual riboflavin testing (Section 5.5) proved effective while highlighting localized areas requiring further geometric refinement. Such as the observation of residual riboflavin at the 90° corner of the mounting interface and near the bayonet lock. This iterative process of design, assessment, and refinement is fundamental to achieving and verifying full regulatory compliance for cleanability and drainability.

7.4. Limitations

While this study provides a robust foundation for the application of compliant mechanisms in aseptic manufacturing, several limitations were encountered:

1. **Material Validation:** The current prototype in Aluminum 7075, experimental validation of production-grade materials like PEEK and SAF2507 stainless steel is still missing, specifically regarding their long term fatigue performance and stability under repeated sterilization cycles (autoclaving, VHP). PEEK's susceptibility to creep and initial deformation cycles [87] specifically asks for testing.
2. **Absence of Experimental Fatigue Testing:** Despite analytical predictions, the mechanical longevity of the flexures under cyclic loading, especially in combination with sterilization cycles, has not been experimentally verified.
3. **Lack of Quantitative Particle Emission and Airflow Assessment:** The study did not include experimental quantification of airborne particle emissions during operation or smoke studies to visually assess airflow turbulence caused by the mechanism. Such data is critical for definitive ISO 14644 Class A compliance verification.
4. **VCA Thermal and Magnetic Considerations:** While passive gripping minimizes VCA heat, the thermal performance under prolonged or high-frequency active actuation remains unexplored. Furthermore, the use of Super Duplex (a potentially magnetic material) with a VCA necessitates further investigation into parasitic magnetic attraction forces or potential demagnetization effects.
5. **Manufacturing Tolerance Impact:** A robust tolerance analysis of the intricate flexure geometries, crucial for consistent performance and interchangeability in scaled production, was beyond the scope of this study.
6. **Rotational Locking System Optimization:** While functional, the bayonet lock's cleanability requires

further optimization. Riboflavin tests identified areas of concern (Section 5.5) where improved radii, drainability, minimization of flat stagnant areas, and a more rigorous tolerance analysis are needed to enhance robustness and ensure absolute hygienic compliance.

7. **Limited Gripper Versatility:** The current two-fingered gripper, while optimized for specific components, has limited versatility for handling irregularly shaped or highly diverse objects.
8. **Economic Scalability:** A detailed analysis of the economic viability and scalability for producing compliant mechanisms from high-performance aseptic-grade materials was not within the scope of this feasibility study.

7.5. Implications for Industry

The compliant gripping mechanism developed in this thesis holds implications for the pharmaceutical industry, particularly in advanced aseptic manufacturing settings.

- **Enhanced Sterility and Product Quality:** By fundamentally eliminating sources of contamination, this technology significantly reduces the risk of batch rejections and ensures higher product quality, directly contributing to patient safety.
- **Operational Efficiency and Cost Savings:** The monolithic design and simplified cleaning protocols promise significant operational time savings. Reduced downtime for cleaning, faster tool changeovers facilitated by the aseptic bayonet lock, and extended maintenance intervals could all contribute to improved efficiency and lower operational costs compared to conventional systems.
- **Regulatory Compliance and Future-Proofing:** This work provides a proactive solution for meeting and exceeding the increasingly stringent requirements of regulatory bodies such as the EU GMP Annex 1, positioning manufacturers favourably for future compliance and market demands.

Beyond pharmaceutical manufacturing, the fundamental principles of lubricant free, particle eliminating, and hygienically designed compliant mechanisms developed here are highly transferable, offering significant potential for other demanding industries such as medical device packaging, food production, or semiconductor manufacturing.

7.6. Future Work

Building upon the insights and limitations identified, future research can be broadly categorized into direct improvements to the current design and exploration of broader applications for compliant mechanisms in aseptic and other demanding industries.

7.6.1. Improvements and Validation of Current Design

Material Transition and Comprehensive Characterization

Immediate next steps include fabricating the mechanism from production-compatible materials (PEEK, SAF2507) followed by experimental testing. This should validate fatigue performance and assess material behaviour under repeated sterilization cycles (autoclaving, VHP), characterizing conditioning effects (e.g., initial deformation in PEEK) to ensure long-term reliability. As well as confirm particle emissions are indeed minimized.

Manufacturing Process Optimization and Tolerance Analysis

Investigation into optimal manufacturing methods for scaled production is crucial. This includes exploring injection moulding for PEEK components and welding or additive manufacturing (DMLS) for metallic ($316\,\mathrm{L}$) components. As the current design is not optimized for manufacturing which results in it leaving room for improvement.

Quantitative Particle Emission and Airflow Assessment

Experimental validation using particle counters and smoke studies is crucial to quantify airborne particle generation and visually assess airflow turbulence caused by the mechanism, directly verifying compliance with ISO 14644 Class A standards. Insights from similar work showed that a compliant gripper already reduced particle generation by a lot and that the Solenoid actuator accounted for most of the particles [55]. As the desing proposed in this thesis uses a frictionless VCA actuator the particle emissions tests should yield even better results but this needs to be verified. The approach [55] can guide methodology for this testing.

Design Refinements for Enhanced Functionality and Safety

Further design refinements include:

1. **Ergonomic and Safety Enhancements:** Optimizing the design even more for glove handling as there are still some outside edges that need refinement. Rounding of all these edges and chamfers to mitigate the risk of tearing sterile gloves during manual handling.
2. **Flexure Profile Optimization:** Further optimization of tapered flexure profiles to achieve even greater stress redistribution and fatigue life.
3. **VCA Integration Alternatives:** Exploring alternative VCA configurations (e.g., internal coil, external magnet) to potentially enable dual-sided flexure support, improve LGM alignment, and simplify the overall layout.

4. **Thermal Management of VCA:** Conducting thermal analysis of the VCA under prolonged active operation, and developing cooling strategies if necessary for specific high-frequency applications.
5. **Magnetic Compatibility:** Specifically investigating the magnetic properties of Super Duplex steel if considered for VCA components, to ensure no adverse impact on actuator performance and to minimize any potential attraction forces.
6. **Rotational Lock Optimization:** Re-evaluating the bayonet lock's geometry to improve drainability, minimize flat areas where residue can accumulate, and optimize the overall design for better stress distribution and robust engagement.
7. **Modelling fillets:** It was observed that the current way of modelling the fillets in the LGM result in stress concentrations on the inside of the arc flexures. By investigating different modelling techniques this could be optimized further improving the fatique life.

Topology Optimization for Hygienic Design

Topology optimization, initial determined to be the approach to design the gripping mechanism but after initial tests deemed too extensive for this feasibility study, should be investigated. This powerful tool can systematically implement stringent hygienic design requirements (e.g., minimum internal cavities and radii) [6], offering a systematic approach to developing inherently hygienic, robust, and optimized compliant mechanisms for Grade A environments.

7.6.2. Broader Applications and Conceptual Extensions

Three Finger End Effector

Future work could explore multi-fingered gripper designs (e.g., three-fingered grippers) the three finger design would improve the stiffness performance of the design as it would be symmetric resulting in even better stiffens ratios as the second mode of the complete system would then be similar to the third mode.

End Effector Design

Alternative end□effector designs can be explored to tailor performance to specific handling tasks. A promising direction is a metamaterial□based gripper tip [93], where a periodic internal lattice (e.g., auxetic or compliant honeycomb) provides engineered compliance and distributed contact. Such tips could be designed to form to the cartridge and grip multiple cartridges simultaneously from a nest while maintaining uniform contact pressure and minimizing localized stress.

Other Applications

The findings of this feasibility study suggest that compliant, flexure-based mechanisms can be applied beyond the end effector. A spin-off thesis project has already started on the redesign identified transport "wagons" (format carriers/fixtures) as compliant assemblies to reduce particle generation and improve cleanability. Several other areas identified in the literature review could also be investigated, where the Linear Guide Mechanism (LGM) and related compliant architectures could provide clear benefits:

Filling needle Z-motion: The LGM's high axial stiffness and low parasitic deflection make it a strong candidate for precise up–down motion of filling needles, with potential to reduce sliding bearings and lubricants in Grade A zones. This would require integration with position feedback, validation of dynamic stability, and airflow impact assessment near exposed product. Stopper/vial handling modules: Compliant linear guides and grippers could replace small stroke slides and pick-and-place units (e.g., stopper feed gates, vial transfers), reducing crevice formation and simplifying CIP. Capping and crimping submechanisms: Compliant couplers and guided flexures could provide controlled, repeatable force application while eliminating lubricated pivots, subject to fatigue and force-capability validation.

Each application should follow the same validation pathway used here: analytical sizing (PRBM/CFLF-based compliance models), FEA (stress, modal separation), cleanability testing (riboflavin), airflow studies (CFD/smoke), and airborne particle measurements under operational cycles.

Alternative LGM Concepts

Research could delve into integrating alternative LGM designs directly into the gripping mechanism for higher monolithic integration. Additionally, investigating designs incorporating negative stiffness in some flexures to achieve a zero-motion stiffness mechanism could offer energy savings and improved VCA efficiency, particularly if applied selectively to the LGM.

Holistic System Validation under GMP Conditions

Beyond component level testing, a crucial next step involves rigorous validation of the entire integrated system under simulated production conditions. This includes multiple sterilization cycles, prolonged cyclic operation, and media fill tests to confirm sterility assurance and compliance with GMP guidelines.

Economic Viability and Cost-Benefit Analysis

A detailed cost-benefit analysis is needed for industrial adoption. This would compare the total lifecycle costs of the compliant mechanism against traditional aseptic robotic solutions, providing critical data for justifying investment and scaling production.

Regulatory Strategy Development

Given the novel nature of compliant mechanisms, a robust regulatory strategy is essential. This includes estab-

lishing clear validation plans, defining acceptance criteria and risks management,

Industry Expansion: Cryogenic and Space Applications

The fundamental principles of lubricant free, particle eliminating, and robust compliant mechanisms developed here are transferable. This technology holds promise for other demanding industries such as cryogenic and space applications. Adapting the material selection and design to specific environmental stresses could result in new findings.

This thesis demonstrates the feasibility of implementing compliant mechanisms tailored for aseptic pharmaceutical manufacturing. By inherently fulfilling stringent sterility requirements through its monolithic, lubricant-free operation, and incorporating advanced hygienic design principles. Offering a path to enhanced sterility assurance, reduced operational complexity, and improved efficiency in advanced pharmaceutical production. The contributions of this research lay a robust foundation for future industrial adoption, highlighting the transformative potential of compliant mechanisms in shaping the future of sterile manufacturing.

8

Conclusion

This Master of Science thesis directly addressed the overarching research question: *Compliant Mechanisms in Aseptic Pharmaceutical Manufacturing: Feasibility Study on Flexure-Based Design for Particle Elimination in Sterile Environments*. The findings strongly demonstrate the promising potential for integrating such mechanisms, effectively showing how the primary functional goal of **enabling a secure, precise grip on small, sensitive components while preserving sterility and cleanliness** can be achieved.

This investigation successfully tackled the **Primary Objectives** set at the start of this research. Firstly, the development of a gripping mechanism capable of securely holding objects between $5\,\mathrm{mm}$ to $10\,\mathrm{mm}$ in size (such as cartridges, vials, and Petri dishes) was confirmed. The Finite Element Analysis (FEA) results verified that the optimized two-fingered gripper successfully achieved a required grip motion of $7.15\,\mathrm{mm}$ with a VCA input displacement of $4\,\mathrm{mm}$. This force output is demonstrably sufficient to securely handle the specified range of objects, effectively showcasing the motion amplification and force transmission capabilities of the design.

Secondly, the objective to eliminate traditional rigid-body joints, thereby preventing sources of contamination like lubricant usage or wear induced particles, was inherently met. By replacing conventional pin joints, bearings, and sliding interfaces with flexural hinges, the primary sources of particle generation (wear debris) and microbial traps (lubricants, crevices) were fundamentally removed. This monolithic design principle represents a significant advantage over traditional robotic grippers, aligning directly with the stringent particle control requirements of Grade A aseptic environments.

Finally, the study aimed to retain operational performance in harsh sterilization conditions, such as autoclaving or exposure to aggressive cleaning agents. While the initial prototype was fabricated in Aluminum 7075 for developmental purposes, the design principles and geometry were proven compatible with pharmaceutical-grade materials. The mechanism was successfully re-optimized for Super Duplex stainless steel, and FEA demonstrated that its flexural elements operate within elastic limits (a peak stress of $403\,\mathrm{MPa}$ versus a Super Duplex yield strength of $580\,\mathrm{MPa}$, providing a safety factor of 1.44) and staying within the fatigue limit for a million cycles of $430\,\mathrm{MPa}$. This confirms the feasibility although further optimization is needed as well as tests under harsh operational and sterilization cycles.

Beyond these primary goals, the study also successfully addressed its **Secondary Objectives**. Compatibility with Clean-In-Place (CIP) or Clean-Out-of-Place (COP) procedures was ensured through the incorporation of an aseptic bayonet lock, designed for quick, tool-less disassembly, alongside rigorous hygienic design principles (e.g., minimum radii, self-draining surfaces, avoidance of dead legs). Preliminary assessments based on riboflavin test principles confirmed high cleanability, with identified areas guiding further geometric refinements. Furthermore, the compact design of both the Linear Guide Mechanism (LGM) and Gripping Mechanism (GM), optimized for the VCA's envelope, facilitates seamless integration into existing robotic manipulators, minimizing overall size and weight. The monolithic nature of compliant mechanisms inherently leads to a reduced part count, which in turn simplifies assembly, reduces potential failure points, and thus enhances overall reliability.

Key Contributions

This work provided several significant contributions to the field. It advanced the design and analysis of compliant mechanisms by refining a analytical model for a linear guiding mechnism to include corner-filleted arc leaf flexures, which accurately predicted stiffness for the LGM. The effective application of Pseudo-Rigid Body Models (PRBMs) for gripper kinematics further enhanced robust analysis of motion amplification and force transmission.

Crucially, the study demonstrated the successful transfer and re-optimization of a complex compliant mechanism design from a prototyping material (Aluminum 7075) to a high-performance, aseptic-grade material (Super Duplex stainless steel) while maintaining validated performance. Ultimately, this research established a comprehensive design methodology that holistically integrates mechanical performance with the stringent material and hygienic requirements unique to Grade A aseptic pharmaceutical manufacturing.

Concluding Outlook

This thesis conclusively demonstrates the feasibility of implementing compliant mechanisms tailored for aseptic pharmaceutical manufacturing. By fulfilling stringent sterility requirements through its monolithic, lubricant-free operation and incorporating advanced hygienic design principles, this work represents a significant step towards next-generation automation. It bridges critical gaps between mechanical innovation and the rigorous demands of Grade A cleanroom compatibility, offering a path to enhanced sterility assurance, reduced operational complexity, and improved efficiency in advanced pharmaceutical production lines. The successful feasibility demonstration in this thesis lays a robust foundation for future industrial adoption, highlighting the transformative potential of compliant mechanisms in shaping the future of sterile manufacturing.

References

[1] Larry L. Howell. “Compliant Mechanisms”. In: *21st Century Kinematics*. Ed. by J. Michael McCarthy. London: Springer London, 2013, pp. 189–216. ISBN: 978-1-4471-4510-3.

[2] Estefania Hermoza Llanos et al. “Systematic mapping of synthesis methods for compliant grippers using PRISMA”. In: *Mechanism and Machine Theory* 206 (2025), p. 105900. ISSN: 0094-114X. DOI: https://doi.org/10.1016/j.mechmachtheory.2024.105900. URL: https://www.sciencedirect.com/science/article/pii/S0094114X24003276.

[3] Minchang Wang et al. “Micro-scale Realization of Compliant Mechanisms: Manufacturing Processes and Constituent Materials—A Review”. In: *Chinese Journal of Mechanical Engineering (English Edition)* 34.1 (2021), pp. 1–22. DOI: 10.1186/s10033-021-00606-y. URL: https://doi.org/10.1186/s10033-021-00606-y.

[4] HBM. *Hygienic design is mandatory*. https://www.hbm.com/3232/hygienic-design-is-mandatory/. Published: January 26, 2021. 2021.

[5] Tim Sandle. “Best Practices for Cleaning and Disinfection”. In: (Nov. 2020).

[6] Dorota Budzyń et al. “Implicit lunar dust mitigation technology: Compliant mechanisms”. In: *Acta Astronautica* 203 (2023), pp. 146–156. ISSN: 0094-5765. DOI: https://doi.org/10.1016/j.actaastro.2022.11.042. URL: https://www.sciencedirect.com/science/article/pii/S0094576522006506.

[7] European Commission. *The Rules Governing Medicinal Products in the European Union*. Volume 4: EU Guidelines for Good Manufacturing Practice for Medicinal Products for Human and Veterinary Use - Annex 1: Manufacture of Sterile Medicinal Products. Published: 22 August 2022. Accessed: [INSERT ACCESS DATE]. 2022. URL: https://health.ec.europa.eu/system/files/2022-08/20220825_gmp-an1_en_0.pdf.

[8] Tim Sandle. “Chapter 3 - GMP, Regulations and Standards”. In: *Biocontamination Control for Pharmaceuticals and Healthcare*. Ed. by Tim Sandle. Academic Press, 2019, pp. 27–46. ISBN: 978-0-12-814911-9. DOI: https://doi.org/10.1016/B978-0-12-814911-9.00003-1. URL: https://www.sciencedirect.com/science/article/pii/B9780128149119000031.

[9] International Organization for Standardization. *ISO 14644-1:2015 Cleanrooms and associated controlled environments — Part 1: Classification of air cleanliness by particle concentration*. International Standard. Confirmed in 2021. Geneva, Switzerland: International Organization for Standardization, Dec. 2015. URL: https://www.iso.org/standard/53394.html.

[10] U.S. National Archives and Records Administration. *21 CFR § 211.67 — Equipment cleaning and maintenance*. Code of Federal Regulations. Current as of May 9, 2023. Amended at 73 FR 51931, Sept. 8, 2008. 2023. URL: https://www.ecfr.gov/current/title-21/section-211.67.

[11] United States Pharmacopeial Convention. *<788> Particulate Matter in Injections*. United States Pharmacopeia-National Formulary. Current through Revision 1, May 1, 2023. 2023. URL: https://www.usp.org/compendium/content/788-particulate-matter-in-injections-general-chapter/ (visited on 10/25/2023).

[12] Matthew J Page et al. “The PRISMA 2020 statement: an updated guideline for reporting systematic reviews”. In: *BMJ* (2021), n71. DOI: 10.1136/bmj.n71.

[13] Mourad Ouzzani et al. “Rayyan—a web and mobile app for systematic reviews”. In: *Syst. Rev.* 5.1 (Dec. 2016).

[14] International Organization for Standardization. *Biological evaluation of medical devices — Part 1: Evaluation and testing within a risk management process*. International Standard. Edition 5. Corrected versions: 2018-10 (en/fr). To be replaced by ISO/FDIS 10993-1. Part of the ISO 10993 series on biological evaluation of medical devices. Geneva, Switzerland, 2018. URL: https://www.iso.org/standard/68936.html (visited on 10/25/2023).

[15] Patrick Dick. *The Importance of USP Class VI Testing*. Sponsored content by SilcoTek Corp. Describes USP Class VI biocompatibility testing protocols and material certification process. 2024. URL: https://www.qmed.com/mpmn/article/importance-usp-class-vi-testing (visited on 06/03/2024).

[16] ASME. *ASME BPE: Bioprocessing Equipment Standard*. Standard. 2022. URL: https://www.asme.org/codes-standards/find-codes-standards/bpe-bioprocessing-equipment-(1) (visited on 10/25/2023).

[17] International Organization for Standardization. *Cleanrooms and associated controlled environments — Part 3: Test methods*. International Standard. 2019. URL: https://www.iso.org/standard/80271.html (visited on 10/25/2023).

[18] International Organization for Standardization. *Cleanrooms and associated controlled environments — Part 1: Classification of air cleanliness by particle concentration*. International Standard. 2022. URL: https://www.iso.org/standard/63841.html (visited on 10/25/2023).

[19] International Organization for Standardization. *Medical devices — Quality management systems — Requirements for regulatory purposes*. International Standard. 2016. URL: https://www.iso.org/standard/56137.html (visited on 10/25/2023).

[20] International Organization for Standardization. *Sterilization of health care products — Moist heat — Requirements for the development, validation and routine control of a sterilization process for medical devices*. International Standard. First edition. Replaces ISO 17665-1:2006, ISO/TS 17665-2:2009, and ISO/TS 17665-3:2013. Part of the ISO 17665 series. 154 pages. ICS 11.080.01. Geneva, Switzerland, 2024. URL: https://www.iso.org/standard/80271.html (visited on 10/25/2023).

[21] International Organization for Standardization. *Sterilization of health care products — Radiation — Part 1: Requirements for the development, validation and routine control of a sterilization process for medical devices*. International Standard. Second edition. Replaces ISO 11137-1:2006. Part of the ISO 11137 series on radiation sterilization. 39 pages. ICS 11.080.01. Geneva, Switzerland, 2025. URL: https://www.iso.org/standard/81721.html (visited on 10/25/2023).

[22] International Organization for Standardization. *Biological evaluation of medical devices — Part 7: Ethylene oxide sterilization residuals*. International Standard. Edition 2. Includes Corrigendum 1:2009 and Amendment 1:2019 (neonatal/infant limits). 86 pages. ICS 11.100.20. To be replaced by ISO/FDIS 10993-7. Part of the ISO 10993 series on biological evaluation. Geneva, Switzerland, 2008. URL: https://www.iso.org/standard/34213.html (visited on 10/25/2023).

[23] International Organization for Standardization. *Sterilization of health care products — Low temperature vaporized hydrogen peroxide — Requirements for the development, validation and routine control of a sterilization process for medical devices*. International Standard. First edition. 79 pages. ICS 11.080.01. Specifies VH□O□ sterilization processes for medical devices, excluding decontamination systems and prion inactivation. References EN 556-1 and ANSI/AAMI ST67. Geneva, Switzerland, 2022. URL: https://www.iso.org/standard/73214.html (visited on 10/25/2023).

[24] International Organization for Standardization. *Sterilization of health care products — Dry heat — Requirements for the development, validation and routine control of a sterilization process for medical devices*. International Standard. First edition. Confirmed in 2022. 58 pages. ICS 11.080.01. Covers dry heat sterilization and depyrogenation processes. Part of ISO sterilization standards series. Geneva, Switzerland, 2010. URL: https://www.iso.org/standard/39778.html (visited on 10/25/2023).

[25] U.S. Food and Drug Administration. *21 CFR § 178.1010 — Sanitizing solutions*. Code of Federal Regulations. Current as of May 12, 2023. Specifies permissible sanitizing solutions for food-contact surfaces, including chemical composition limits. Includes multiple subsections detailing allowed components and concentrations. May 12, 2023. URL: https://www.ecfr.gov/current/title-21/chapter-I/subchapter-B/part-178/subpart-B/section-178.1010 (visited on 10/25/2023).

[26] William A. Rutala and David J. Weber. "301 - Disinfection, Sterilization, and Control of Hospital Waste". In: *Mandell, Douglas, and Bennett's Principles and Practice of Infectious Diseases (Eighth Edition)*. Ed. by John E. Bennett, Raphael Dolin, and Martin J. Blaser. Eighth Edition. Philadelphia: W.B. Saunders, 2015, 3294–3309.e4. ISBN: 978-1-4557-4801-3. DOI: https://doi.org/10.1016/B978-1-4557-4801-3.00301-5. URL: https://www.sciencedirect.com/science/article/pii/B9781455748013003015.

[27] Tim Sandle. "Chapter 17 - Assessing, Controlling, and Removing Contamination Risks From the Process". In: *Biocontamination Control for Pharmaceuticals and Healthcare*. Ed. by Tim Sandle. Academic Press, 2019, pp. 287–314. ISBN: 978-0-12-814911-9. DOI: https://doi.org/10.1016/B978-0-12-814911-9.00017-1. URL: https://www.sciencedirect.com/science/article/pii/B9780128149119000171.

[28] Igor Gorsky. "Chapter 4 - Equipment Cleaning Process". In: *Principles of Parenteral Solution Validation*. Ed. by Igor Gorsky and Harold S. Baseman. Academic Press, 2020, pp. 81–96. ISBN: 978-0-12-809412-9. DOI: https://doi.org/10.1016/B978-0-12-809412-9.00003-4. URL: https://www.sciencedirect.com/science/article/pii/B9780128094129000034.

[29] European Medicines Agency. *Guideline on the sterilisation of the medicinal product, active substance, excipient and primary container*. Scientific guideline EMA/CHMP/CVMP/QWP/850374/2015. Effective from 1 October 2019. Replaces CPMP/QWP/054/98 and EMEA/CVMP/065/99.

Adopted by CHMP: 15 Nov 2018, CVMP: 6 Dec 2018. EMA, 2019. URL: https://www.ema.europa.eu/en/documents/scientific-guideline/guideline-sterilisation-medicinal-product-active-substance-excipient-primary-container_en.pdf (visited on 10/25/2023).

[30] U.S. Food and Drug Administration. *Aseptic Processing and Packaging for the Food Industry*. Inspection Guide GUIDE TO INSPECTIONS OF ASPECTIC PROCESSING AND PACKAGING FOR THE FOOD INDUSTRY. Updated: 2005-07-14. Reference materials for investigators and FDA personnel. FDA, 2005. URL: https://www.fda.gov/inspections-compliance-enforcement-and-criminal-investigations/inspection-guides/aseptic-processing-and-packaging-food-industry (visited on 10/25/2023).

[31] SECU-CHEK GmbH. *Riboflavin test for Cleaning Validation*. Product page describing UV-LED lamps for industrial riboflavin testing in cleaning validation. 2023. URL: https://www.secu-chek.de/en/riboflavin-testing/ (visited on 10/25/2023).

[32] STERIS. *Biological Indicators. STERIS Knowledge Center - Sterile Processing*. Published April 12, 2017; Updated February 5, 2020. STERIS Healthcare. Feb. 5, 2020. URL: https://www.steris.com/healthcare/knowledge-center/sterile-processing/biological-indicators (visited on 10/25/2023).

[33] Jyoti Salgar, Sanjay Bais, and Reshma Mule. "Review on Biological Indicator". In: *International Journal of Advanced Research in Science, Communication and Technology* (Dec. 2023), pp. 22–43. DOI: 10.48175/IJARSCT-14302.

[34] STERIS. *What is a Chemical Indicator? STERIS Knowledge Center - Sterile Processing*. References ANSI/AAMI ST79:2017 and ISO 14161 standards. STERIS Healthcare. June 16, 2022. URL: https://www.steris.com/healthcare/knowledge-center/sterile-processing/what-is-a-chemical-indicator (visited on 10/25/2023).

[35] STERIS Applied Sterilization Technologies (AST). *EO Residual Testing Solutions | Laboratory Testing Services | STERIS AST. Laboratory Testing Services for Ethylene Oxide Residuals*. References ISO 10993-7 and AAMI TIR 19 standards. STERIS Applied Sterilization Technologies. 2023. URL: https://www.steris-ast.com/services/laboratory-testing-services/eo-residual-testing/ (visited on 10/25/2023).

[36] Frits A. Boom et al. "Microbiological monitoring during aseptic handling: Methods, limits and interpretation of results". In: *European Journal of Pharmaceutical Sciences* 155 (2020), p. 105540. ISSN: 0928-0987. DOI: https://doi.org/10.1016/j.ejps.2020.105540. URL: https://www.sciencedirect.com/science/article/pii/S0928098720303286.

[37] STERIS plc. *Riboflavin Coverage Test. Validation of Clean-in-Place (CIP) System Spray Coverage*. Technical Tip from STERIS Technical Learning Library. STERIS Life Sciences. Dec. 1, 2020. URL: https://www.steris.com/tech-lab/riboflavin-coverage-test (visited on 10/25/2023).

[38] Quadrant Engineering Plastic Products. *Technical Data Sheet: PEEK (PolyEtherketone)*. Tech. rep. Properties include mechanical, thermal, electrical characteristics for virgin and filled PEEK grades. Covers ASTM test methods and typical values for injection molded, extruded, and compression molded forms. Quadrant EPP, 2023. URL: https://www.quadrantepp.com/products/peek/ (visited on 10/25/2023).

[39] Pedro Rendas et al. "High-Cycle Fatigue Behaviour of Polyetheretherketone (PEEK) Produced by Additive Manufacturing". In: *Polymers* 16 (Dec. 2023), p. 18. DOI: 10.3390/polym16010018.

[40] .

[41] K. Saeidi et al. "316L stainless steel designed to withstand intermediate temperature". In: *Materials Design* 135 (2017), pp. 1–8. ISSN: 0264-1275. DOI: https://doi.org/10.1016/j.matdes.2017.08.072. URL: https://www.sciencedirect.com/science/article/pii/S026412751730833X.

[42] Andrea Zaffora, Francesco Di Franco, and Monica Santamaria. "Corrosion of stainless steel in food and pharmaceutical industry". In: *Current Opinion in Electrochemistry* 29 (2021), p. 100760. ISSN: 2451-9103. DOI: https://doi.org/10.1016/j.coelec.2021.100760. URL: https://www.sciencedirect.com/science/article/pii/S2451910321000740.

[43] The Chemours Company. *Technical Data Sheet: Teflon® (PTFE) - Polytetrafluoroethylene Resin*. Tech. rep. Typical properties of unfilled, 25% glass-filled, and 25% carbon-filled PTFE. Includes mechanical, thermal, and electrical characteristics. Values for reference only - not for design specifications. Wilmington, DE, USA: Chemours, 2023. URL: https://www.chemours.com/en/brands/teflon (visited on 10/25/2023).

[44] Andrea Tanzini et al. “Robotics and Aseptic Processing in View of Regulatory Requirements”. In: *Pharmaceutics* 15.6 (2023). ISSN: 1999-4923. DOI: 10.3390/pharmaceutics15061581. URL: https://www.mdpi.com/1999-4923/15/6/1581.

[45] LifeSciences Lab Automation. *LGR Pneumatic Gripper - Laboratory Automation Gripping System*. Product page for low-profile pneumatic gripper with 62mm stroke, dual piston design, and ISO-compliant mounting. Features landscape/portrait orientation handling and 3 million cycle durability. 2023. URL: https://www.lifesciencesla bautomation.com/products/pneumatic-gripper (visited on 05/04/2023).

[46] Weiss Robotics GmbH & Co. KG. *STERIGRIP Series Servo-electric Grippers*. Aseptic servo-electric gripper modules for pharmaceutical cleanrooms, GMP Class A certified. Weiss Robotics. Ludwigsburg, Germany, 2023. URL: https://www.weiss-robotics.com/en/products/servo-electric-grippers/sterigrip-series/ (visited on 10/25/2023).

[47] GripWiq ApS. *SofTouch Robotic Vacuum Grippers*. Product page detailing FDA/EC-compliant vacuum grippers (GR-400/500/600 series) for food packaging applications. Features include flexible vacuum range (200-400 mbar), payloads up to 6kg, and hygienic design. 2024. URL: https://www.gripwiq.com/solutions/robotic-vacuum-grippers/ (visited on 10/25/2023).

[48] Patrick Jahn et al. “Roboterkomponenten für den kryogenen Arbeitsraum: Entwicklung von Festkörpergelenken und monolithischen Greifersystemen für eine Parallelroboterstruktur”. In: *Deutsche Kälte- und Klimatagung 2020*. Conference paper on cryogenic robotic components (in German). Hannover, Germany: DKV, 2020. DOI: 10.15488/13371.

[49] IGUS GmbH. *Clean bearing arrangement in the cost-effective gripper for microtiter plates in the laboratory*. Product page for laboratory automation grippers. 2023. URL: https://www.igus.eu/info/gripper-for-handling-unit-in-labs (visited on 05/04/2023).

[50] MONOLITIX GmbH. *Produktübersicht Rote Serie*. Product catalog for MONOLITIX Red Series components. 2023. URL: http://www.monolitix.com/117-0-Produktuebersicht-Rote-Serie.html (visited on 05/04/2023).

[51] Philipp Jahn, Frank Ihmig, and Annika Raatz. “Design of a parallel robot with additively manufactured flexure hinges for a cryogenic work environment”. In: *Procedia CIRP* 103 (2021). 9th CIRP Global Web Conference – Sustainable, resilient, and agile manufacturing and service operations : Lessons from COVID-19, pp. 280–285. ISSN: 2212-8271. DOI: https://doi.org/10.1016/j.procir.2021.10.045. URL: https://www.sciencedirect.com/science/article/pii/S2212827121008866.

[52] Hanwen Cao et al. “Design and Optimization of an Origami Gripper for Versatile Grasping and Manipulation”. In: *Advanced Intelligent Systems* 6 (Oct. 2024). DOI: 10.1002/aisy.202400271.

[53] Nicolas Mouazé and Lionel Birglen. “Bistable compliant underactuated gripper for the gentle grasp of soft objects”. In: *Mechanism and Machine Theory* 170 (2022), p. 104676. ISSN: 0094-114X. DOI: https://doi.org/10.1016/j.mechmachtheory.2021.104676. URL: https://www.sciencedirect.com/science/article/pii/S0094114X21004067.

[54] F. Ruiz, B.C. Arrue, and A. Ollero. “Thermally-Resilient Soft Gripper for On-Orbit Operations”. In: *2024 IEEE/RSJ International Conference on Intelligent Robots and Systems (IROS)*. 2024, pp. 14050–14055. DOI: 10.1109/IROS58592.2024.10801537.

[55] Leon Budde et al. “Achieving near-zero particle generation by simplicity of design—A compliant-mechanism-based gripper for clean-room environments”. In: *SLAS Technology* 29.4 (2024), p. 100148. ISSN: 2472-6303. DOI: https://doi.org/10.1016/j.slast.2024.100148. URL: https://www.sciencedirect.com/science/article/pii/S247263032400030X.

[56] Philipp Jahn et al. “Roboterkomponenten für den kryogenen Arbeitsraum: Entwicklung von Festkörpergelenken und monolithischen Greifersystemen für eine Parallelroboterstruktur”. In: *Deutsche Kälte- und Klimatagung (DKV-Tagung) 2020*. Conference paper on cryogenic robotics components for parallel manipulator systems. Online: Deutscher Kälte- und Klimatechnischer Verein e.V. (DKV), 2020, pp. 2–14.

[57] Chih-Hsing Liu, Fu-Ming Chung, and Yuan-Ping Ho. “Topology Optimization for Design of a 3D-Printed Constant-Force Compliant Finger”. In: *IEEE/ASME Transactions on Mechatronics* PP (May 2021), pp. 1–1. DOI: 10.1109/TMECH.2021.3077947.

[58] Zhaoqi Zheng et al. “Design and Optimization of Electromagnetically Driven End-Effector”. In: *Proceedings of the Institution of Mechanical Engineers, Part C: Journal of Mechanical Engineering Science* 239 (Nov. 2024). DOI: 10.1177/09544062241296809.

[59] Matthew Lofroth and Ebubekir Avci. “Development of a Novel Modular Compliant Gripper for Manipulation of Micro Objects”. In: *Micromachines* 10.5 (2019). ISSN: 2072-666X. DOI: 10.3390/mi10050313. URL: https://www.mdpi.com/2072-666X/10/5/313.

[60] Chih-Hsing Liu, Fu-Ming Chung, and Yuan-Ping Ho. “Topology Optimization for Design of a 3D-Printed Constant-Force Compliant Finger”. In: *IEEE/ASME Transactions on Mechatronics* PP (May 2021), pp. 1–1. DOI: 10.1109/TMECH.2021.3077947.

[61] Mingdong Zhou et al. “Minimum length scale in topology optimization by geometric constraints”. In: *Computer Methods in Applied Mechanics and Engineering* 293 (2015), pp. 266–282. ISSN: 0045-7825. DOI: https://doi.org/10.1016/j.cma.2015.05.003. URL: https://www.sciencedirect.com/science/article/pii/S0045782515001693.

[62] Eduardo Fernández et al. “Imposing minimum and maximum member size, minimum cavity size, and minimum separation distance between solid members in topology optimization”. In: *Computer Methods in Applied Mechanics and Engineering* 368 (2020), p. 113157. ISSN: 0045-7825. DOI: https://doi.org/10.1016/j.cma.2020.113157. URL: https://www.sciencedirect.com/science/article/pii/S004578252030342X.

[63] JPE, Inc. *Cryogenic Voice Coil Actuator Series Technical Specifications*. High-precision linear actuators for cryogenic environments (4K-300K). Features include ultra-high vacuum compatibility, non-magnetic variants, and custom stroke/force configurations. Dayton, OH, USA, 2023. URL: https://www.jpe.com/products/cryo-voice-coil-actuators (visited on 10/25/2023).

[64] S.K. Nah and Z.W. Zhong. “A microgripper using piezoelectric actuation for micro-object manipulation”. In: *Sensors and Actuators A: Physical* 133.1 (2007), pp. 218–224. ISSN: 0924-4247. DOI: https://doi.org/10.1016/j.sna.2006.03.014. URL: https://www.sciencedirect.com/science/article/pii/S0924424706002305.

[65] Guancheng Liu et al. “Magnetic Levitation Actuation and Motion Control System with Active Levitation Mode Based on Force Imbalance”. In: *Applied Sciences* 13.2 (2023). ISSN: 2076-3417. DOI: 10.3390/app13020740. URL: https://www.mdpi.com/2076-3417/13/2/740.

[66] Ganapathy Then Mozhi, Kaliaperumal Dhanalakshmi, and Seung-Bok Choi. “Design and Control of Monolithic Compliant Gripper Using Shape Memory Alloy Wires”. In: *Sensors* 23.4 (2023). ISSN: 1424-8220. DOI: 10.3390/s23042052. URL: https://www.mdpi.com/1424-8220/23/4/2052.

[67] S. Lakshmana Prabu et al. “Chapter 3 - GMP in Pharma Manufacturing—Description of GMP as Related to Air-Handling Units and Prevention of Contamination and Implementation of GMP Regulatory Requirements”. In: *Developments in Surface Contamination and Cleaning: Types of Contamination and Contamination Resources*. Ed. by Rajiv Kohli and K.L. Mittal. William Andrew Publishing, 2017, pp. 85–123. ISBN: 978-0-323-43158-3. DOI: https://doi.org/10.1016/B978-0-323-43158-3.00005-8. URL: https://www.sciencedirect.com/science/article/pii/B9780323431583000058.

[68] Ram Alloys, LLC. *Duplex S31803 (2205) & Super Duplex S32750 (2507) Stainless Steel*. Product page detailing chemical/mechanical properties of duplex stainless steels S31803 and S32750. Includes composition tables and mechanical specs. 2023. URL: https://www.ramalloys.com/stainless-nickel-products/stainless-round-bar/duplex-s31803-2205-super-duplex-s32750/ (visited on 10/25/2023).

[69] Silvia Cecchel, Davide Ferrario, and Giovanna Cornacchia. “Heat treatments of EN AW 6082 aluminum forging alloy: effect on microstructure and mechanical properties”. In: *La Metallurgia Italiana* 112.3 (2020). Study of T5/T6 heat treatments on EN AW 6082 aluminum forgings for automotive applications. Includes DOE methodology and mechanical characterization., pp. 6–13. URL: https://www.aimnet.it/lmi/2020/03/ (visited on 10/25/2023).

[70] Gallagher Corporation. *Polyurethane’s Temperature Range: Minimum and Maximum Operational Temperatures*. Tech. rep. Technical guide on polyurethane performance across temperature ranges (-62°C to 150°C). Includes DMA analysis, thermal expansion data, and application design considerations. Warsaw, IN, USA: Gallagher Corporation, 2023. URL: https://www.gallaghercorp.com/resources/polyurethane-temperature-range (visited on 10/25/2023).

[71] Gteek Ltd. *High Temperature Resistant EPDM Rubber Sheet*. Product page detailing high-temp EPDM rubber sheets (-40°C to +150°C). Includes WRAS certification, FDA compliance options, and industrial applications. 2023. URL: https://www.gteek.com/elastomeric-products/epdm-sheetings/high-temperature-resistant-epdm-rubber (visited on 10/25/2023).

[72] K.D. Feddersen GmbH & Co. KG. *Polypropylene (PP) Technical Data Sheet*. Technical datasheet for PP including thermal, electrical, mechanical properties and processing methods. Covers applications in injection molding, extrusion, and blow molding. 2023. URL: https://www.kdfeddersen.

com / polymers / polypropylene - pp/ (visited on 10/25/2023).

[73] Magnetic Innovations. *Direct Drive Technology: Torque Motors, Linear Voice Coil Actuator, EC Fan Motor, Belt Drive Motor*. Accessed: 2025-12-05. 2025. URL: https://www.magneticinnovations.com/?utm_term&utm_campaign=Torque%20motor%20-%20Test%20Doelgroepen&utm_source=adwords&utm_medium=ppc&hsa_acc=1696433178&hsa_cam=22150531560&hsa_grp=177494371361&hsa_ad=730227940227&hsa_src=g&hsa_tgt=dsa-3500001&hsa_kw&hsa_mt=b&hsa_net=adwords&hsa_ver=3&gad_source=1&gad_campaignid=22150531560&gclid=Cj0KCQiAosrJBhD0ARIsAHebCNq_v7P6010o-8ThumGe5F8z_Iqcrah7OMpcq-w014XJy3cMSZTolMcaAjw3EALw_wcB.

[74] Miao Yang et al. "A Long-Stroke Nanopositioning Stage With Annular Flexure Guides". In: *IEEE/ASME Transactions on Mechatronics* PP (July 2021), pp. 1–1. DOI: 10.1109/TMECH.2021.3100537.

[75] Tinghao Liu and Guangbo Hao. "Design of a Cylindrical Compliant Linear Guide with Decoupling Parallelogram Mechanisms". In: *Micromachines* 13.8 (2022). ISSN: 2072-666X. DOI: 10.3390/mi13081275. URL: https://www.mdpi.com/2072-666X/13/8/1275.

[76] Fujun Wang et al. "A 2-DOF nano-positioning scanner with novel compound decoupling-guiding mechanism". In: *Mechanism and Machine Theory* 155 (2021), p. 104066. ISSN: 0094-114X. DOI: https://doi.org/10.1016/j.mechmachtheory.2020.104066. URL: https://www.sciencedirect.com/science/article/pii/S0094114X2030286X.

[77] Shorya Awtar and Alexander H. Slocum. "Flexure Systems based on a Symmetric Diaphragm Flexure". In: *Proceedings of ASME IDETC/CIE* (2005). Paper 85440; Precision Engineering Research Group, Massachusetts Institute of Technology.

[78] Ruiqi Li et al. "Analytical solutions for nonlinear deflections of corner-fillet leaf-springs". In: *Mechanism and Machine Theory* 157 (2021), p. 104182. ISSN: 0094-114X. DOI: https://doi.org/10.1016/j.mechmachtheory.2020.104182. URL: https://www.sciencedirect.com/science/article/pii/S0094114X20303992.

[79] Walter Crupano et al. "Investigating mechanical properties of 3D printed polylactic acid / poly-3-hydroxybutyrate composites. Compressive and fatigue performance". In: *Heliyon* 10.18 (2024), e38066. ISSN: 2405-8440. DOI: https://doi.org/10.1016/j.heliyon.2024.e38066. URL: https://www.sciencedirect.com/science/article/pii/S2405844024140972.

[80] Z. Lyu, A. Purwar, and W. Liao. "A Unified Real-Time Motion Generation Algorithm for Approximate Position Analysis of Planar N-Bar Mechanisms". In: *ASME. Journal of Mechanical Design* 146.6 (2024), p. 063302. DOI: 10.1115/1.4064132. URL: https://doi.org/10.1115/1.4064132.

[81] M. Schevenels, B.S. Lazarov, and O. Sigmund. "Robust topology optimization accounting for spatially varying manufacturing errors". In: *Computer Methods in Applied Mechanics and Engineering* 200.49 (2011), pp. 3613–3627. ISSN: 0045-7825. DOI: https://doi.org/10.1016/j.cma.2011.08.006. URL: https://www.sciencedirect.com/science/article/pii/S0045782511002611.

[82] Alexander Slocum. "Kinematic couplings: A review of design principles and applications". In: *International Journal of Machine Tools and Manufacture* 50.4 (2010). Design of Ultraprecision and Micro Machine Tools and their Key Enabling Technologies, pp. 310–327. ISSN: 0890-6955. DOI: https://doi.org/10.1016/j.ijmachtools.2009.10.006. URL: https://www.sciencedirect.com/science/article/pii/S0890695509002090.

[83] Bayer MaterialScience. *Snap-Fit Joints for Plastics: A Design Guide*. Technical brochure / design guide (online or print). Includes design principles, calculation examples, and tables for cantilever, torsion, and annular snap joints; health and safety information. Bayer MaterialScience LLC, 100 Bayer Road, Pittsburgh, PA 15205, USA, n.d. URL: n.d..

[84] Gerrit Newton. *Releasable fastening without fasteners: An overview of snap-fit connections in sheet metal and tube assemblies*. The Fabricator (online). Article; Assembly and Joining. Newton Innovations — van der Kamlaan 62, Delft, 2625 KN Netherlands. Publisher: FMA Communications, Inc. Accessed: 2025-12-05. 2023. URL: https://www.thefabricator.com/articles/assembly/releasable-fastening-without-fasteners.

[85] Larry L. Howell, Spencer P. Magleby, and Brian M. Olsen, eds. *Handbook of Compliant Mechanisms*. 1st. Editors: Larry L. Howell, Spencer P. Magleby, Brian M. Olsen. Hoboken, NJ, USA: John Wiley Sons, 2013. ISBN: 978-1119998126.

[86] Hemesh Patil and P V Jeyakarthikeyan. "Mesh convergence study and estimation of discretization error of hub in clutch disc with integration of ANSYS". In: *IOP Conference Series: Materials Science and Engineering* 402 (Oct. 2018), p. 012065. DOI: 10.1088/1757-899X/402/1/012065.

[87] Pedro Rendas et al. “High-Cycle Fatigue Behaviour of Polyetheretherketone (PEEK) Produced by Additive Manufacturing”. In: *Polymers* 16 (Dec. 2023), p. 18. DOI: 10.3390/polym16010018.

[88] Andrew Sales, Andrei Kotousov, and Ling Yin. “Design against Fatigue of Super Duplex Stainless Steel Structures Fabricated by Wire Arc Additive Manufacturing Process”. In: *Metals* 11.12 (2021). ISSN: 2075-4701. DOI: 10.3390/met11121965. URL: https://www.mdpi.com/2075-4701/11/12/1965.

[89] Dalian Yang et al. “Effects of Prebending Radii on Microstructure and Fatigue Performance of Al-Zn-Mg-Cu Aluminum Alloy after Creep Age Forming”. In: *Metals* 9 (May 2019), p. 630. DOI: 10.3390/met9060630.

[90] M.M. Rababah et al. “Continuum damage analysis, experimental and simulation for investigating the fatigue life performance of 316L steel at high temperatures”. In: *International Journal of Materials and Structural Integrity* 11 (Jan. 2017), p. 175. DOI: 10.1504/IJMSI.2017.10010823.

[91] Freek Broeren. *CV$_{c}ompliantGripper$*. GitLab repository. Project ID: 26957; files include src/, main.py, pyproject.toml, .gitignore, uv.lock. Auto DevOps enabled. 2025. URL: https://gitlab.com/USERNAME/CV_compliantGripper.

[92] Jon Freire G’omez, Julian D. Booker, and Phil H. Mellor. *Stress optimization of leaf-spring crossed flexure pivots for an active Gurney flap mechanism*. University of Bristol Research Repository (preprint / institutional record). Link to published version: 10.1117/12.2082890. Copyright 2016 SPIE. Replace URL with the actual Bristol Research Portal link if available. 2015. URL: https://research-information.bris.ac.uk/ENRICHED_RECORD_LINK_OR_PDF.

[93] Ahmad Rafsanjani, Abdolhamid Akbarzadeh, and Damiano Pasini. “Snapping Mechanical Metamaterials under Tension”. In: *Advanced Materials* 27 (2015). Communication. Published online: 28 August 2015. Copyright 2015 WILEY-VCH Verlag GmbH Co. KGaA, Weinheim., pp. 5931–5935. DOI: 10.1002/adma.201502809. URL: https://doi.org/10.1002/adma.201502809.

A

Analytical Five-bar Compliant Gripper Mechanism (PRBM Based)

```
clear; clc; close all;

%% ===== MECHANISM PARAMETERS =====
params = struct();

% Ground and slider coordinates
params.GAx = 8e-3;          % Ground pivot A, x-coordinate (m)
params.GAy = 40e-3;         % Ground pivot A, y-coordinate (m)
params.y0  = 5e-3;          % Slider height (m)

% Link lengths
params.la = 47.27e-3;       % Bar A length (m)
params.lb = 53.15e-3;       % Bar B length (m)
params.lc = 7.071e-3;       % Coupler length (m)

% Initial stress-free angles (calculated from nominal geometry at x_ref = 20mm)
A_vec = [55e-3 - params.GAx; 45e-3 - params.GAy];
params.theta_A0_nominal = atan2(A_vec(2), A_vec(1));

B_vec = [60e-3 - 20e-3; 40e-3 - params.y0];
params.theta_B0_nominal = atan2(B_vec(2), B_vec(1));

C_vec = [60e-3 - 55e-3; 40e-3 - 45e-3];
params.theta_C0_nominal = atan2(C_vec(2), C_vec(1));

fprintf('====␣MECHANISM␣ANALYSIS␣-␣SIMPLIFIED␣SINGLE␣DOF␣METHOD␣====\n');
fprintf('Nominal␣Stress-Free␣Angles:\n');
fprintf('␣␣ _A0_nominal␣=␣%.6f␣rad␣(%.3f°)\n', params.theta_A0_nominal, rad2deg(params.theta_A0_nominal));
fprintf('␣␣ _B0_nominal␣=␣%.6f␣rad␣(%.3f°)\n', params.theta_B0_nominal, rad2deg(params.theta_B0_nominal));
fprintf('␣␣ _C0_nominal␣=␣%.6f␣rad␣(%.3f°)\n', params.theta_C0_nominal, rad2deg(params.theta_C0_nominal));

% Solve kinematics at reference position
x_ref = 20e-3;
[theta_A_solved, theta_B_solved, theta_C_solved, success] = solveKinematics_initial(x_ref, params);

if success
    % Use solved values (these ensure kinematic consistency)
    params.theta_A0 = theta_A_solved;
    params.theta_B0 = theta_B_solved;
    params.theta_C0 = theta_C_solved;

    fprintf('\nCorrected␣Stress-Free␣Angles␣(from␣kinematic␣solver):\n');
    fprintf('␣␣ _A0␣=␣%.6f␣rad␣(%.3f°)\n', params.theta_A0, rad2deg(params.theta_A0));
    fprintf('␣␣ _B0␣=␣%.6f␣rad␣(%.3f°)\n', params.theta_B0, rad2deg(params.theta_B0));
    fprintf('␣␣ _C0␣=␣%.6f␣rad␣(%.3f°)\n', params.theta_C0, rad2deg(params.theta_C0));

    fprintf('\nAngle␣Corrections:\n');
```

```
    fprintf('  Δ_A = %.6f rad (%.4f°)\n', theta_A_solved - params.theta_A0_nominal, ...
        rad2deg(theta_A_solved - params.theta_A0_nominal));
    fprintf('  Δ_B = %.6f rad (%.4f°)\n', theta_B_solved - params.theta_B0_nominal, ...
        rad2deg(theta_B_solved - params.theta_B0_nominal));
else
    error('Failed to solve kinematics at reference position!');
end

% Material and cross-sections
params.E  = 71.9e9;         % Young's modulus (Pa)
params.wa = 10e-3;          % Bar A width (m)
params.ta = 1e-3;           % Bar A thickness (m)
params.wb = 10e-3;          % Bar B width (m)
params.tb = 1.5e-3;         % Bar B thickness (m)

% Moments of inertia
Ia = params.wa * params.ta^3 / 12;
Ib = params.wb * params.tb^3 / 12;

% PRBM constants
params.gamma_A = 0.5;       % Characteristic radius factor for Bar A
params.gamma_B = 0.85;      % Characteristic radius factor for Bar B
params.KTheta = 2.65;       % Stiffness coefficient

% Torsional spring stiffnesses (ONE spring per bar)
params.KA_base = params.gamma_A * params.KTheta * params.E * Ia / params.la;
params.KB_base = params.gamma_B * params.KTheta * params.E * Ib / params.lb;

% Characteristic pivot offsets for visualization
params.A_pivot_offset = (1-params.gamma_A) * params.la;
params.B_pivot_offset = (1-params.gamma_B) * params.lb;

fprintf('\nSpring Stiffnesses (per bar):\n');
fprintf('  KA_base = %.4f N·m/rad\n', params.KA_base);
fprintf('  KB_base = %.4f N·m/rad\n', params.KB_base);
fprintf('  Ratio KB/KA = %.2f\n', params.KB_base/params.KA_base);
fprintf('============================================================\n\n');

%% ===== ANALYSIS RANGE =====
x_slider_range = linspace(15e-3, 25e-3, 50);
n_positions = length(x_slider_range);

% Pre-allocate result arrays
F_total = zeros(n_positions, 1);
K_mech = zeros(n_positions, 1);
U_total = zeros(n_positions, 1);
tau_A_array = zeros(n_positions, 1);
tau_B_array = zeros(n_positions, 1);
angles_A = zeros(n_positions, 1);
angles_B = zeros(n_positions, 1);
angles_C = zeros(n_positions, 1);

%% ===== MAIN ANALYSIS LOOP =====
fprintf('Computing forces at %d positions using simplified method...\n', n_positions);
fprintf('Progress: ');

% Find resting position index
[~, rest_idx] = min(abs(x_slider_range - 20e-3));

% Solve kinematics and forces at all positions
theta_guess = [];
for i = 1:n_positions
    if mod(i, 10) == 0
        fprintf('%d%% ', round(i/n_positions*100));
    end

    x_slider = x_slider_range(i);

    % Solve kinematics
    [theta_A, theta_B, theta_C, success] = solveKinematics(x_slider, params, theta_guess);

```

```
    if ~success
        warning('Kinematics␣failed␣at␣x␣=␣%.2f␣mm', x_slider*1000);
        F_total(i) = NaN;
        U_total(i) = NaN;
        continue;
    end

    % Store angles
    angles_A(i) = theta_A;
    angles_B(i) = theta_B;
    angles_C(i) = theta_C;

    % Update guess for next iteration
    theta_guess = [theta_A; theta_B; theta_C];

    % Calculate force using simplified direct method
    [F_total(i), tau_A, tau_B] = calculateForceSimplified(x_slider, theta_A, theta_B, params);
    tau_A_array(i) = tau_A;
    tau_B_array(i) = tau_B;

    % Calculate total strain energy
    U_total(i) = calculateEnergy(theta_A, theta_B, params);
end

fprintf('100%%␣Complete!\n\n');

%% ===== CALCULATE MECHANISM STIFFNESS =====
for i = 2:n_positions-1
    if ~isnan(F_total(i))
        dx = x_slider_range(i+1) - x_slider_range(i-1);
        K_mech(i) = (F_total(i+1) - F_total(i-1)) / dx;
    else
        K_mech(i) = NaN;
    end
end

% Extrapolate endpoints
K_mech(1) = K_mech(2);
K_mech(end) = K_mech(end-1);

% Calculate displacement from rest position
displacement_from_rest = (x_slider_range - 20e-3) * 1000;

%% ===== RESULTS SUMMARY =====
fprintf('====␣ANALYSIS␣RESULTS␣====\n');
valid_idx = ~isnan(F_total);

if any(valid_idx)
    fprintf('\nResults␣at␣x=20mm␣(rest␣position):\n');
    fprintf('␣␣Force:␣␣␣␣␣␣␣␣F␣=␣%.6f␣N\n', F_total(rest_idx));
    fprintf('␣␣Stiffness:␣␣␣␣K␣=␣%.2f␣N/m\n', K_mech(rest_idx));
    fprintf('␣␣Energy:␣␣␣␣␣␣␣U␣=␣%.6f␣mJ\n', U_total(rest_idx)*1000);
    fprintf('␣␣Torque␣A:␣␣␣␣␣ _A␣=␣%.6f␣N·m\n', tau_A_array(rest_idx));
    fprintf('␣␣Torque␣B:␣␣␣␣␣ _B␣=␣%.6f␣N·m\n', tau_B_array(rest_idx));

    fprintf('\nForce␣Range:\n');
    fprintf('␣␣Min:␣%.2f␣N␣at␣x=%.2f␣mm\n', min(F_total(valid_idx)), ...
        x_slider_range(F_total == min(F_total(valid_idx)))*1000);
    fprintf('␣␣Max:␣%.2f␣N␣at␣x=%.2f␣mm\n', max(F_total(valid_idx)), ...
        x_slider_range(F_total == max(F_total(valid_idx)))*1000);

    fprintf('\nStiffness␣Range:\n');
    fprintf('␣␣Min:␣%.0f␣N/m\n', min(K_mech(valid_idx)));
    fprintf('␣␣Max:␣%.0f␣N/m\n', max(K_mech(valid_idx)));

    fprintf('\nAngle␣Range:\n');
    fprintf('␣␣Bar␣A:␣%.2f°␣to␣%.2f°\n', min(rad2deg(angles_A)), max(rad2deg(angles_A)));
    fprintf('␣␣Bar␣B:␣%.2f°␣to␣%.2f°\n', min(rad2deg(angles_B)), max(rad2deg(angles_B)));
end
fprintf('============================\n\n');

```

```
%% ===== COMPREHENSIVE PLOTTING =====
figure('Position', [50, 50, 1600, 1000]);

% Plot 1: Input Force vs Slider Position
subplot(3,3,1);
plot(x_slider_range*1000, F_total, 'b-', 'LineWidth', 2); hold on;
plot(20, F_total(rest_idx), 'ro', 'MarkerSize', 10, 'LineWidth', 2, 'MarkerFaceColor', 'r');
yline(0, 'k:', 'LineWidth', 1);
grid on;
xlabel('Slider Position (mm)');
ylabel('Input Force (N)');
title('Input Force vs Slider Position');
xlim([15 25]);
legend('Force', 'Rest Position', 'Location', 'best');

% Plot 2: Mechanism Stiffness
subplot(3,3,2);
plot(x_slider_range*1000, K_mech, 'r-', 'LineWidth', 2); hold on;
plot(20, K_mech(rest_idx), 'ko', 'MarkerSize', 10, 'LineWidth', 2, 'MarkerFaceColor', 'k');
grid on;
xlabel('Slider Position (mm)');
ylabel('Stiffness (N/m)');
title('Mechanism Stiffness');
xlim([15 25]);
legend('Stiffness', 'Rest', 'Location', 'best');

% Plot 3: Total Stored Energy
subplot(3,3,3);
plot(x_slider_range*1000, U_total*1000, 'g-', 'LineWidth', 2); hold on;
plot(x_slider_range*1000, U_total*1000/2, 'g--', 'LineWidth', 1.5);
plot(20, U_total(rest_idx)*1000, 'ko', 'MarkerSize', 10, 'LineWidth', 2, 'MarkerFaceColor', 'k');
grid on;
xlabel('Slider Position (mm)');
ylabel('Energy (mJ)');
title('Total Stored Energy');
xlim([15 25]);
legend('Total', 'Per side', 'Rest', 'Location', 'best');

% Plot 4: Link Angles
subplot(3,3,4);
plot(x_slider_range*1000, rad2deg(angles_A), 'b-', 'LineWidth', 1.5); hold on;
plot(x_slider_range*1000, rad2deg(angles_B), 'r-', 'LineWidth', 1.5);
plot(x_slider_range*1000, rad2deg(angles_C), 'g-', 'LineWidth', 1.5);
plot(20, rad2deg(angles_A(rest_idx)), 'bo', 'MarkerSize', 8, 'MarkerFaceColor', 'b');
plot(20, rad2deg(angles_B(rest_idx)), 'ro', 'MarkerSize', 8, 'MarkerFaceColor', 'r');
plot(20, rad2deg(angles_C(rest_idx)), 'go', 'MarkerSize', 8, 'MarkerFaceColor', 'g');
grid on;
xlabel('Slider Position (mm)');
ylabel('Angle (degrees)');
title('Link Angles');
legend('Bar A', 'Bar B', 'Coupler', 'Location', 'best');
xlim([15 25]);

% Plot 5: Angular Deflections
subplot(3,3,5);
delta_A = angles_A - params.theta_A0;
delta_B = angles_B - params.theta_B0;
plot(x_slider_range*1000, rad2deg(delta_A), 'b-', 'LineWidth', 1.5); hold on;
plot(x_slider_range*1000, rad2deg(delta_B), 'r-', 'LineWidth', 1.5);
yline(0, 'k:', 'LineWidth', 1);
grid on;
xlabel('Slider Position (mm)');
ylabel('Angular Deflection (degrees)');
title('Angular Deflections from Neutral');
xlim([15 25]);
legend('Δ_A', 'Δ_B', 'Location', 'best');

% Plot 6: Spring Torques
subplot(3,3,6);
plot(x_slider_range*1000, tau_A_array*1000, 'b-', 'LineWidth', 1.5); hold on;
plot(x_slider_range*1000, tau_B_array*1000, 'r-', 'LineWidth', 1.5);
```

```
yline(0, 'k:', 'LineWidth', 1);
grid on;
xlabel('Slider Position (mm)');
ylabel('Torque (N·mm)');
title('Spring Torques (per side)');
xlim([15 25]);
legend(' _A', ' _B', 'Location', 'best');

% Plot 7: MECHANISM VISUALIZATION
subplot(3,3,7);
positions_to_show = [15e-3, 20e-3, 25e-3];
colors = {'b', 'k', 'r'};
labels = {'15mm', '20mm (rest)', '25mm'};

for k = 1:length(positions_to_show)
    x_show = positions_to_show(k);
    [~, idx] = min(abs(x_slider_range - x_show));
    theta_A_show = angles_A(idx);
    theta_B_show = angles_B(idx);

    if ~isnan(theta_A_show)
        % TOP SIDE
        GA_top = [params.GAx; params.GAy];
        A_tip_top = GA_top + params.la * [cos(theta_A_show); sin(theta_A_show)];
        B_base_top = [x_show; params.y0];
        B_top_top = B_base_top + params.lb * [cos(theta_B_show); sin(theta_B_show)];

        A_pivot_top = GA_top + params.A_pivot_offset * [cos(theta_A_show); sin(theta_A_show)];
        B_pivot_top = B_base_top + params.B_pivot_offset * [cos(theta_B_show); sin(theta_B_show)];

        % Draw bars
        plot([GA_top(1), A_tip_top(1)]*1000, [GA_top(2), A_tip_top(2)]*1000, ...
            colors{k}, 'LineWidth', 2.5); hold on;
        plot([B_base_top(1), B_top_top(1)]*1000, [B_base_top(2), B_top_top(2)]*1000, ...
            colors{k}, 'LineWidth', 2.5);
        plot([A_tip_top(1), B_top_top(1)]*1000, [A_tip_top(2), B_top_top(2)]*1000, ...
            colors{k}, 'LineWidth', 1.5, 'LineStyle', '--');

        % Draw springs
        drawSpringSpiral(A_pivot_top*1000, theta_A_show, colors{k}, 1.0);
        drawSpringSpiral(B_pivot_top*1000, theta_B_show, colors{k}, 1.0);

        % BOTTOM SIDE (mirror)
        GA_bot = [params.GAx; -params.GAy];
        A_tip_bot = GA_bot + params.la * [cos(-theta_A_show); sin(-theta_A_show)];
        B_base_bot = [x_show; -params.y0];
        B_top_bot = B_base_bot + params.lb * [cos(-theta_B_show); sin(-theta_B_show)];

        A_pivot_bot = GA_bot + params.A_pivot_offset * [cos(-theta_A_show); sin(-theta_A_show)];
        B_pivot_bot = B_base_bot + params.B_pivot_offset * [cos(-theta_B_show); sin(-theta_B_show)];

        plot([GA_bot(1), A_tip_bot(1)]*1000, [GA_bot(2), A_tip_bot(2)]*1000, colors{k}, 'LineWidth', 2.5)
            ;
        plot([B_base_bot(1), B_top_bot(1)]*1000, [B_base_bot(2), B_top_bot(2)]*1000, colors{k}, '
            LineWidth', 2.5);
        plot([A_tip_bot(1), B_top_bot(1)]*1000, [A_tip_bot(2), B_top_bot(2)]*1000, colors{k}, 'LineWidth'
            , 1.5, 'LineStyle', '--');

        drawSpringSpiral(A_pivot_bot*1000, -theta_A_show, colors{k}, 1.0);
        drawSpringSpiral(B_pivot_bot*1000, -theta_B_show, colors{k}, 1.0);
    end
end

% Draw slider rails
plot([0, 70], [params.y0, params.y0]*1000, 'k-', 'LineWidth', 3);
plot([0, 70], [-params.y0, -params.y0]*1000, 'k-', 'LineWidth', 3);

% Draw ground pivots
plot(params.GAx*1000, params.GAy*1000, 'ko', 'MarkerSize', 10, 'MarkerFaceColor', 'k');
plot(params.GAx*1000, -params.GAy*1000, 'ko', 'MarkerSize', 10, 'MarkerFaceColor', 'k');

```

```
% Draw centerline
plot([0, 70], [0, 0], 'k:', 'LineWidth', 1);

grid on; axis equal;
xlabel('x (mm)');
ylabel('y (mm)');
title('Mechanism Configuration');
xlim([-5, 70]);
ylim([-50, 50]);
legend(labels, 'Location', 'northeast');

% Plot 8: Force vs Displacement from Rest
subplot(3,3,8);
plot(displacement_from_rest, F_total, 'b-', 'LineWidth', 2.5); hold on;
plot(0, F_total(rest_idx), 'ro', 'MarkerSize', 10, 'LineWidth', 2, 'MarkerFaceColor', 'r');

% Reference data (if available)
slope_ref = 41.4 / 2.35;
plot([0, 5], [0, slope_ref*5], 'g--', 'LineWidth', 1.5);
plot(2.35, 41.4, 'go', 'MarkerSize', 8, 'MarkerFaceColor', 'g');

% Smooth reference curve
x_ref_points = [0, 1.49, 2.93, 4.84];
y_ref_points = [0, 25, 50, 75];
x_smooth = linspace(0, 5, 100);
y_smooth = spline(x_ref_points, y_ref_points, x_smooth);
plot(x_smooth, y_smooth, 'm-', 'LineWidth', 1.5);
plot(x_ref_points(2:end), y_ref_points(2:end), 'mo', 'MarkerSize', 8, 'MarkerFaceColor', 'm');

grid on;
xlabel('Displacement from Rest (mm)');
ylabel('Force (N)');
title('Force vs Displacement');
xlim([-5 5]);
legend('Calculated', 'Rest', 'Linear ref', 'Spline ref', 'Ref points', 'Location', 'best');

% Plot 9: Energy Components
subplot(3,3,9);
U_A = 0.5 * params.KA_base * (angles_A - params.theta_A0).^2;
U_B = 0.5 * params.KB_base * (angles_B - params.theta_B0).^2;
plot(x_slider_range*1000, U_A*1000*2, 'b-', 'LineWidth', 1.5); hold on;
plot(x_slider_range*1000, U_B*1000*2, 'r-', 'LineWidth', 1.5);
plot(x_slider_range*1000, U_total*1000, 'k-', 'LineWidth', 2);
grid on;
xlabel('Slider Position (mm)');
ylabel('Energy (mJ)');
title('Energy Components (both sides)');
xlim([15 25]);
legend('U_A (both)', 'U_B (both)', 'Total', 'Location', 'best');

%% ===== DETAILED RESULTS TABLE =====
fprintf('==== DETAILED RESULTS AT KEY POSITIONS ====\n');
fprintf('Position | Force | Stiffness | Energy | Angle A | Angle B | Torque A | Torque B\n');
fprintf('  (mm)  |  (N)  |  (N/m)    |  (mJ)  |  (deg)  |  (deg)  |  (N·mm)  |  (N·mm)\n');
fprintf('---------|-------|-----------|--------|---------|---------|----------|----------\n');

key_positions = [15, 17.5, 20, 22.5, 25];
for pos = key_positions
    [~, idx] = min(abs(x_slider_range - pos*1e-3));
    if ~isnan(F_total(idx))
        fprintf(' %6.2f  | %6.2f | %9.0f | %6.3f | %7.2f | %7.2f | %8.3f | %8.3f\n', ...
            pos, F_total(idx), K_mech(idx), U_total(idx)*1000, ...
            rad2deg(angles_A(idx)), rad2deg(angles_B(idx)), ...
            tau_A_array(idx)*1000, tau_B_array(idx)*1000);
    end
end
fprintf('================================================================================\n\n');

%% ===== EXPORT RESULTS =====
results = struct();
results.x_slider = x_slider_range;
```

```
results.F_total = F_total;
results.K_mech = K_mech;
results.U_total = U_total;
results.angles_A = angles_A;
results.angles_B = angles_B;
results.angles_C = angles_C;
results.tau_A = tau_A_array;
results.tau_B = tau_B_array;
results.params = params;

% Save to file
save('mechanism_results_simplified.mat', 'results');
fprintf('Results saved to: mechanism_results_simplified.mat\n\n');

%% ===== FUNCTIONS =====

function [theta_A, theta_B, theta_C, success] = solveKinematics_initial(x_slider, params)
    % Initial solve using nominal angles as guess
    theta0 = [params.theta_A0_nominal; params.theta_B0_nominal; params.theta_C0_nominal];

    options = optimoptions('fsolve', 'Display', 'off', ...
        'TolFun', 1e-12, 'TolX', 1e-12, 'Algorithm', 'levenberg-marquardt', ...
        'MaxIterations', 1000);

    [theta_sol, fval, exitflag] = fsolve(@(th) loopClosure(th, x_slider, params), ...
        theta0, options);

    theta_A = theta_sol(1);
    theta_B = theta_sol(2);
    theta_C = theta_sol(3);

    success = (exitflag > 0) && (norm(fval) < 1e-8);
end

function [theta_A, theta_B, theta_C, success] = solveKinematics(x_slider, params, theta_guess)
    % Solve kinematics with optional initial guess
    if isempty(theta_guess)
        theta0 = [params.theta_A0; params.theta_B0; params.theta_C0];
    else
        theta0 = theta_guess;
    end

    options = optimoptions('fsolve', 'Display', 'off', ...
        'TolFun', 1e-10, 'TolX', 1e-10, 'Algorithm', 'levenberg-marquardt');

    [theta_sol, fval, exitflag] = fsolve(@(th) loopClosure(th, x_slider, params), ...
        theta0, options);

    theta_A = theta_sol(1);
    theta_B = theta_sol(2);
    theta_C = theta_sol(3);

    success = (exitflag > 0) && (norm(fval) < 1e-6);
end

function residual = loopClosure(theta, x_slider, params)
    % Loop-closure equations for five-bar mechanism
    theta_A = theta(1);
    theta_B = theta(2);
    theta_C = theta(3);

    % Ground pivot A
    GA = [params.GAx; params.GAy];

    % Tip of Bar A
    A_tip = GA + params.la * [cos(theta_A); sin(theta_A)];

    % Base of Bar B (on slider)
    B_base = [x_slider; params.y0];

    % Top of Bar B
```

```
    B_top = B_base + params.lb * [cos(theta_B); sin(theta_B)];

    % Coupler vector (actual)
    coupler_vec = B_top - A_tip;

    % Coupler vector (expected)
    coupler_expected = params.lc * [cos(theta_C); sin(theta_C)];

    % Residuals
    residual = zeros(3,1);
    residual(1) = coupler_vec(1) - coupler_expected(1);
    residual(2) = coupler_vec(2) - coupler_expected(2);
    residual(3) = norm(coupler_vec) - params.lc;
end

function U_total = calculateEnergy(theta_A, theta_B, params)
    % Total elastic strain energy (both sides of symmetric mechanism)
    delta_A = theta_A - params.theta_A0;
    delta_B = theta_B - params.theta_B0;

    % Energy in one side
    U_one_side = 0.5 * params.KA_base * delta_A^2 + ...
                 0.5 * params.KB_base * delta_B^2;

    % Total energy (symmetric mechanism)
    U_total = 2 * U_one_side;
end

function [F, tau_A, tau_B] = calculateForceSimplified(x_slider, theta_A, theta_B, params)
    % SIMPLIFIED FORCE CALCULATION using virtual work principle
    % For single DOF mechanism: F = Σ(_i * d_i/dx)

    % Angular deflections from neutral position
    delta_A = theta_A - params.theta_A0;
    delta_B = theta_B - params.theta_B0;

    % Spring torques (per side)
    tau_A = params.KA_base * delta_A;
    tau_B = params.KB_base * delta_B;

    % Get kinematic Jacobian: relates [d_A; d_B] to slider motion
    J_kin = constructJacobian2x2(theta_A, theta_B, params);

    % Right-hand side: [dx/dx; dy/dx] = [1; 0] since slider moves only in x
    rhs = [-1; 0];

    % Solve for angle derivatives: [d_A/dx; d_B/dx]
    dtheta_dx = J_kin \ rhs;

    % Virtual work: force per side
    % dW = F·dx = _A·d_A + _B·d_B
    % Therefore: F = _A·(d_A/dx) + _B·(d_B/dx)
    F_one_side = tau_A * dtheta_dx(1) + tau_B * dtheta_dx(2);

    % Total force (symmetric mechanism has two sides)
    F = 2 * F_one_side;
end

function J_kin = constructJacobian2x2(theta_A, theta_B, params)
    % Construct 2×2 kinematic Jacobian from loop closure equations
    % Relates changes in [_A; _B] to changes in slider position

    J_kin = zeros(2, 2);

    % (x-component) /_A and (x-component) /_B
    J_kin(1, 1) = params.la * sin(theta_A);
    J_kin(1, 2) = -params.lb * sin(theta_B);

    % (y-component) /_A and (y-component) /_B
    J_kin(2, 1) = -params.la * cos(theta_A);
    J_kin(2, 2) = params.lb * cos(theta_B);
```

```
end

function drawSpringSpiral(pos, link_angle, color, scale_factor)
    % Draw spring visualization as a spiral
    if nargin < 4
        scale_factor = 1.5;
    end

    radius = 1.5 * scale_factor;
    n_turns = 2.5;
    n_points = 50;

    % Create spiral in local coordinates
    t = linspace(0, n_turns * 2 * pi, n_points);
    r = linspace(0, radius, n_points);
    x_local = r .* cos(t);
    y_local = r .* sin(t);

    % Rotate spiral to align with link
    spiral_angle = link_angle + pi/2;
    cos_a = cos(spiral_angle);
    sin_a = sin(spiral_angle);

    x_rot = x_local * cos_a - y_local * sin_a;
    y_rot = x_local * sin_a + y_local * cos_a;

    % Translate to position
    x_spring = pos(1) + x_rot;
    y_spring = pos(2) + y_rot;

    % Draw spiral
    plot(x_spring, y_spring, 'Color', color, 'LineWidth', 1.2);

    % Draw center point
    plot(pos(1), pos(2), 'o', 'Color', color, 'MarkerSize', 2, 'MarkerFaceColor', color);
end
```

B

Code for Joint Location Optimization GM

```
%% %% Comprehensive Compliant Mechanism Analysis with Interactive Features
clc; clear; close all;

% Fixed parameters
output_initial = [12, 2];  % Output position
slider_initial = [2, 0];   % Slider initial position (x=2)

% Adjusted parameter ranges
ground_y_values = linspace(3, 5, 10);  % Ground joint Y positions (3-5)
F_x_values = linspace(4, 9, 50);       % Joint F X positions (4-9)
F_y_values = linspace(3, 6, 20);       % Joint F Y positions (3-6)

% Initialize storage
all_configs = [];
pareto_front = [];

% Main analysis loop
for g_idx = 1:length(ground_y_values)
    ground = [0, ground_y_values(g_idx)];

    for Fy_idx = 1:length(F_y_values)
        for Fx_idx = 1:length(F_x_values)
            F_initial = [F_x_values(Fx_idx), F_y_values(Fy_idx)];
            L_A1 = norm(F_initial - ground);
            L_B = norm(F_initial - slider_initial);

            if L_B < 4, continue; end

            try
                % Constrain slider to 2-2.25 range
                slider_min = max(2, F_initial(1) - sqrt(L_B^2 - F_initial(2)^2));
                slider_max = min(2.25, F_initial(1) + sqrt(L_B^2 - F_initial(2)^2));
                valid_slider_x = linspace(slider_min, slider_max, 50);
            catch
                continue;
            end

            % Process slider positions
            temp_angles = [];
            for s_idx = 1:length(valid_slider_x)
                B = [valid_slider_x(s_idx), 0];
                options = optimoptions('fsolve', 'Display', 'off');
                [F, ~, exitflag] = fsolve(@(x) root2d(x, ground, B, L_A1, L_B), F_initial, options);

                if exitflag > 0 && isreal(F) && F(2) > 2.5
                    % Calculate bar A angle with vertical
                    vec_A = F - ground;
                    angle = 90 - atan2d(vec_A(2), vec_A(1));
                    temp_angles = [temp_angles; angle];
                end
```

```
            end

            if numel(temp_angles) > 1
                % Calculate metrics
                input_disp = valid_slider_x(end) - valid_slider_x(1);
                output_disp = norm(F + (output_initial - F_initial) - output_initial);
                disp_ratio = output_disp / input_disp;
                angle_diff = temp_angles(1) - temp_angles(end);  % Start - End angle

                % Store configuration
                all_configs = [all_configs;
                               ground(2), F_initial(1), F_initial(2), disp_ratio, angle_diff];
            end
        end
    end
end

% Identify Pareto-optimal configurations
is_pareto = true(size(all_configs,1),1);
for i = 1:size(all_configs,1)
    for j = 1:size(all_configs,1)
        if (all_configs(j,4) >= all_configs(i,4) && all_configs(j,5) <= all_configs(i,5)) && ...
           (all_configs(j,4) > all_configs(i,4) || all_configs(j,5) < all_configs(i,5))
            is_pareto(i) = false;
            break;
        end
    end
end
pareto_front = all_configs(is_pareto,:);

% Create interactive visualization
figure('Position', [100 100 1400 600]);

% 3D Parameter Space Plot
subplot(1,2,1);
h_3d = scatter3(all_configs(:,1), all_configs(:,2), all_configs(:,3), ...
        40, all_configs(:,4), 'filled', 'UserData', all_configs);
hold on;
scatter3(pareto_front(:,1), pareto_front(:,2), pareto_front(:,3), ...
        120, 'r', 'filled', 'MarkerEdgeColor', 'k', 'UserData', pareto_front);
xlabel('Ground␣Y␣(3-5)');
ylabel('F␣X␣(4-9)');
zlabel('F␣Y␣(3-6)');
title('3D␣Parameter␣Space␣(Color:␣Displacement␣Ratio)');
colorbar;
view(3);
grid on;

% Trade-off Plot
subplot(1,2,2);
h_2d = scatter(all_configs(:,4), all_configs(:,5), 40, all_configs(:,1), 'filled', ...
        'UserData', all_configs);
hold on;
scatter(pareto_front(:,4), pareto_front(:,5), 120, 'r', 'filled', ...
        'MarkerEdgeColor', 'k', 'UserData', pareto_front);
xlabel('Displacement␣Ratio␣(Input:␣2-2.25)');
ylabel('Angle␣Difference␣(°)');
title('Performance␣Trade-off␣(Color:␣Ground␣Y␣Position)');
colorbar;
grid on;

% Configure interactive data tips
dcm = datacursormode(gcf);
set(dcm, 'UpdateFcn', @customDataTip, 'Enable', 'on');

% Custom data tip function
function output_txt = customDataTip(~, event_obj)
    pos = get(event_obj, 'Position');
    target = get(event_obj, 'Target');
    user_data = get(target, 'UserData');
    idx = get(event_obj, 'DataIndex');
```

```
122
123     % Extract parameters from stored data
124     if size(user_data,2) == 5  % Full configuration data
125         config = user_data(idx,:);
126         ground_y = config(1);
127         F_x = config(2);
128         F_y = config(3);
129         disp_ratio = config(4);
130         angle_diff = config(5);
131     else  % Pareto front data
132         config = user_data(idx,1:5);
133         ground_y = config(1);
134         F_x = config(2);
135         F_y = config(3);
136         disp_ratio = config(4);
137         angle_diff = config(5);
138     end
139
140     % Create tooltip text
141     output_txt = {
142         ['Ground Y: ', num2str(ground_y, '%.2f')],
143         ['F Position: (', num2str(F_x, '%.1f'), ', ', num2str(F_y, '%.1f'), ')'],
144         ['Disp Ratio: ', num2str(disp_ratio, '%.2f')],
145         ['Angle Diff: ', num2str(angle_diff, '%.1f'), '°']
146     };
147 end
148
149 % Mechanism constraint function
150 function F = root2d(x, ground, B, L_A1, L_B)
151     F(1) = (x(1)-ground(1))^2 + (x(2)-ground(2))^2 - L_A1^2;
152     F(2) = (x(1)-B(1))^2 + (x(2)-B(2))^2 - L_B^2;
153 end
```

C

Linear Guide Mechanism Analytical Code With Corner Fillets and Linear Taper Included

```
function nanopositioning_stage_analysis_with_fillets()

% LGM Paper (motion in z):
%
% FILLET ORIENTATION CORRECTION:
%   - Fillet affects WIDTH (w)

%% Geometry and material
R0 = 40e-3;                         % Median radius [m]
t_LGM = 5e-3;                       % Thickness [m] (constant for all leaves)
R = R0 - t_LGM/2;

% Constant widths
w_LGM_38 = 0.54e-3;                 % Width for small leaves [m]
w_LGM_47 = 0.54e-3;                 % Width for non-tapered big leaf [m]

% Tapered width for the tapered leaf:
wA_LGM_47 = 0.6e-3;                 % Width at fixed end A [m]
wB_LGM_47 = 1.03e-3;                % Width at free end B [m]

% Fillet parameters
r_fillet38 = 0e-3;                  % Fillet radius for 38° leaves [m]
r_fillet47 = 0e-3;                  % Fillet radius for 47° leaves [m]

E = 70e9;                           % Young's modulus [Pa]
nu = 0.33;                          % Poisson's ratio
mu = 6/5;                           % Shear coefficient (rectangular)

% Layout
n = 3;                              % Number of FPM guides in parallel (stage-level)
angles = [45.865, 52.8];            % degrees

%Fillet size
r_fillet_38 = 2.5e-3;
r_fillet_47 = 2.5e-3;


fprintf('========================================\n');
fprintf('LGM: Motion in z');
fprintf('========================================\n\n');

fprintf('Geometry:\n');
fprintf('  Median radius R = %.2f mm\n', R*1e3);
```

```
fprintf('  Width w (radial) = %.2f mm', w_LGM_38*1e3);
fprintf('  Thickness t (axial) = %.2f mm\n', t_LGM*1e3);
fprintf('  Fillet r = %.2f mm (%.0f%% of w)\n\n', r_fillet_38*1e3, 100*r_fillet_38/w_LGM_38);

%% Calculate with fillets (using unified taper function)
k38_f = calc_arc_general(angles(1), R, w_LGM_38, w_LGM_38, t_LGM, r_fillet_38, E, nu, mu);
k47_f = calc_arc_general(angles(2), R, w_LGM_47, w_LGM_47, t_LGM, r_fillet_47, E, nu, mu);
k47t_f = calc_arc_general(angles(2), R, wA_LGM_47, wB_LGM_47, t_LGM, r_fillet_47, E, nu, mu);

%% Calculate without fillets (using unified taper function, r=0)
k38_o = calc_arc_general(angles(1), R, w_LGM_38, w_LGM_38, t_LGM, 0, E, nu, mu);
k47_o = calc_arc_general(angles(2), R, w_LGM_47, w_LGM_47, t_LGM, 0, E, nu, mu);
k47t_o = calc_arc_general(angles(2), R, wA_LGM_47, wB_LGM_47, t_LGM, 0, E, nu, mu);

%% Combine
kFPM1_f = 1/(1/k38_f + 1/k38_f + 1/k47_f);
kFPM2_f = 1/(1/k38_f + 1/k38_f + 1/k47t_f);
kstage_f = n * (2*kFPM1_f + 2*kFPM2_f);

kFPM1_o = 1/(1/k38_o + 1/k38_o + 1/k47_o);
kFPM2_o = 1/(1/k38_o + 1/k38_o + 1/k47t_o);
kstage_o = n * (2*kFPM1_o + 2*kFPM2_o);

%% Results
fprintf('\n========================================\n');
fprintf('RESULTS\n');
fprintf('========================================\n');
fprintf('Leaf Stiffness (N/mm):\n');
fprintf('  38°:  %.3f → %.3f (%.2f%%)\n', k38_o/1e3, k38_f/1e3, 100*(k38_o-k38_f)/k38_o);
fprintf('  47°:  %.3f → %.3f (%.2f%%)\n', k47_o/1e3, k47_f/1e3, 100*(k47_o-k47_f)/k47_o);
fprintf('  47°t: %.3f → %.3f (%.2f%%)\n', k47t_o/1e3, k47t_f/1e3, 100*(k47t_o-k47t_f)/k47t_o);
fprintf('\nStage: %.3f → %.3f (%.2f%%)\n', ...
    kstage_o/1e3, kstage_f/1e3, 100*(kstage_o-kstage_f)/kstage_o);
fprintf('Target: ~23%%\n');
fprintf('========================================\n');

%% Plot
max_disp = 5e-3;
x = linspace(0, max_disp, 100);

%Actualmessurment
new_disp3 = [0, 2];                         % mm
new_force3 = [0, 25];                       % N

figure('Position', [100 100 1000 700])
hold on; grid on; box on
plot(x*1e3, 13e3*x, '--', 'Color', [0,25,101]/255, 'LineWidth', 2.5)
plot(x*1e3, kstage_f*x, 'Color', [220,50,50]/255, 'LineWidth', 2.5)
%plot(x*1e3, kstage_o*x, 'Color', [59,151,222]/255, 'LineWidth', 2.5)
%plot([0,5.78], [0,55], 's', 'Color', [42,145,139]/255, 'MarkerSize', 10, ...
    %'LineWidth', 2, 'MarkerFaceColor', [42,145,139]/255)
plot(new_disp3, new_force3, 's', 'Color', [10,10,139]/255, 'MarkerSize', 10, ...
    'LineWidth', 2, 'MarkerFaceColor', [10,10,139]/255)

xlabel('Displacement (mm)', 'FontSize', 14, 'FontWeight', 'bold')
ylabel('Force (N)', 'FontSize', 14, 'FontWeight', 'bold')
title('Corrected Fillet Orientation: Affects Width (w)', 'FontSize', 15, 'FontWeight', 'bold')
legend({'FEA', 'With Fillets', 'No Fillets', 'FEM'}, 'Location', 'northwest')
xlim([0 6]); ylim([0 70])
hold off
end

%% UNIFIED FUNCTION: General arc beam with optional taper and fillet
function kuz = calc_arc_general(alpha_deg, R, wA, wB, t, r, E, nu, mu)
% Universal function for arc beam analysis
% - Handles constant width (wA = wB) or tapered (wA  wB)
% - Handles with fillet (r > 0) or without (r = 0)
%
% Fillet affects Witdh (w)
% Section properties with fillet:
% - A () = w () × () × t
```

```
% - Iy () = [w () × ()]³×t / 12
% - Iz () = [w () × ()]×t³ / 12
% - Ip ()   [w () × ()]³×t × ...

alpha_total = deg2rad(alpha_deg);
L = R * alpha_total;
G = E / (2 * (1 + nu));

% Width taper function
wfun = @(alpha) wB + (wA - wB) .* (alpha / alpha_total);

% Base section properties
Afun_base = @(alpha) wfun(alpha) .* t;
Iyfun_base = @(alpha) (wfun(alpha).^3 .* t) / 12;                    % w³ - strongly affected by fillet
Izfun_base = @(alpha) (wfun(alpha) .* t.^3) / 12;                    % w - linearly affected by fillet
Ipfun_base = @(alpha) wfun(alpha).^3 .* t .* (1/3 - 0.21*(wfun(alpha)./t) + 0.0175*(wfun(alpha)./t).^5);

% Check if fillet is present
has_fillet = (r > 1e-6);

if has_fillet
    % Use average width for fillet parameters
    w_avg = (wA + wB) / 2;
    a = r / w_avg;
    b = L / w_avg;

    % Shape function - based on width coordinate
    zeta_fun = @(alpha) arrayfun(@(a_val) calc_zeta(R*a_val/w_avg, a, b), alpha);

    % Fillet region boundaries
    alpha1 = min((a*w_avg)/R, alpha_total);
    alpha2 = max(0, min(((b-a)*w_avg)/R, alpha_total));
else
    % No fillet: zeta = 1 everywhere
    zeta_fun = @(alpha) ones(size(alpha));
    alpha1 = 0;
    alpha2 = alpha_total;
end

opt = {'ArrayValued', true, 'RelTol', 1e-9, 'AbsTol', 1e-12};

% Calculate integrals with appropriate powers of :
% - Area (w×t):  ^1
% - Iy (w³×t):  ^3 ←  BIG EFFECT from fillet
% - Iz (w×t³):  ^1
% - Ip (w³×t):  ^3 ←  BIG EFFECT from fillet

if has_fillet && alpha1 > 0 && alpha2 > alpha1 && alpha2 < alpha_total
    % Split integration over three regions
    [JA1, JA3, JA4, JA0, JIy1, JIy3, JIy4, JIz0, JIz2, JIz3, JIz5, JIz6, JIz8, ...
     JIp1, JIp2, JIp3, JIp4, JIp5, JIp7] = ...
        calc_integrals_split(Afun_base, Iyfun_base, Izfun_base, Ipfun_base, ...
                             zeta_fun, alpha1, alpha2, alpha_total, opt);
else
    % Single region integration (no fillet or fillet covers entire beam)
    [JA1, JA3, JA4, JA0, JIy1, JIy3, JIy4, JIz0, JIz2, JIz3, JIz5, JIz6, JIz8, ...
     JIp1, JIp2, JIp3, JIp4, JIp5, JIp7] = ...
        calc_integrals_single(Afun_base, Iyfun_base, Izfun_base, Ipfun_base, ...
                              zeta_fun, alpha_total, opt);
end

% Build compliance matrix
C = build_compliance_matrix(R, E, G, mu, ...
    JA1, JA3, JA4, JA0, JIy1, JIy3, JIy4, JIz0, JIz2, JIz3, JIz5, JIz6, JIz8, ...
    JIp1, JIp2, JIp3, JIp4, JIp5, JIp7);

% Solve for stiffness
t_vec = [0;0;0;0;0;1];
w_sol = C\t_vec;
kuz = w_sol(3);
end
```

```
187
188 %% HELPER: Calculate integrals over three regions (fillet zones)
189 function [JA1, JA3, JA4, JA0, JIy1, JIy3, JIy4, JIz0, JIz2, JIz3, JIz5, JIz6, JIz8, ...
190           JIp1, JIp2, JIp3, JIp4, JIp5, JIp7] = ...
191     calc_integrals_split(Afun_base, Iyfun_base, Izfun_base, Ipfun_base, ...
192                          zeta_fun, alpha1, alpha2, alpha_total, opt)
193
194 % Area integrals (^1)
195 JA1 = integrate_three_regions(@(a) cos(a).^2 ./ (Afun_base(a).*zeta_fun(a)), ...
196                               alpha1, alpha2, alpha_total, opt);
197 JA3 = integrate_three_regions(@(a) sin(a).^2 ./ (Afun_base(a).*zeta_fun(a)), ...
198                               alpha1, alpha2, alpha_total, opt);
199 JA4 = integrate_three_regions(@(a) sin(a).*cos(a) ./ (Afun_base(a).*zeta_fun(a)), ...
200                               alpha1, alpha2, alpha_total, opt);
201 JA0 = integrate_three_regions(@(a) 1 ./ (Afun_base(a).*zeta_fun(a)), ...
202                               alpha1, alpha2, alpha_total, opt);
203
204 % Iy integrals (^3 - strong fillet effect)
205 JIy1 = integrate_three_regions(@(a) cos(a).^2 ./ (Iyfun_base(a).*zeta_fun(a).^3), ...
206                                alpha1, alpha2, alpha_total, opt);
207 JIy3 = integrate_three_regions(@(a) sin(a).^2 ./ (Iyfun_base(a).*zeta_fun(a).^3), ...
208                                alpha1, alpha2, alpha_total, opt);
209 JIy4 = integrate_three_regions(@(a) sin(a).*cos(a) ./ (Iyfun_base(a).*zeta_fun(a).^3), ...
210                                alpha1, alpha2, alpha_total, opt);
211
212 % Iz integrals (^1 - linear fillet effect)
213 JIz0 = integrate_three_regions(@(a) 1 ./ (Izfun_base(a).*zeta_fun(a)), ...
214                                alpha1, alpha2, alpha_total, opt);
215 JIz2 = integrate_three_regions(@(a) (1-cos(a)).^2 ./ (Izfun_base(a).*zeta_fun(a)), ...
216                                alpha1, alpha2, alpha_total, opt);
217 JIz3 = integrate_three_regions(@(a) sin(a).^2 ./ (Izfun_base(a).*zeta_fun(a)), ...
218                                alpha1, alpha2, alpha_total, opt);
219 JIz5 = integrate_three_regions(@(a) sin(a).*(1-cos(a)) ./ (Izfun_base(a).*zeta_fun(a)), ...
220                                alpha1, alpha2, alpha_total, opt);
221 JIz6 = integrate_three_regions(@(a) (1-cos(a)) ./ (Izfun_base(a).*zeta_fun(a)), ...
222                                alpha1, alpha2, alpha_total, opt);
223 JIz8 = integrate_three_regions(@(a) sin(a) ./ (Izfun_base(a).*zeta_fun(a)), ...
224                                alpha1, alpha2, alpha_total, opt);
225
226 % Ip integrals (^3 - strong fillet effect)
227 JIp1 = integrate_three_regions(@(a) cos(a).^2 ./ (Ipfun_base(a).*zeta_fun(a).^3), ...
228                                alpha1, alpha2, alpha_total, opt);
229 JIp2 = integrate_three_regions(@(a) (1-cos(a)).^2 ./ (Ipfun_base(a).*zeta_fun(a).^3), ...
230                                alpha1, alpha2, alpha_total, opt);
231 JIp3 = integrate_three_regions(@(a) sin(a).^2 ./ (Ipfun_base(a).*zeta_fun(a).^3), ...
232                                alpha1, alpha2, alpha_total, opt);
233 JIp4 = integrate_three_regions(@(a) sin(a).*cos(a) ./ (Ipfun_base(a).*zeta_fun(a).^3), ...
234                                alpha1, alpha2, alpha_total, opt);
235 JIp5 = integrate_three_regions(@(a) sin(a).*(1-cos(a)) ./ (Ipfun_base(a).*zeta_fun(a).^3), ...
236                                alpha1, alpha2, alpha_total, opt);
237 JIp7 = integrate_three_regions(@(a) cos(a).*(1-cos(a)) ./ (Ipfun_base(a).*zeta_fun(a).^3), ...
238                                alpha1, alpha2, alpha_total, opt);
239 end
240
241 %% HELPER: Calculate integrals over single region (no fillet or uniform fillet)
242 function [JA1, JA3, JA4, JA0, JIy1, JIy3, JIy4, JIz0, JIz2, JIz3, JIz5, JIz6, JIz8, ...
243           JIp1, JIp2, JIp3, JIp4, JIp5, JIp7] = ...
244     calc_integrals_single(Afun_base, Iyfun_base, Izfun_base, Ipfun_base, ...
245                           zeta_fun, alpha_total, opt)
246
247 % Area integrals (^1)
248 JA1 = integral(@(a) cos(a).^2 ./ (Afun_base(a).*zeta_fun(a)), 0, alpha_total, opt{:});
249 JA3 = integral(@(a) sin(a).^2 ./ (Afun_base(a).*zeta_fun(a)), 0, alpha_total, opt{:});
250 JA4 = integral(@(a) sin(a).*cos(a) ./ (Afun_base(a).*zeta_fun(a)), 0, alpha_total, opt{:});
251 JA0 = integral(@(a) 1 ./ (Afun_base(a).*zeta_fun(a)), 0, alpha_total, opt{:});
252
253 % Iy integrals (^3)
254 JIy1 = integral(@(a) cos(a).^2 ./ (Iyfun_base(a).*zeta_fun(a).^3), 0, alpha_total, opt{:});
255 JIy3 = integral(@(a) sin(a).^2 ./ (Iyfun_base(a).*zeta_fun(a).^3), 0, alpha_total, opt{:});
256 JIy4 = integral(@(a) sin(a).*cos(a) ./ (Iyfun_base(a).*zeta_fun(a).^3), 0, alpha_total, opt{:});
257
```

```
% Iz integrals (^1)
JIz0 = integral(@(a) 1 ./ (Izfun_base(a).*zeta_fun(a)), 0, alpha_total, opt{:});
JIz2 = integral(@(a) (1-cos(a)).^2 ./ (Izfun_base(a).*zeta_fun(a)), 0, alpha_total, opt{:});
JIz3 = integral(@(a) sin(a).^2 ./ (Izfun_base(a).*zeta_fun(a)), 0, alpha_total, opt{:});
JIz5 = integral(@(a) sin(a).*(1-cos(a)) ./ (Izfun_base(a).*zeta_fun(a)), 0, alpha_total, opt{:});
JIz6 = integral(@(a) (1-cos(a)) ./ (Izfun_base(a).*zeta_fun(a)), 0, alpha_total, opt{:});
JIz8 = integral(@(a) sin(a) ./ (Izfun_base(a).*zeta_fun(a)), 0, alpha_total, opt{:});

% Ip integrals (^3)
JIp1 = integral(@(a) cos(a).^2 ./ (Ipfun_base(a).*zeta_fun(a).^3), 0, alpha_total, opt{:});
JIp2 = integral(@(a) (1-cos(a)).^2 ./ (Ipfun_base(a).*zeta_fun(a).^3), 0, alpha_total, opt{:});
JIp3 = integral(@(a) sin(a).^2 ./ (Ipfun_base(a).*zeta_fun(a).^3), 0, alpha_total, opt{:});
JIp4 = integral(@(a) sin(a).*cos(a) ./ (Ipfun_base(a).*zeta_fun(a).^3), 0, alpha_total, opt{:});
JIp5 = integral(@(a) sin(a).*(1-cos(a)) ./ (Ipfun_base(a).*zeta_fun(a).^3), 0, alpha_total, opt{:});
JIp7 = integral(@(a) cos(a).*(1-cos(a)) ./ (Ipfun_base(a).*zeta_fun(a).^3), 0, alpha_total, opt{:});
end

%% HELPER: Integrate over three regions
function result = integrate_three_regions(fun, alpha1, alpha2, alpha_total, opt)
result = integral(fun, 0, alpha1, opt{:}) + ...
         integral(fun, alpha1, alpha2, opt{:}) + ...
         integral(fun, alpha2, alpha_total, opt{:});
end

%% HELPER: Build compliance matrix from integrals
function C = build_compliance_matrix(R, E, G, mu, ...
    JA1, JA3, JA4, JA0, JIy1, JIy3, JIy4, JIz0, JIz2, JIz3, JIz5, JIz6, JIz8, ...
    JIp1, JIp2, JIp3, JIp4, JIp5, JIp7)

% Direct compliance terms
C_uxfx = (R/E)*JA1 + (R^3/E)*JIz2 + (mu*R/G)*JA3;
C_uyfy = (R/E)*JA3 + (R^3/E)*JIz3 + (mu*R/G)*JA1;
C_uzfz = (R^3/E)*JIy3 + (R^3/G)*JIp2 + (mu*R/G)*JA0;

C_theta_xmx = (R^2/G)*JIp1 + (R/E)*JIy3;
C_theta_ymy = (R/E)*JIy1 + (R/G)*JIp3;
C_theta_zmz = (R/E)*JIz0;

% Cross-coupling terms
C_uxfy = (R/E)*JA4 - (R^3/E)*JIz5 - (mu*R/G)*JA4;
C_uyfx = C_uxfy;

C_uxmz = -(R^2/E)*JIz6;
C_theta_zfx = C_uxmz;

C_uymz = (R^2/E)*JIz8;
C_theta_zfy = -C_uymz;

C_uzmx = (R^2/E)*JIy3 - (R^2/G)*JIp7;
C_theta_xfz = C_uzmx;

C_uzmy = -(R^2/E)*JIy4 - (R^3/G)*JIp5;
C_theta_yfz = C_uzmy;

C_theta_xmy = -(R/E)*JIy4 + (R/G)*JIp4;
C_theta_ymx = C_theta_xmy;

% Assemble compliance matrix
C = [0, 0, C_theta_xfz, C_theta_xmx, C_theta_xmy, 0;
     0, 0, C_theta_yfz, C_theta_ymx, C_theta_ymy, 0;
     C_theta_zfx, C_theta_zfy, 0, 0, 0, C_theta_zmz;
     C_uxfx, C_uxfy, 0, 0, 0, C_uxmz;
     C_uyfx, C_uyfy, 0, 0, 0, C_uymz;
     0, 0, C_uzfz, C_uzmx, C_uzmy, 0];
end

%% HELPER: Zeta function (fillet shape)
function z = calc_zeta(xi, a, b)
if xi >= 0 && xi < a
    term = a - xi;
    z = 2*(a - sqrt(max(a^2 - term^2, 0))) + 1;
```

```
elseif xi >= a && xi <= (b - a)
    z = 1.0;
elseif xi > (b - a) && xi <= b
    term = xi - b + a;
    z = 2*(a - sqrt(max(a^2 - term^2, 0))) + 1;
else
    z = 1.0;
end
z = max(z, 1.0);
z = min(z, 1 + 2*a);
end
```

D

Actuator Characteristics

This are the data sheets provided by MagnaticInnovation on the Moving magnet actuator 5536.[73]

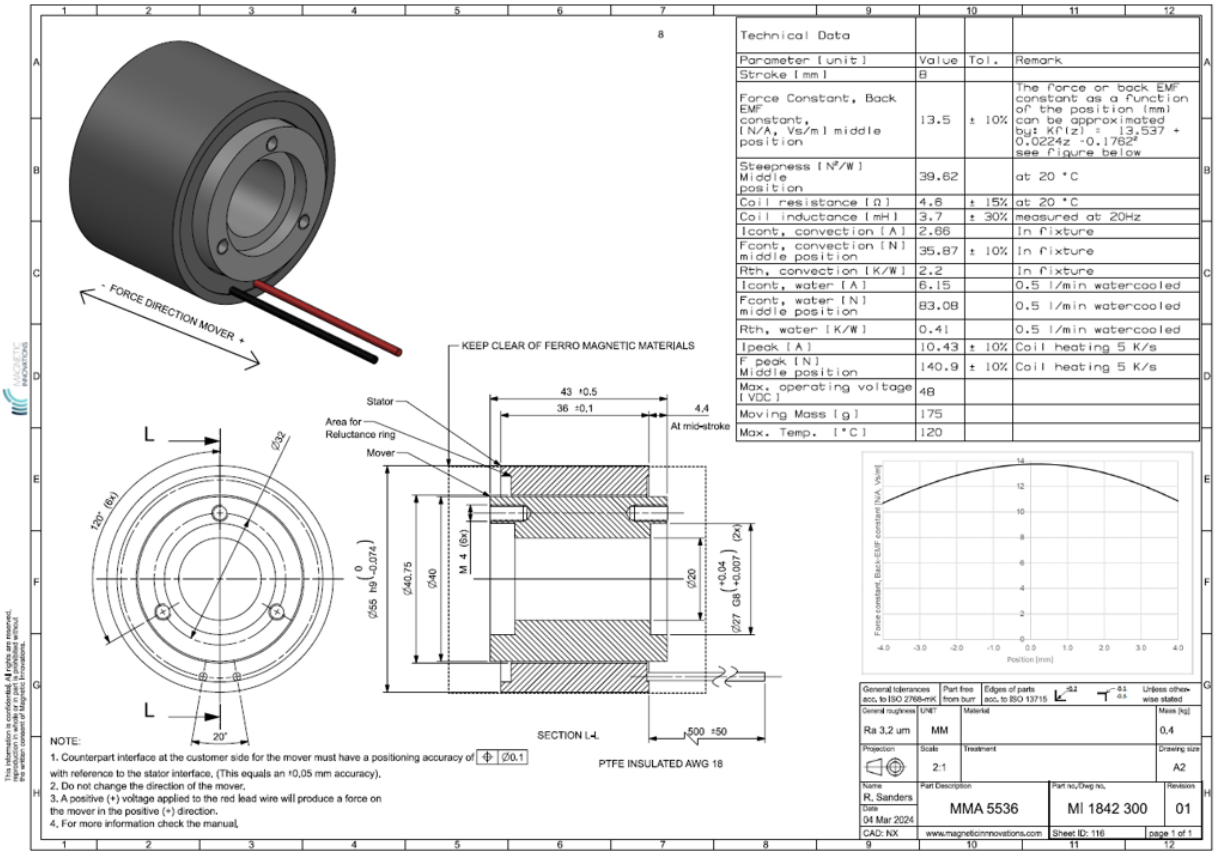

Figure D.1: 5536 moving magnet datasheet

Type	Continuous force [N]	Peak Force [N]
**1525	2.0	5.8
**1555	2.1	8.0
**3070	13	61
**5536	39	130
**9054	113	605

** Type moving magnet actuator (MMA of MMB)

Figure D.2: Peak force for the different VCA models

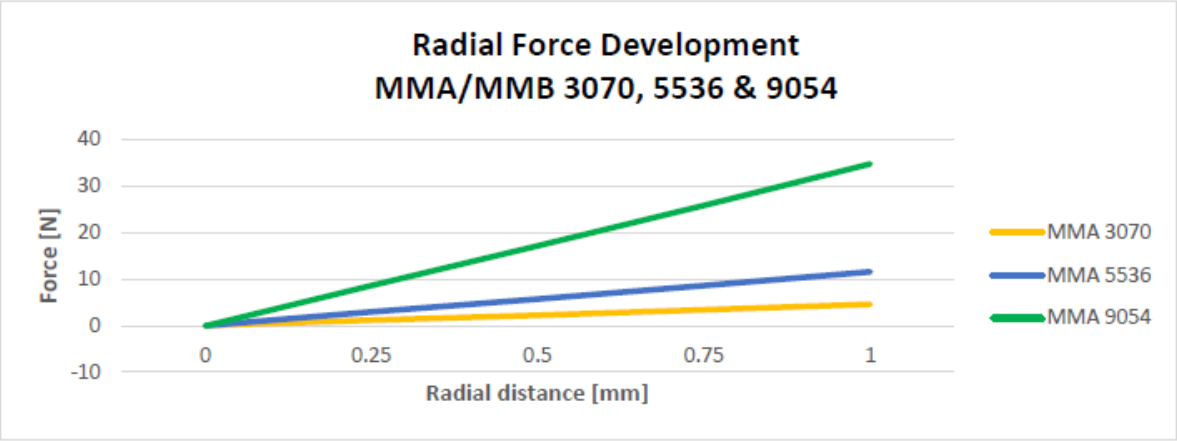

Figure D.3: Radial force between moving magnet and coil for different models

E

Final Design Compliant Gripping Mechanism Prototype AL7075

This chapter details the design specifications of the al7075 prototype such as it is ordered.

Figure E.1: LGM detailed view

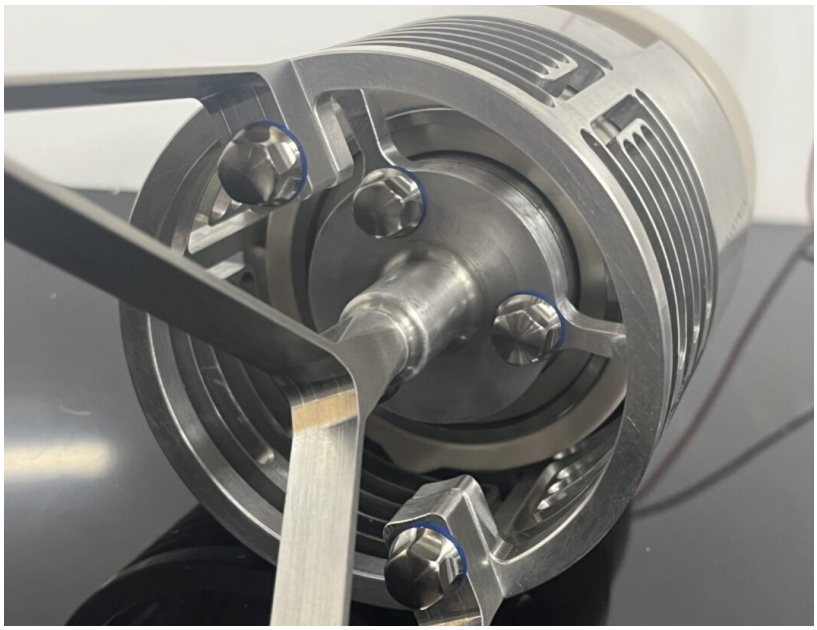

Figure E.2: Air gap of the VCA

Figure E.3: Engaged snap fit locking mechanism

Figure E.4: Final design Disassembled

Figure E.5: Final design assembled total weight

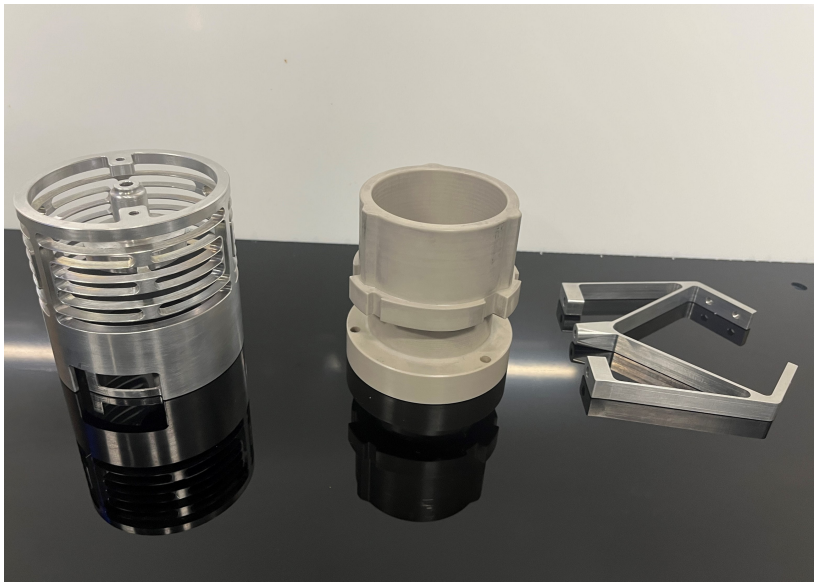

Figure E.6: Final design separate parts

F

Riboflavin Coverage Test

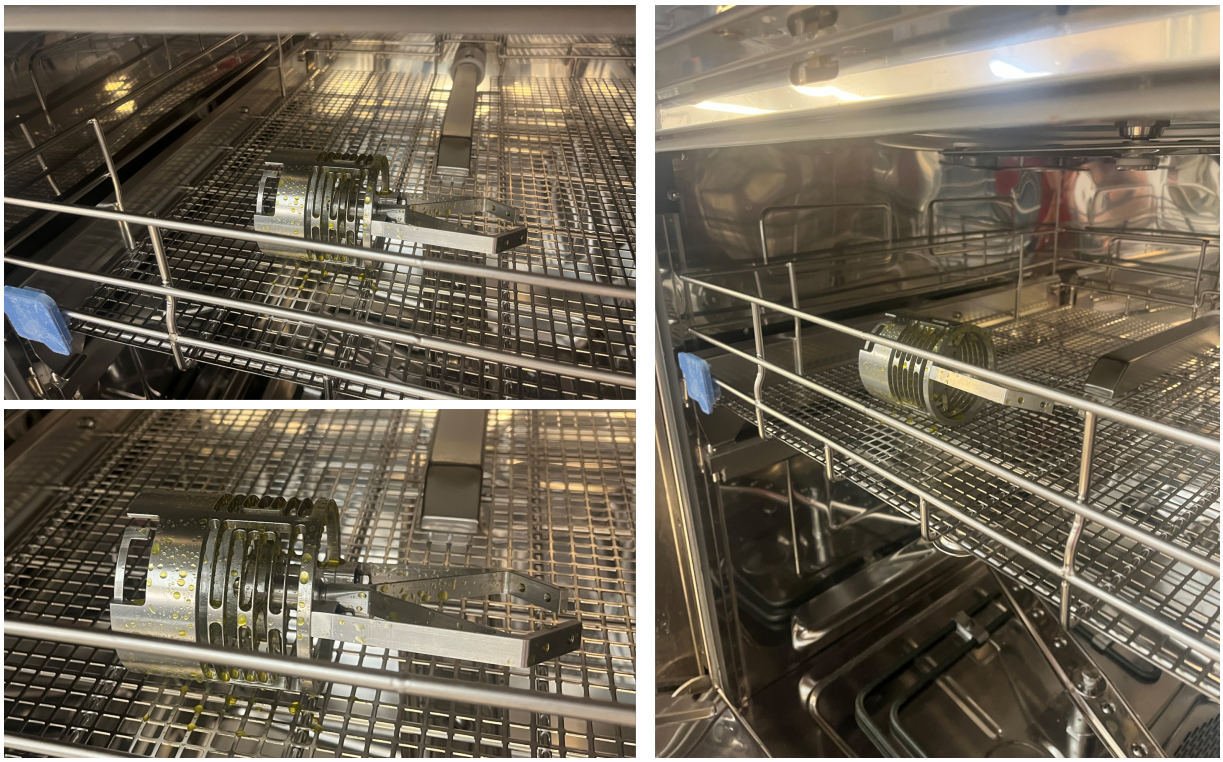

Figure F.1: Coverage test assembled before

Figure F.2: Coverage test assembled while washing

F.0.1. Assembled coverage test

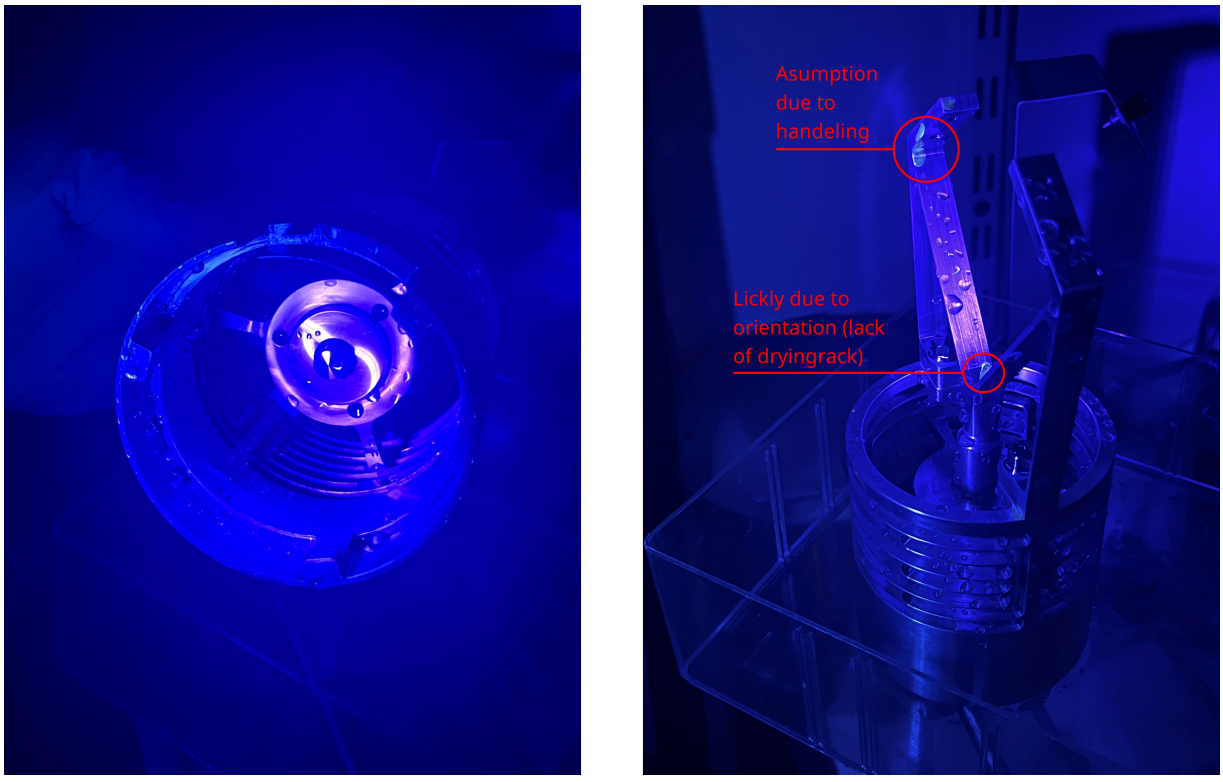

Figure F.3: Coverage test assembled

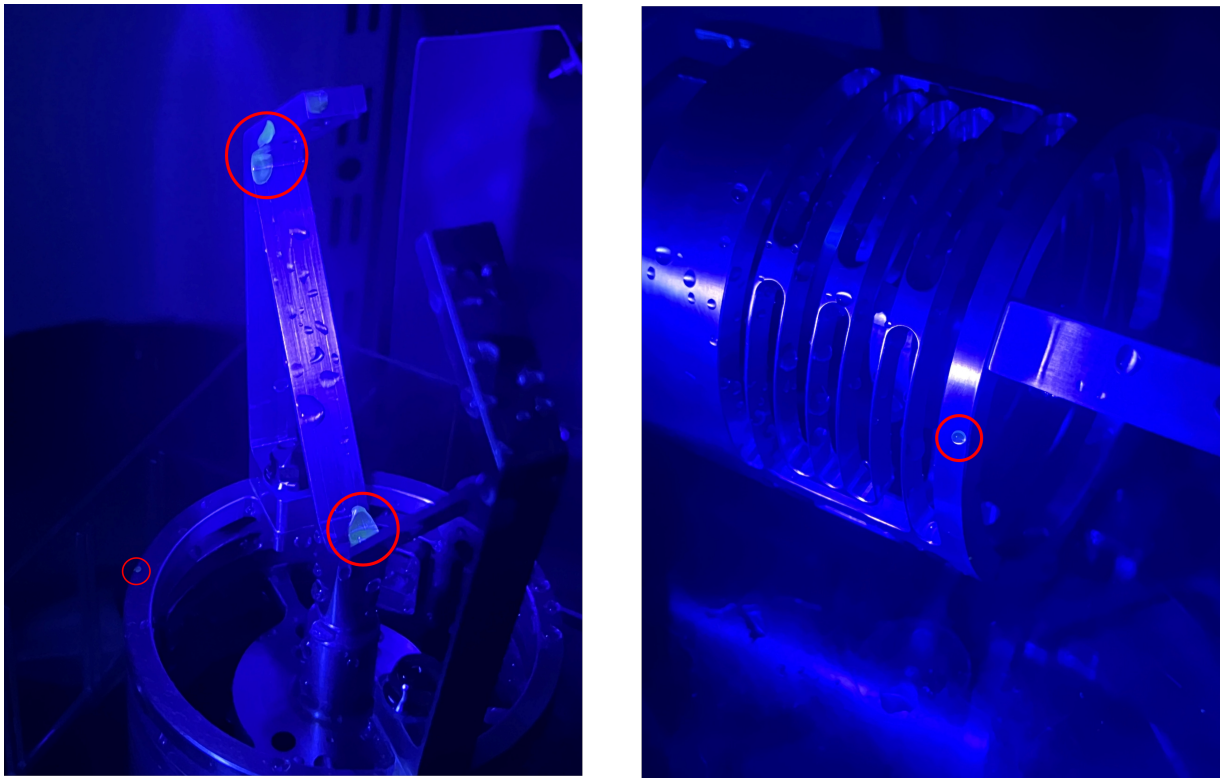

Figure F.4: Coverage test assembled

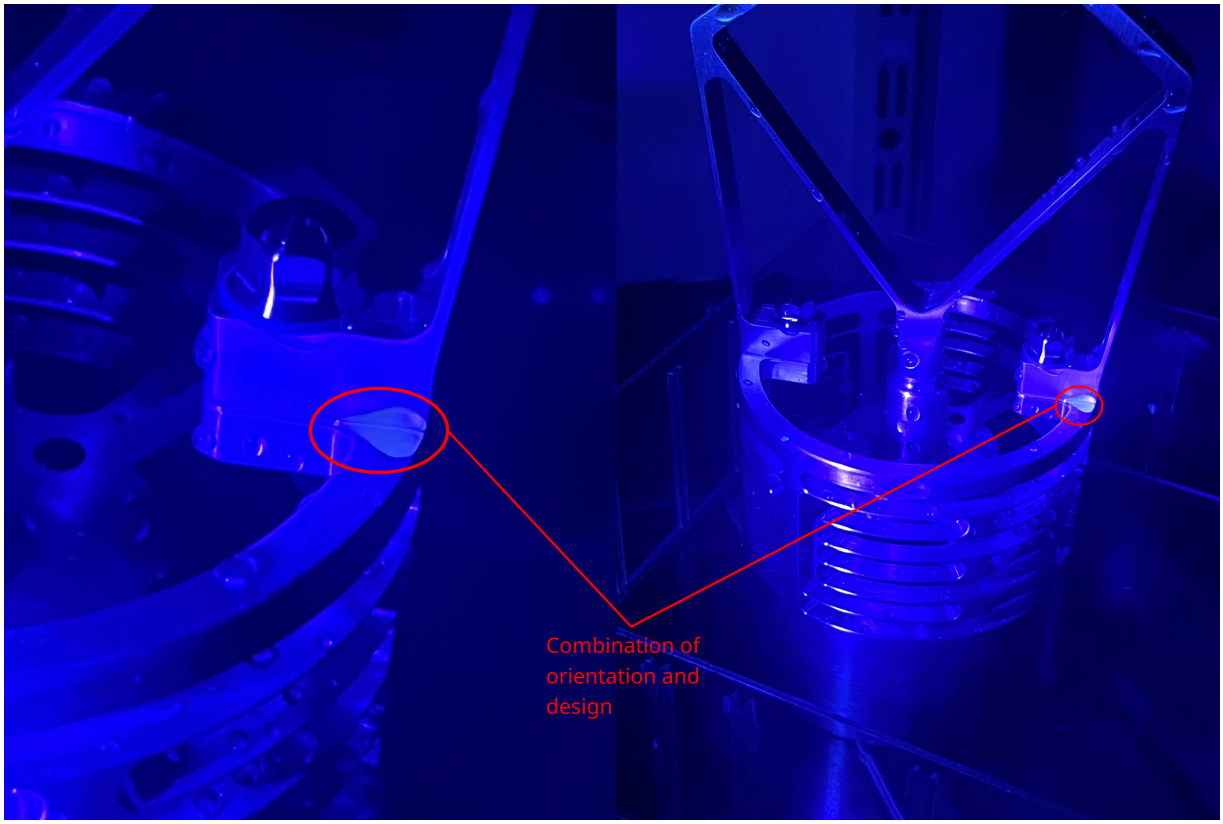

Figure F.5: Coverage test assembled

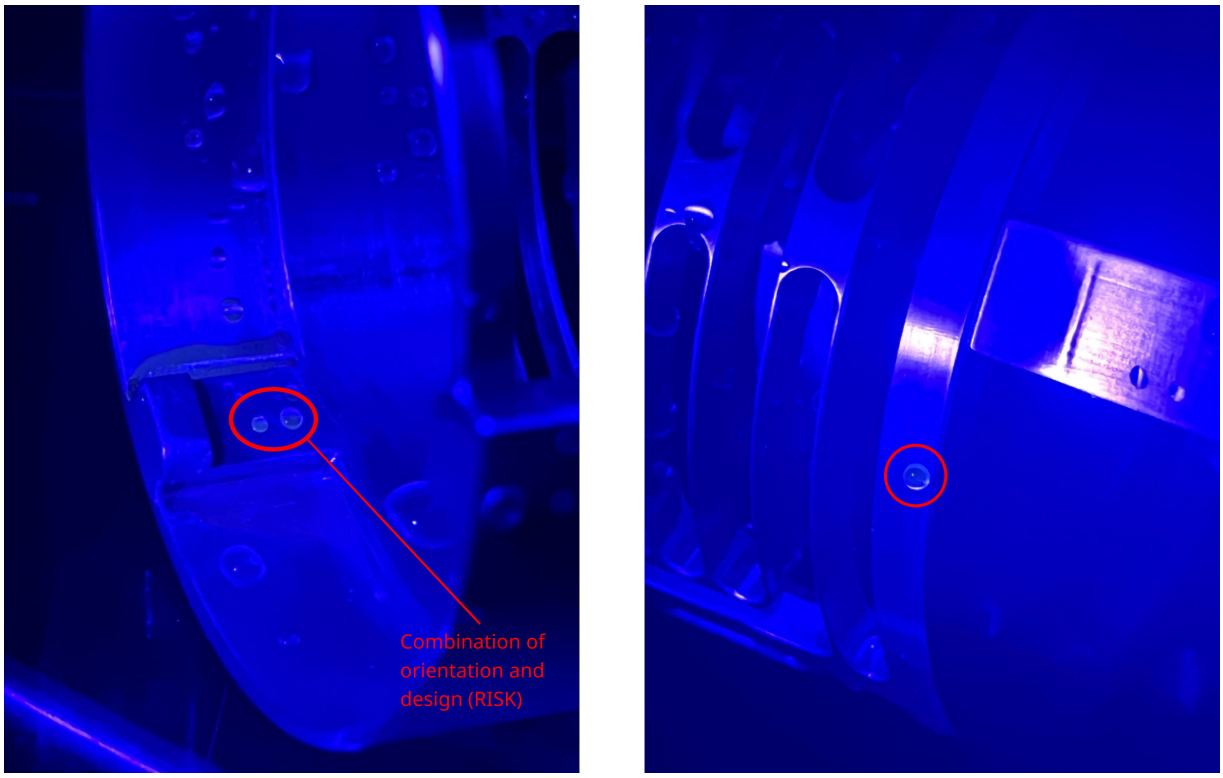

Figure F.6: Coverage test assembled

F.0.2. Disassembled coverage test

Figure F.7: Coverage test disassembled before wash cycle

Figure F.8: Coverage test disassembled after wash cycle

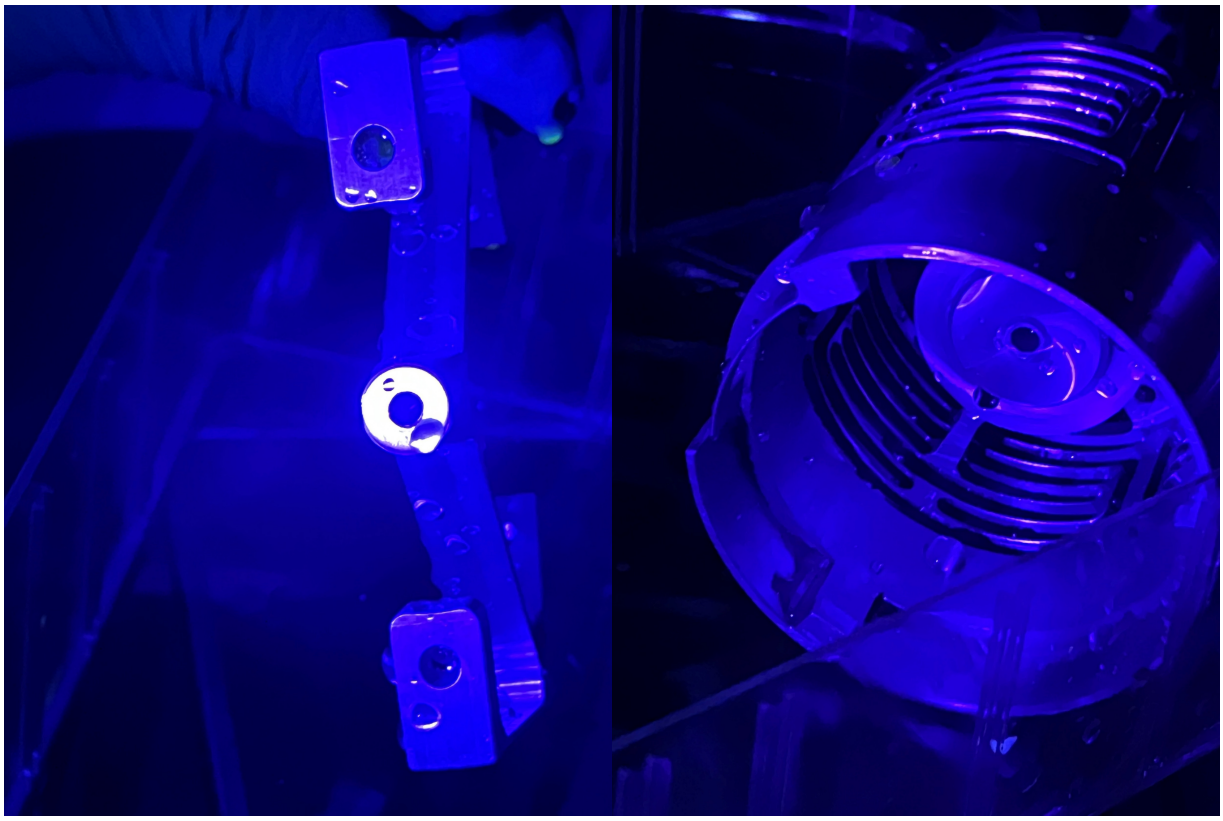

Figure F.9: Coverage test disassembled

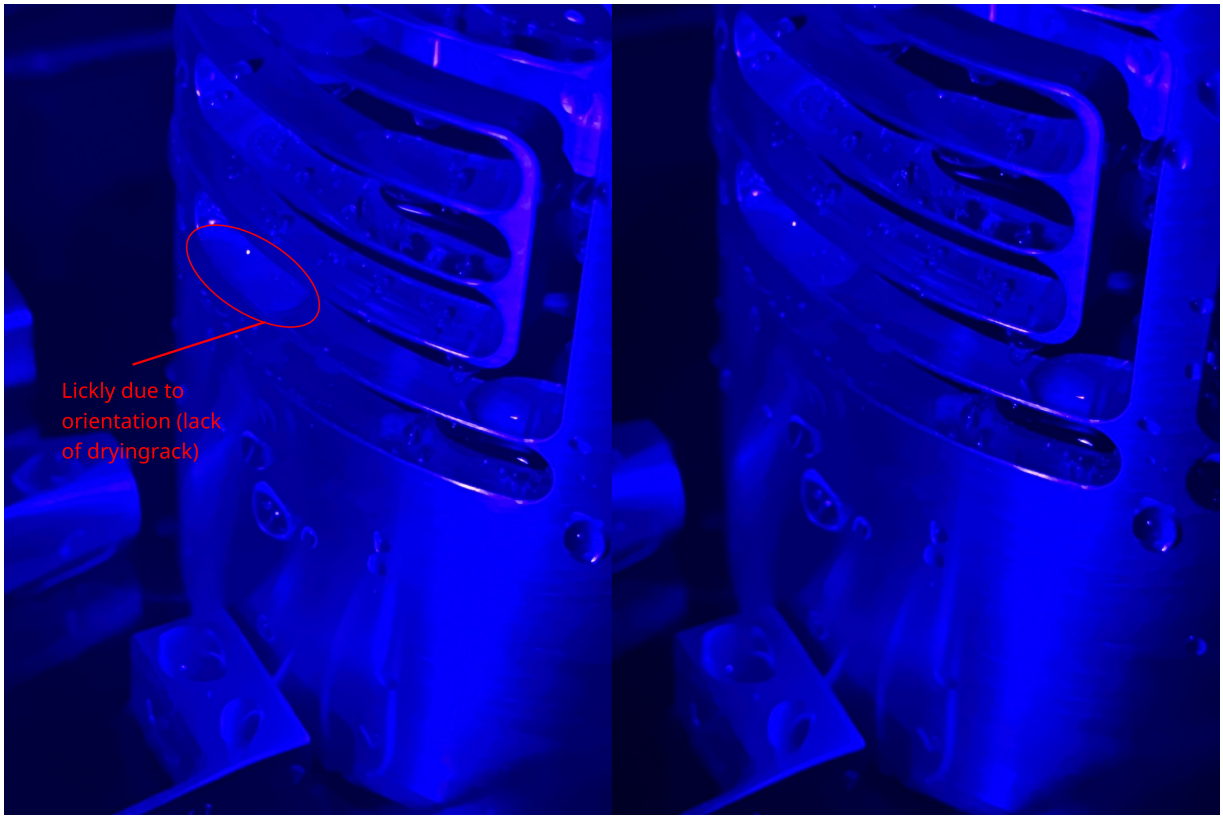

Figure F.10: Coverage test disassembled

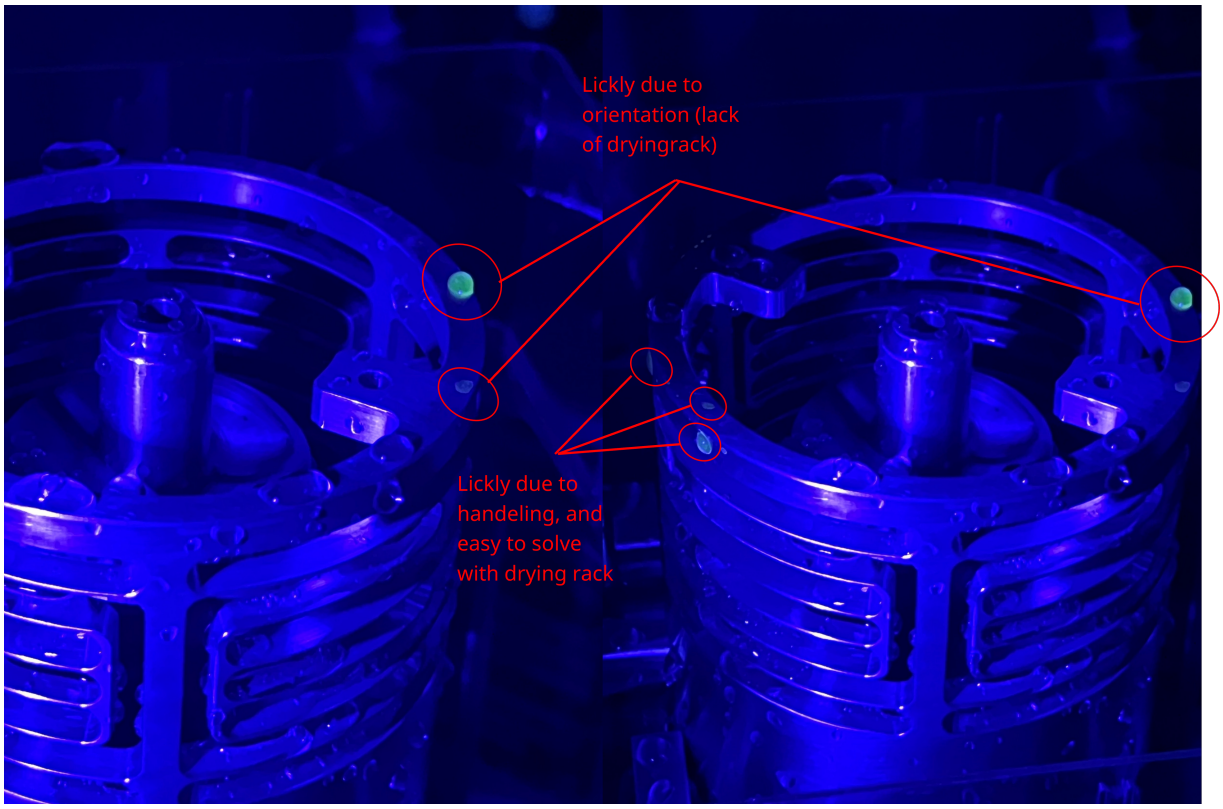

Figure F.11: Coverage test disassembled

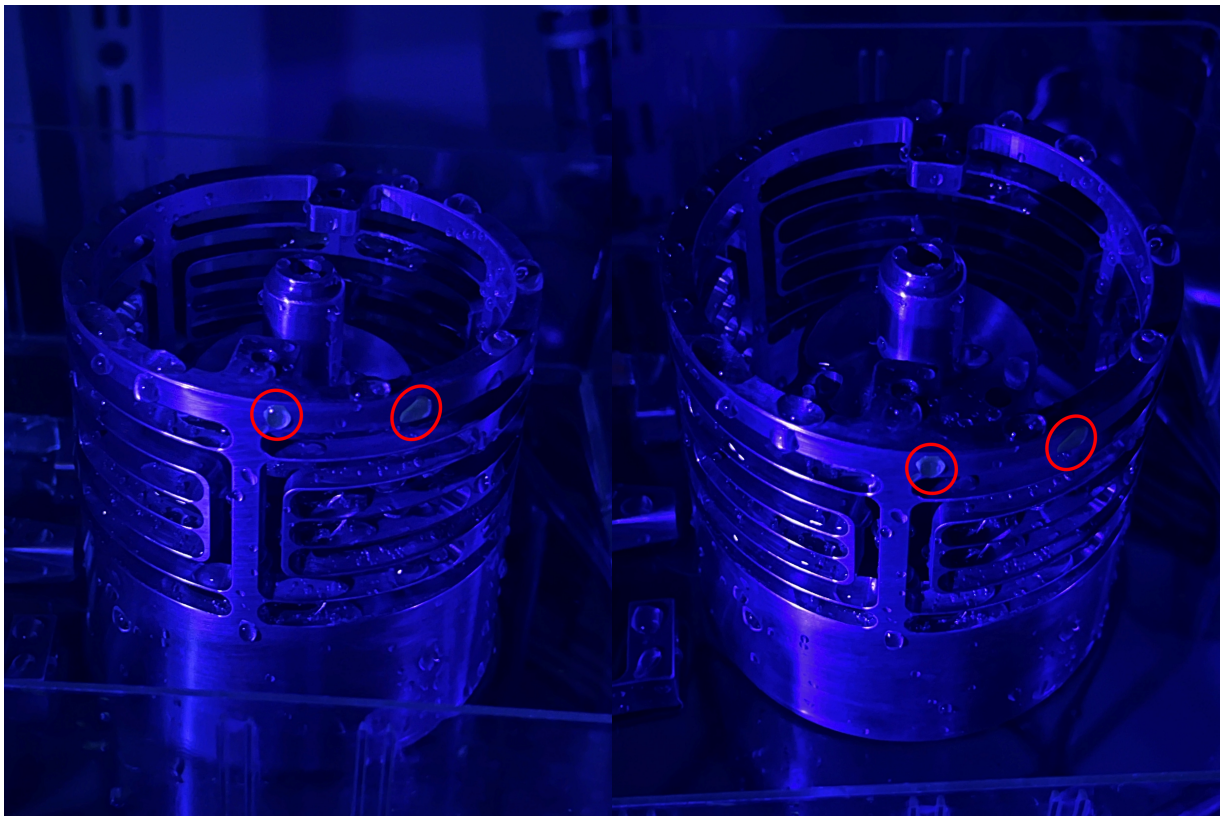

Figure F.12: Coverage test disassembled

G

Extra Validation Test Data

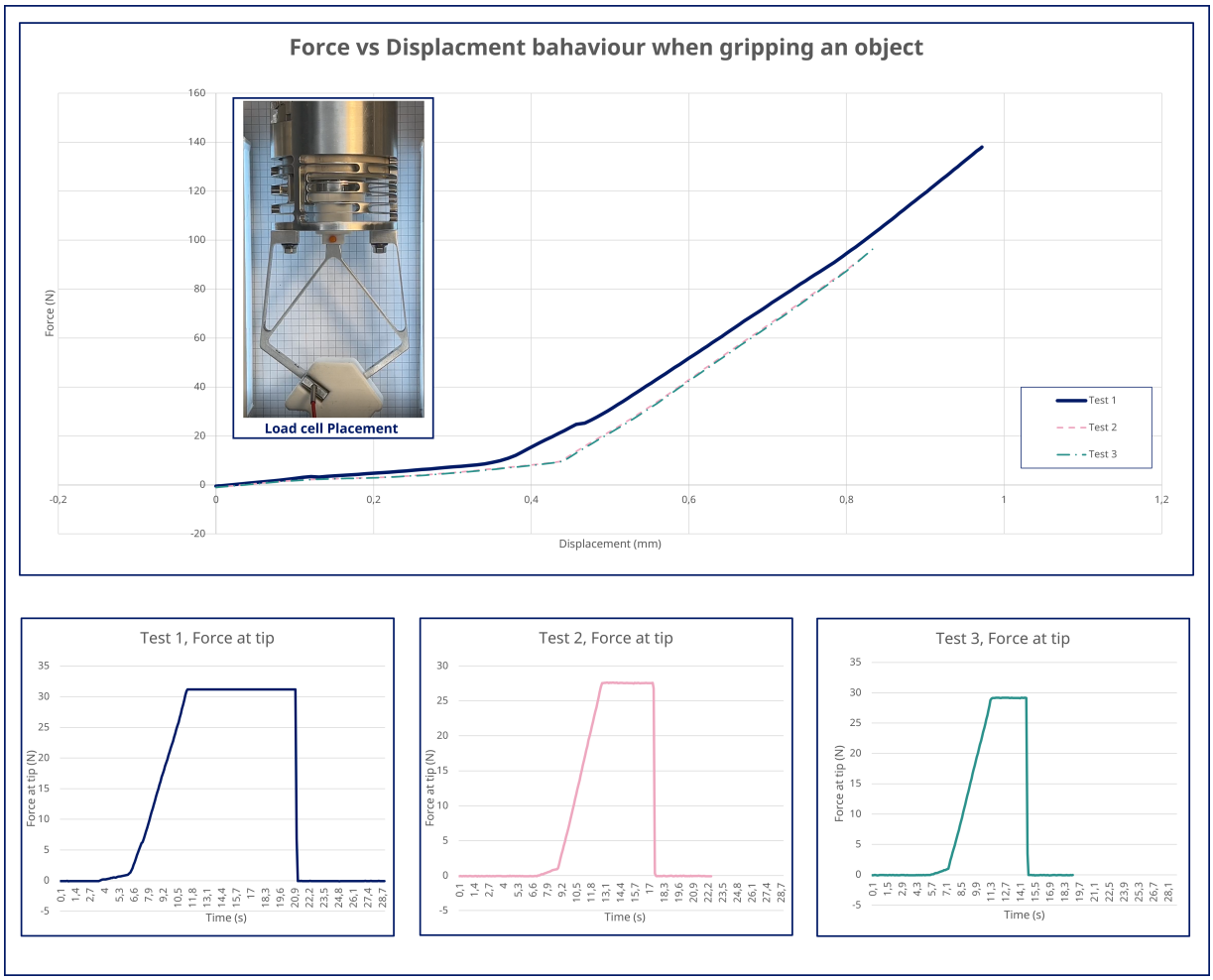

Figure G.1: Active force at the tip when actuated by Instron

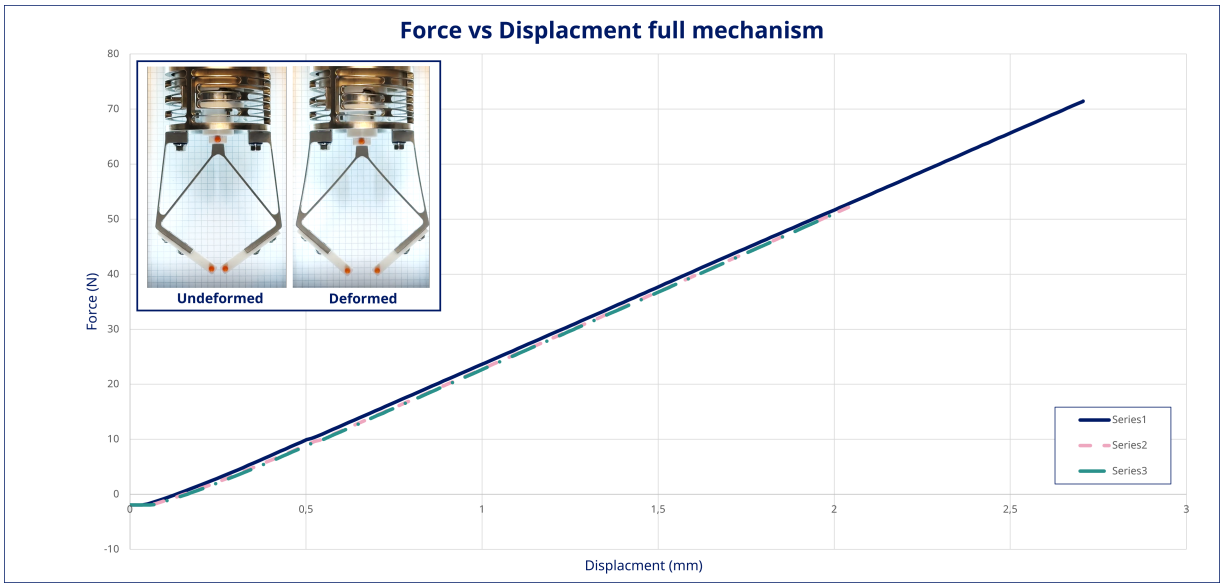

Figure G.2: Force displacement graph of the full mechanism actuated by Instron

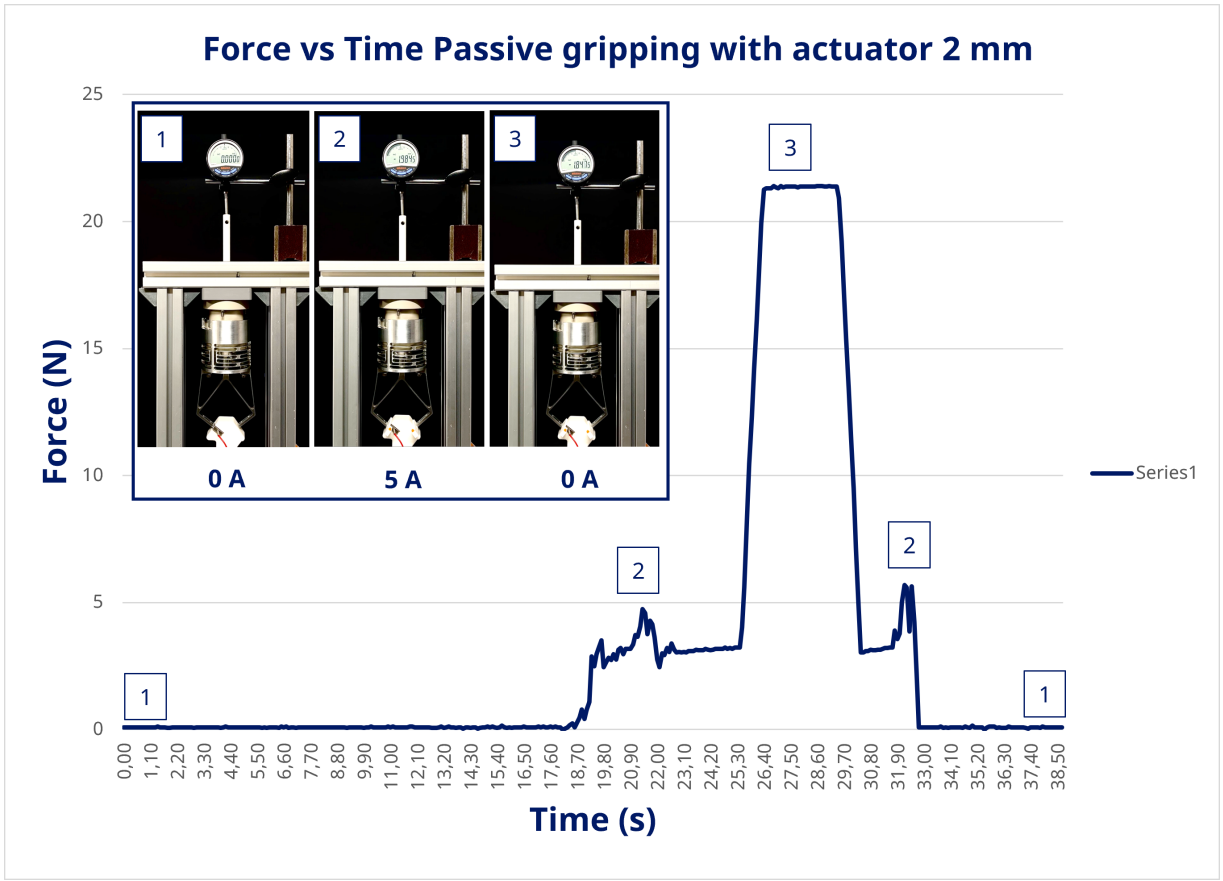

Figure G.3: Passive force at the tip when 2 mm is put in-between

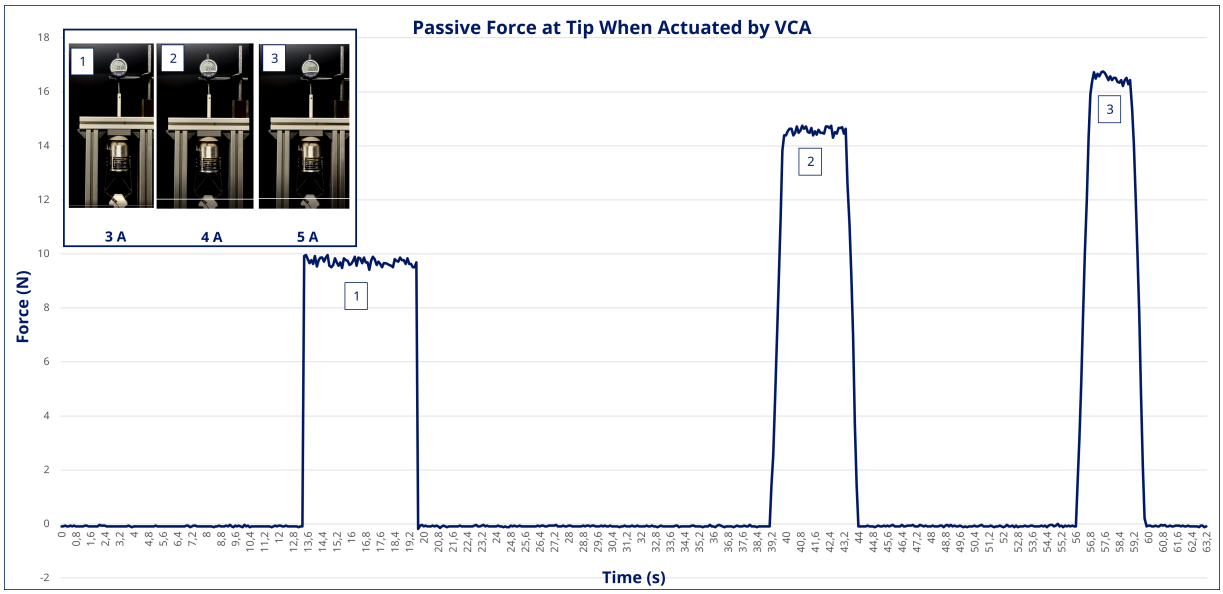

Figure G.4: Active gripping data input loadcell

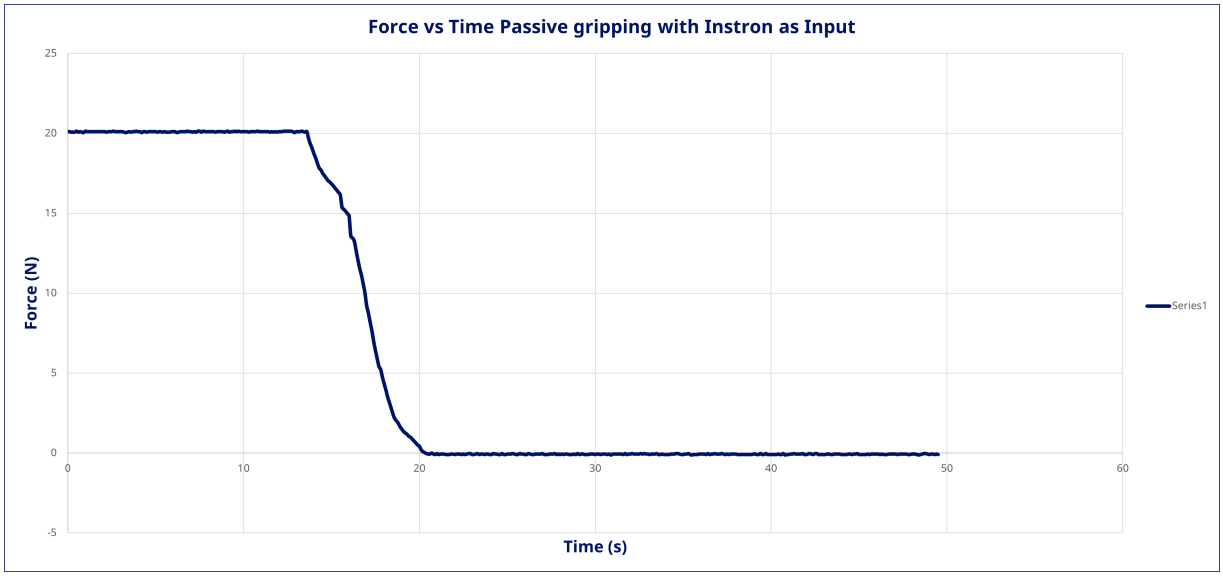

Figure G.5: Passive data loadcell at the tip when 2 mm is put in-between Instron